McGill University

# Investigating the role of ferrous iron in the arsenic(V)-iron(II,III) coprecipitation process system

Renaud Daenzer

Department of Mining and Materials Engineering
McGill University
Montréal, Québec
Canada

February, 2011

A thesis submitted to McGill University
in partial fulfillment of the requirements of the degree of
Master of Engineering

# Abstract

In this thesis, the effects of iron(II) on arsenic(V) removal from acidic sulphate solutions in lime neutralization systems were investigated. The role of Fe(II) was analyzed via different types of experiments. Firstly, 2-stage continuous coprecipitation (CCPTN) circuit experiments were run, involving variable Fe(II)/Fe(III) fractions whilst maintaining an Fe(tot)/As(V) molar ratio of 4, and the resultant products were subjected to stability testing. It was found that CCPTN results were reproducible; that increasing the Fe(II) content resulted in somewhat lower initial arsenic(V) removal, but still better results than those obtained from equimolar Fe(III)-As(V) solutions in the absence of ferrous pointing to the latter's beneficial effect on arsenic(V) precipitation and retention. Coprecipitates aged at constant pH 8, drifting pH and at various temperatures reached pseudoequilibrium after several months. Notably, long term stability testing of the coprecipitates showed that up to an Fe(II)/Fe(III) ratio of 1 at 20 °C, As(V) release was maintained below 1 mg/L after 463 days with "drifting pH" stabilized at 5 increasing only to 1.9 mg/L upon pH adjustment to 8.

Secondly, the behaviour of Fe(II) was studied in batch reactor set-ups as part of hydrolysis and oxidation experiments with and without As(V). It was shown in the absence of As(V), Fe(II) precipitated out of solution completely between pH 7.5 and 8.5. Subsequent oxidation of the ferrous hydroxide slurry was found to proceed via a series of transformations starting from ferrous hydroxide to green rust, to magnetite and finally goethite. The oxidation kinetics were governed by oxygen mass transfer. In the presence of As(V) both Fe(II) and As(V) precipitated from solution starting at pH 3 with the latter ultimately dropping below 1 mg/L between pH 6.5 to 9 via the proposed precipitation of a ferrous arsenate compound (symplesite). Subsequent oxidation of the Fe(II)-As(V) slurry at constant pH 8 led to destabilization of the ferrous arsenate phase and concomitant partial release of As(V). The bulk control of As(V) in the latter case switched from ferrous arsenate to ferric arsenate or arsenate adsorption on freshly formed iron(III) hydroxide.

# Résumé

Cette thèse à pour objet d'étudier les effets des ions ferreux (Fe(II)) sur la stabilisation, par neutralisation à base de chaux, de l'arsenic (As(V)) contenu dans des solutions acides sulfatées. Le rôle des ions ferreux a été analysé à l'aide de différents types d'expériences. Premièrement, des essais de co-précipitation en circuit continu (CCPTN) comprenant deux étapes ont été réalisés pour différentes fractions de Fe(II)/Fe(III), tout en conservant un rapport molaire Fe(tot.)/As(V) égal à 4; les produits obtenus ont par la suite été soumis à des tests de stabilité à long terme. Les résultats de ces tests ont montré de façon reproductible qu'une augmentation de la teneur en ions ferreux réduisait l'effet de stabilisation de l'As(V) initialement présent; ces résultats étaient cependant meilleurs que dans le cas de tests de stabilisation de l'As(V) présent dans des solutions équimolaires de Fe(III)-As(V), en l'absence d'ions ferreux, validant l'effet positif des ces derniers sur la précipitation et la rétention de l'As(V). Après plusieurs mois de vieillissement dans des conditions variées de pH constant (ajusté à pH 8), de pH non-ajusté et de températures, les produits de co-précipitation ont fini par atteindre un état de pseudo-équilibre. Notamment, les tests de stabilité à long terme ont montré que pour une fraction molaire Fe(II)/Fe(III) allant jusqu'à 1 et une température de 20 °C, la libération d'As(V) en solution après 463 jours était maintenue en-dessous de 1 mg/L, respectivement 1.9 mg/L, dans le cas d'une solution au pH non-ajusté (se stabilisant à pH 5), respectivement d'une solution au pH constamment ajusté à pH 8.

Deuxièmement, le comportement des ions ferreux a été étudié à l'aide d'un réacteur discontinu, dans le cadre de tests d'hydrolyse et d'oxydation, en présence ou non d'As(V). Les résultats de cette partie de l'étude ont montré qu'en l'absence d'As(V), les ions ferreux précipitent intégralement entre pH 7.5 et 8.5. Par la suite, l'oxydation de la suspension d'hydroxyde de fer (II) procède selon une série de transformations allant de la rouille verte, à la magnétite et finalement à la goethite. Les résultats ont également montré que la cinétique d'oxydation était gouvernée par le transfert de masse d'oxygène. En présence d'As(V), la précipitation du Fe(II) et de l'As(V) à été observée à partir de pH 3, sous la forme suggérée d'un composé d'arséniate de fer (II) (symplésite), la concentration finale d'As(V) non-précipité atteignant moins d'1 mg/L entre pH 6.5 et 9. Par la suite, l'oxydation de la suspension de Fe(II)-As(V) à pH 8 constant a entrainé la déstabilisation de la phase d'arséniate de fer et la remise en solution partielle d'As(V). En effet, dans ce cas particulier, le control de l'As(V) à entrainé la conversion de la majorité de la phase

d’arséniate de fer (II) en arséniate de fer (III) ou possiblement son adsorption à la surface d’hydroxyde de fer (III) fraichement oxydé.

# Acknowledgements

First and foremost my utmost gratitude goes to Prof. Demopoulos for giving me the opportunity to join his research group. His patience, his generosity, his fatherly approach and his unfathomable knowledge are the best attributes a student can ever wish for in a supervisor.

I take this opportunity to also thank the hydrometallurgy group as a whole (Levente, Guo-Bin, Mario, Kee Eun, Lydia, Nick, JC, Jessica, Cesar, Sonia, Cecile, Sebastian, Nima, Jack, Jordan) for being a very outgoing, friendly, fun, -and when it matters most, an incredibly supportive and helpful group of people. Special mention goes to Derek for his friendship, inspiring life, motivational speeches, the English language and sense of humor. I also want to acknowledge the following people for their contribution and expertise enabling my thesis project: Mr. Golsztajn, Mr. Roy, Ms. Riendeau, Ms. Hanley, and particularly Philippe T. Pinard. I see it fit to also salute the Blades of Steel, all my friends from school, my Professors throughout University, Pauli and Mitch.

On a more personal level, I wish to thank my Mom (for everything that she’s been doing and still does for her grownup son – no questions asked), my Dad, Samy and Aline for making us a great family with unconditional love and support for one another. I also want to thank the O’Donnell family for their generosity and influence on my life. And lastly, I want to express how grateful I am to be able to share my life with my best friend, my travel partner, my confidant, my sunshine, the love of my life Katherine who has encouraged me and been there for me every step of the way.

# Table of Contents

# List of Figures

# List of Tables

# 1 Introduction

Uranium mills in northern Saskatchewan are processing ores that contain high concentrations of arsenic. Before acidic effluent waters may be released back into the environment, they must first be neutralized in order to precipitate out toxic elements like arsenic, nickel, selenium and molybdenum just to name a few. Following precipitation, the neutralization sludge is deposited in a tailings pond where the pore waters are subjected to regular toxic element analysis [1]. The major and long term goal is to produce a stable form of arsenic-bearing precipitate, which will not dissolve back into the environment for literally tens of thousands of years. Although initial arsenic removal is very effective and the average concentrations are in general below regulatory limits it is of interest to understand the stability of such arsenic-bearing precipitates and its relation to the method of production if further improvements to the tailings management practice are to be made.

Arsenic (preferably as As(V)) removal in such neutralization operations is achieved by continuous coprecipitation (CCPTN) involving excess iron in solution so that arsenic “coprecipitates” with iron upon pH adjustment. Such co-precipitation process has always been considered to require the excess iron to be in ferric form with molar ratio Fe(III)/As(V) >3 [2]. However, actual process effluents from uranium mills contain significant levels of soluble ferrous iron ($Fe(II)/Fe_{tot}$=10 % [3], 44-93 % [4], 37 % [5], 57 % [6-7]). As a result, the role of ferrous iron on arsenic(V) removal and retention in the CCPTN system deserves to be studied. The available literature on the effect of ferrous on the removal of arsenic(V) is limited compared to what is available on the subject of ferric iron and arsenic precipitation.

Previous research by the McGill Hydrometallurgy group has focused on the effect of process parameters on the efficiency of the Fe(III)/As(V) CCPTN circuit and the stability of the generated coprecipitates [8]. In this thesis, the role of ferrous iron during coprecipitation of As(V) with mixed Fe(II,III) media is investigated at different levels. First the best conditions for operating the Fe(III)/As(V) CCPTN process as determined by De Klerk [8] were validated and subsequently the CCPTN circuit was operated with increasing amounts of ferrous iron in the initial solution followed by accelerated ageing/stability testing of the newly formed precipitates. This part of the work is described in Chapter 4. Chapters 2 and 3 cover the background technical literature and experimental methods respectively.

With the objective of interpreting the behaviour of ferrous iron during arsenic(V) coprecipitation in the continuous circuit additional tests were performed involving various batch investigations. Thus, in addition to CCPTN, this thesis includes a chapter dedicated to the hydrolysis of ferrous iron alone and in mixture with arsenic(V) over a wide range of pH (Chapter 5). In Chapter 6 the oxidation kinetics of ferrous iron in solution or as ferrous hydroxide slurry by oxygen/air sparging at various pH set points are investigated. The final chapter provides a summary of the major findings from the preceding chapters and makes suggestions for future work.

# 2 Literature Review

This literature review comprises two distinct sections concerned with the removal of arsenic from solution. The first section (2.1) focuses on the coprecipitation of arsenic(V) with iron(III) by neutralization of acidic effluent solutions in terms of the effects of process parameters on the production (removal of arsenic) as well as the ageing (long term stability) of the generated products. In particular, the nature of the various phases in which arsenic(V) is removed from solution are discussed.

The second part provides a comprehensive review on the chemical behaviour of ferrous iron(II) that can have an influence on the performance of continuous coprecipitation circuits aimed at removing arsenic(V) from solution. The review includes the hydrolysis of ferrous iron over a wide range of pH, the oxidation reaction kinetics of ferrous ion and ferrous hydroxide, the formation of mixed-valent iron(II,III) phases and their behaviour in an oxidizing environment together with arsenic(V), and finally the solubility of various precipitated ferrous arsenate phases (read symplesite).

## 2.1 Coprecipitation of Ferric Arsenate and Arsenical Ferrihydrite

### 2.1.1 Introduction

Arsenic a is poisonous element that is typically found in process effluent solutions in two oxidation states, as arsenate ($AsO_4^{3-}$) and arsenite ($AsO_3^{3-}$) species, with the latter one being 6 times more cytotoxic [9]. Some parts of the world contain naturally occurring high arsenic concentrations (e.g. Taiwan, India, Chile, Bangladesh and southern US [10-12]) in ground water, that can affect human populations thus requiring effective arsenic removal technologies for ground water purification. Recently, the US Environmental Protection Agency maximum contaminant level (MCL) [13] and Canadian maximum acceptable concentration (MAC) [14] for arsenic have been decreased from 0.05 to 0.01 mg/L for drinking water.

On a different note, arsenic is the 33rd most abundant element on the earth's crust (2ppm) [15] and a major impurity in several valuable mineral feedstocks that inevitably ends up accumulating in waste effluent streams of mining and milling operations of gold [16], uranium [3] and copper industries to name a few [17-19]. In Canada, regulations such as the MMER [20] are put into effect limiting the discharge concentration of arsenic into the environment in a controlled site at 1 mg/L for a grab sample and 0.5 mg/L as the monthly mean concentration of a deposit site.

Thus, it is of great significance to improve arsenic removal technologies for humanitarian and environmental reasons. Among the various arsenic removal technologies the most notable one, at least in the case of mining/metallurgical process effluents, is the coprecipitation of arsenic with iron by neutralization. A good example of such coprecipitation process is the McClean Lake uranium mill that involves processing of arsenic-bearing raffinate solution through a two tank continuous lime neutralization circuit [6]. The performance of the process in terms of effective arsenic removal and stability of the produced coprecipitated solids depends on a number of parameters. These are discussed in the next section.

### 2.1.2 Coprecipitation

Previous research has investigated the effect of the Fe(III)/As(V) molar ratio during coprecipitation [2, 4, 21]. Figure 1 taken from the work of Robins *et al.* [21] clearly indicates that at a ratio greater than three acceptable arsenic removal is achieved. Furthermore it can be seen that as the Fe/As ratio increases the effectiveness of arsenic removal is extended to wider pH range.

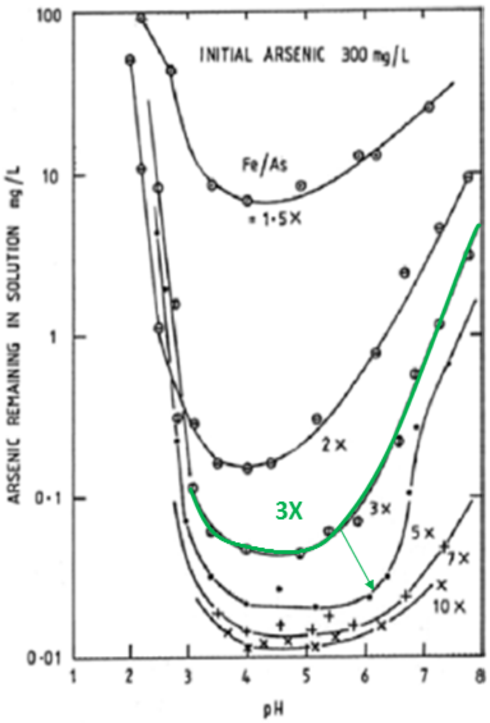

**Figure 1: Effect of pH and Fe/As molar ratio on the removal of arsenic from solution [21]**

Other research has looked into the effect of co-ion solutes on the "batch" coprecipitation process indicating that sulphate media [22], calcium [22-24], nickel [24-25], ferrous (albeit for groundwater arsenic removal) [26], and aluminum [27] provide improved arsenic removal. Furthermore, it has been demonstrated that both calcium [22, 24] and aluminum [27] provide improved arsenic retention over time. Until recently, there was only one published study where the investigation used a continuous coprecipitation (CCPTN) circuit (mill scale) [3]. All other studies involved batch experiments.

De Klerk of the McGill Hydrometallurgy Group [8] conducted the first laboratory scale continuous coprecipitation (CCPTN) circuit experiments and successfully correlated various process parameters to arsenic removal and retention. It was shown that the use of slaked lime, as opposed to more aggressive sodium hydroxide, as the base of choice and the use of a two reactor CCPTN circuit yielded the best results in terms of arsenic retention and subsequent ageing.

It is worthy to discuss the arsenic removal efficiency observed as a function of staging in CCPTN as compared to batch reactor coprecipitation. Neutralization to pH 8 by NaOH of an initial solution containing 1400 mg/L arsenic at a Fe/As molar ratio of four in a single continuous reactor provided effluent arsenic concentrations of 150 and 26 µg/L with NaOH and $Ca(OH)_2$ base respectively [8]. These results show the benefits of using slaked lime as a base in order to yield lower residual arsenic concentrations. Moreover, it was shown that using two or three continuous reactors resulted in an effluent with lower arsenic concentrations when compared to a single continuous reactor [8]. Although the difference in residual arsenic concentration between the two and three stage circuits was relatively small (8 vs. 10 µg/L), the two stage circuit was deemed as the optimal choice for future experiments due to better coprecipitate ageing results.

### 2.1.3 Nature of As-bearing Coprecipitates

Currently, there is an ongoing debate on the type(s) of arsenic-bearing phase(s) that form as a result of coprecipitation. Clearly, neutralizing solutions of high Fe/As molar ratios will yield ferrihydrite (FH) due to the excess iron. This dominant phase having a high surface to volume ratio has the capacity to adsorb arsenates and arsenites via surface complexation [17, 21]. The precipitation and subsequent adsorption reactions can be represented by Equations (1) & (2) [17].

$$Fe^{3+} + (3+x)H_2O = FeO(OH)(H_2O)_{1+x} + 3H^+ \quad (1)$$

$$FeO(OH)(H_2O)_{1+x} + AsO_4^{3-} = AsO_4^{3-} \cdot FeO(OH)(H_2O)_{1+x} \quad (2)$$

Fuller *et al.* [28] showed that the co-precipitation of Fe(III) and As(V) in the pH range 7.5-9 resulted in the fast adsorption of arsenates up to a density of 0.7 mole As(V) per mole Fe. Despite the high concentrations of arsenic in the precipitates, EXAFS spectroscopy did not find evidence for ferric arsenate or any other As-bearing surface precipitates [28]. They suggested the high adsorption of As(V) is due to the extremely small FH particles which during polymerization were "poisoned" by strong arsenate bidentate adsorption [29]. These arsenates subsequently inhibit the normal crystallization of FH to more stable products such hematite [30]. In other words the adsorbed arsenates stabilize the structure of FH and prevent particle growth and transformation [17].

On the other hand, results from mill-scale experiments correlated with a geochemical model (taking into account both scorodite and FH as equilibrium phases) have suggested that between pH 2.4 and 3.1 arsenic is controlled by "scorodite" (although more likely this is poorly crystalline scorodite or ferric arsenate (FA)) before dissolving incongruently at pH>3.1. The latter involves re-precipitation of dissolved iron into FH which becomes the dominant phase that adsorbs the arsenate anions at higher pH region [3]. Langmuir *et al.* [4] on the other hand showed that during neutralization of solutions containing Fe and As at a molar ratio between 3-5, ferric arsenate began to precipitate at pH 1 and persisted to higher pH regions becoming the dominant form of arsenate in the tailings. Subsequent ageing tests suggested the breakdown of FA to explain the rate of release of dissolved arsenate into porewaters. In 2006, the same authors conducted an extensive review of the available literature on the solubilities of crystalline scorodite and amorphous ferric arsenate [5]. They showed that as the Fe/As molar ratio of an acidic solution being neutralized (generating a mixture of ferric arsenate and ferric hydroxide) is increased (1.6, 5.8 & 14.4), the solubility product, $K_{sp}$, of ferric arsenate decreases at pH 2. Furthermore, they showed that increasing the pH set points for neutralization of an actual raffinate solution with an Fe/As molar ratio of 3.72 decreased the solubility of FA indicating a more crystalline scorodite present at higher pH values, a rather unexpected postulation. Concurrently, over the same pH range the solubility of precipitated ferric oxyhydroxide (FO) (equivalent to ferrihydrite) increased indicating an amorphous FO unable to crystallize due to arsenate and sulphate adsorption onto its surface. In sum, Langmuir *et al.* attributed the low concentrations of arsenic in tailings pore waters at near neutral pH to the stability of partially crystalline scorodite (very small fraction) with respect to a rather unstable amorphous FO. This is represented by the ferric arsenate/iron hydroxide equilibrium reaction (3):

$$FeAsO_4 \cdot 2H_2O(s) + H_2O = Fe(OH)_3(s) + HAsO_4^{-2} + 2H^+ \tag{3}$$

Jia *et al.* [31] used X-ray diffraction to compare prepared standards of poorly crystalline ferric arsenate to As-FH adsorption samples prepared from solutions of relatively high arsenic concentration (1400 mg/L) with Fe(III)/As(V) molar ratios ranging between 2 and 8 and final pH values between 3 and 8. It was proposed that at acidic pH (~3-4), adsorption of arsenate on FH and the ensuing surface complexation transitioned to a ferric arsenate surface precipitate showing up as a similar XRD spectrum to poorly crystalline FA. Between pH 4-5, both FA and FH are equally important as indicated by the two components on the first band (28º & 34º 2θ in Figure 2). However, at higher pH (~8), the surface complexation dominates the process and the XRD of coprecipitates resemble those of plain FH.

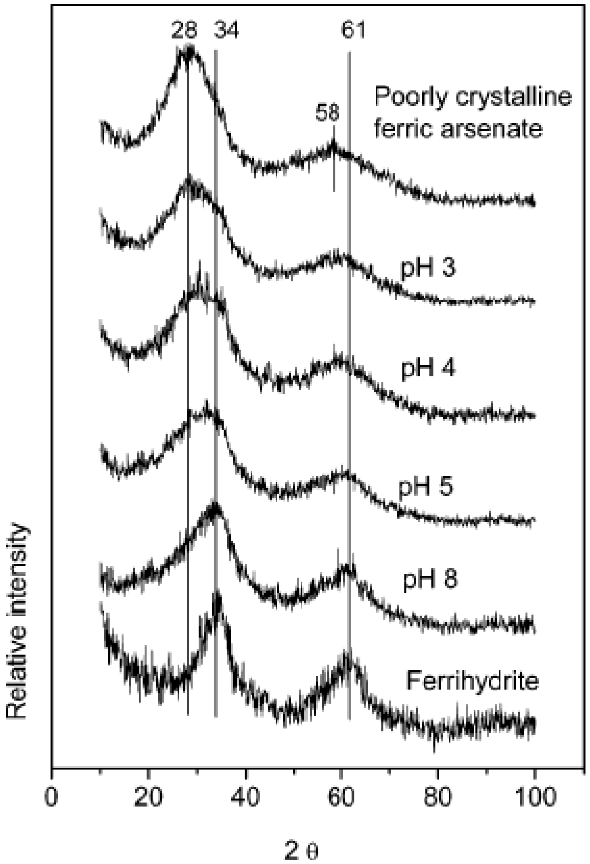

**Figure 2:Effect of pH on the XRD patterns of arsenate-ferrihydrite sorption materials with initial molar ratio Fe/As=2 and equilibrium time of two weeks [31]**

Chen *et al.* [7] undertook the task of characterizing coprecipitates obtained from actual raffinate solutions with an Fe/As molar ratio of 4.4 ([As]=732 mg/L, [Fe]=2400 mg/L) from AREVA's McClean Lake uranium ore processing facility by means of x-ray absorption fine structure spectroscopy. These researchers prepared and characterized crystalline scorodite (CS), poorly crystalline scorodite (PCS), arsenic-adsorbed goethite (As-G and/or As-FH) and Fe/As=4 coprecipitates neutralized to pH 4 & 8 using NaOH (CPT) reference materials to be compared with coprecipitates from the raffinate solution neutralized with $Ca(OH)_2$ or NaOH (indicated by pH values in *italic*) up to pH set points *2.01*, 2.18, 3.15, 4.04, 6.09, *7.08*. Firstly, the results showed that the synthetic Fe/As=4 solution neutralized to pH 4 produced CPTs that had As-Fe inter-atomic distance and coordination numbers close to those of PCS. Nevertheless, the same solution neutralized to pH 8 produced CPT much closer to As-G. Next, they showed that raffinate solution neutralization up to pH 7 resulted in coprecipitates that had the same local structure as that of PCS and that only at high enough terminal pH values (pH>8), the As-FH species becomes dominating. One may now plead the case that coprecipitates with Fe/As molar ratios greater than 1 may be composed of PCS and arsenate adsorbed ferric oxyhydroxide or equivalently ferrihydrite). According to Chen *et al.*, the PCS features stand out until a threshold pH value (pH 7-8) beyond which the coprecipitate structure resembles that of the As-FH phase. Coincidentally, this pH region is also known to be the upper region of scorodite stability in the Fe-As-$H_2O$ $E_h$-pH diagram published by Langmuir *et al.* [4].

Ultimately, regardless of the actual phase in which arsenic is bound, at high Fe/As molar ratio the removal of arsenic has been shown to be effective up to pH 8 and deemed stable enough for long term stability in tailings management facilities.

## 2.2 The Chemical Behaviour of Ferrous Iron

### 2.2.1 Introduction

Previous research involving the removal of arsenic, whether be from industrial process solutions and effluents, acid mine drainage or naturally occurring toxic arsenic cycling in the subsurface such as in ground waters, was mainly preoccupied with the use of ferric iron to precipitate and/or adsorb the arsenic out of solution. Not much attention has been given to ferrous iron (Fe(II)). It is conceivable that this species of iron may oxidize during coprecipitation and report as ferrihydrite or ferric arsenate in the solids. Alternatively it may precipitate first as ferrous hydroxide and later be oxidized to ferric hydroxide (ferrihydrite) on which arsenic adsorbs or simply precipitate as ferrous arsenate. Hence it is essential to investigate the behaviour (in terms of oxidation and precipitation) of ferrous iron in solutions similar to those encountered in Fe/As coprecipitation operations.

## 2.2.2 Effect of pH on Ferrous Iron Oxidation

### 2.2.2.1 Ferrous Oxidation at pH<4

At low pH, although the oxidation of Fe(II) with oxygen is thermodynamically favorable it is considered extremely slow. Sato *et al.* [32] briefly reported that the oxidation of iron(II) sulphate at pH<3 with oxygen at both 25 °C and 50 °C is very slow. They attempted to increase the rate of ferrous oxidation by addition of a catalyst and various complex-forming agents. It was found that the copper(II) sulphate catalyst slightly increased the rate of oxidation yet not as successfully as complex-forming species such as ethylenediaminetetraacetic acid and sodium triphosphate, whose effects were limited to their added concentration.

### 2.2.2.2 Rate Laws for the Oxidation of Ferrous Iron at Near Neutral pH

The most commonly verified rate equation for the oxidation of ferrous iron at near neutral pH is represented by Equation (4) [33]:

$$-\frac{d[Fe(II)]}{dt} = k(OH^-)^2 P_{O_2}[Fe(II)] \tag{4}$$

Where Fe(II) is given in mol $L^{-1}$, $O_2$ as a partial pressure (atm) and $OH^-$ as an activity [33] or as the concentration of hydroxyl ions [34]. If conditions are such that the pH and oxygen partial pressure remain constant, this equation reduces to a pseudo first order rate expression:

$$-\frac{d[Fe(II)]}{dt} = k_1[Fe(II)] \tag{5}$$

Where $k_1 = k(OH^-)^2 P_{O_2}$ has units of inverse time. By integrating Equation (5) we yield (6), which should give a linear curve with slope $-k_1$ when the natural logarithm of iron concentration is plotted over time.

$$ln[Fe(II)] = -k_1\mathrm{t} + \ln\,[Fe(II)]_0 \tag{6}$$

Multiple authors have performed oxidation experiments at different constant pH and oxygen partial pressures to confirm this general rate law [33-35].

As Davidson and Seed [33] discuss, in the range of pH investigated and reviewed (5.6-8.2), the rate constant k is highly sensitive to the precision of pH measurements such that values of k measured by different workers could effectively differ by up to a factor of 6 (based on a possible error in the absolute determination of pH of only ±0.2 units). Based on their review and own experimental results, Davidson and Seed provide the justification for a "universal" rate constant of $2\times10^{13}$ $M^{-2}$ $atm^{-1}$ $min^{-1}$ for pH range 6.5-7.4. It must be noted that their rate constant is the result of the evaluation of homogeneous systems.

It has been shown [36] and confirmed [34] that a decrease in oxidation rate can be attributed to the presence of some anions (rate constant k decreasing in the order $ClO_4^-$, $NO_3^-$, $Cl^-$, $H_3SiO_4^-$, $Br^-$, $I^-$, $SO_4^-$), which have a tendency to form complexes with ferrous iron. However, phosphate and fluorides were shown to have catalytic effects [36] and ferric iron (due to adsorption) had an autocatalytic effect on the rate constant [33-34, 37].

### 2.2.2.3 Rate of Oxidation at pH>7

At pH values above 7, the formation of ferric hydroxides as the oxidation of ferrous progresses, has an increasingly important heterogeneous catalytic effect [34]. This effect is incorporated in the rate law by the addition of a second rate constant, Equation (7):

$$-\frac{d[Fe(II)]}{dt} = (k_1 + k_2[Fe(III)])[\mathrm{Fe(II)}] \tag{7}$$

Where $k_1$ is the homogenous rate constant and $k_2$ is the heterogeneous rate constant (given in $M^{-1}$ $min^{-1}$). Furthermore, it was shown that $k_2 = k_s\,[O_2]K/[H^+]$ where $k_s$ is the surface rate in $M^{-1}$ $min^{-1}$, $[O_2]$ is the concentration of oxygen in solution and K is the adsorption constant of ferrous iron on ferric hydroxide. Further manipulation of Equation (7) by Sung and Morgan [34] revealed good agreement between predicted values and their experimental results along with data from other researchers [36].

Moreover, based on their "universal" rate constant (see Section 2.2.2.2), Davidson and Seed [33] calculated half-lives for ferrous iron at pH values of 6.5, 7.0, 7.5, 8.0 to be 361, 36, 3.6 and 0.36 minutes respectively at 20 °C. This demonstrates that beyond pH 7.5, ferrous oxidation and the ensuing autocatalysis is so rapid to the point where the rate of oxidation is limited by other factors such as the rate of oxygen mass transfer. The latter can be manipulated by gas flow rate, gas type, agitation speed and impeller type [38].

Tamura *et al.* [36] make a final remark concerning the oxygenation of ferrous ions at pH of 9 or higher. They observed a very fast reaction start, which slowed down considerably towards the end with the formation of magnetite ($Fe_3O_4$) and no further oxidation. This presents a situation where the reaction product has a negative impact of the reaction rate.

#### 2.2.2.4 Generalized View on Ferrous Oxidation Over a Wide Range of pH

Morgan and Lahav [39] attempted to generalize the oxidation kinetics of soluble ferrous iron in solution over a wide range of pH. In their review, the rate of oxidation of Fe(II) with $O_2$ was presented using log Fe(II) species-pH diagrams in order to correlate the rates of oxidation split into three distinct regions with regards to the species present. It was explained that hydrolyzed ferrous species, such as $Fe(OH)_2$ and $FeOH^+$, are more readily oxidized than $Fe^{2+}$ likely due to the efficiency of the $OH^-$ ligands to donate electron density towards the reduced metal ion thus facilitating its oxidation. Furthermore, the authors highlight the fact that once $Fe(OH)_2$ precipitates its oxidation depends only on the rate of introduction of the oxidant into the solution. As such, a rate constant separating the individual species that may be present at a given pH was proposed by Millero (8) [40].

$$\frac{-d[Fe^{2+}]}{dt} = \left(k_0[Fe^{2+}] + k_1[Fe(OH)^+] + k_2\left[Fe(OH)^0_{2(aq)}\right] + k_3[Fe(OH)_3^-]\right)C_{O_2(aq)} \qquad (8)$$

Based on this rate equation, Morgan and Lahav [39] graphically and logically explained the rationale behind the pH dependant region between ~5<pH<~8 that is flanked by two pH independent regions at pH<5 and pH>8. In short, below pH ~4, $Fe^{2+}$ cations dominate and are independent of the hydroxyl group hence the oxidation rate is pH independent. Above pH ~5, the concentrations of the $Fe(OH)_2$ and $FeOH^+$ species rise steeply and linearly with pH therefore establishing an oxidation rate that is pH dependant up to pH 8. In other words, the first two terms of Equation (8) are dropped giving rise to an oxidation rate that is second order with respect to $[OH^-]$. Finally, beyond pH 8, $FeOH^+$ and $Fe^{2+}$ concentrations drop significantly leaving $Fe(OH)_2$ as the dominant species. Since its concentration remains constant with respect to pH the rate of oxidation of ferrous iron reverts back to a pH independent region.

It is important to reiterate that the anions present in a solution tend to slow the rate of oxidation down due to the formation of complexes that are less favorable for oxidation compared to hydroxyl complexes [39]. This is the case when preparing Fe(II) solution from ferrous sulphate or ferrous chloride with the former one being relevant to the present study.

### 2.2.3 Products of Ferrous Iron Oxygenation

Randall *et al*. [41] highlighted the fact that air oxidation of precipitated intermediate ferrous compounds produces either lepidocrocite (γ-FeOOH) or magnetite ($Fe_3O_4$) depending on the rate and pH of oxidation. In particular, Misawa *et al.* [42] reported on the end products of the oxidation of dissolved ferrous iron (0.4 M) in neutral and slightly basic solutions (NaOH) at constant pH. Their results indicated that rapid aerial oxidation converted the intermediate products into γ-FeOOH and slow oxidation yielded $Fe_3O_4$. Similarly, Sung and Morgan [34] have characterized their oxidation products via infrared spectroscopy and X-ray diffraction to reveal that ultimately the product of oxidation was γ-FeOOH irrelevant of the type of media (e.g. $Cl^-$ or $SO_4^{2-}$). They conclude that in the long run lepidocrocite is unstable with respect to goethite but that the short term sorption behaviour is governed by the nature of this intermediate oxygenation product.

#### 2.2.3.1 Formation of Magnetite in Aqueous Solutions

Perez and Umetsu [43] were able to produce crystalline magnetite without the use of a high temperature process and time consuming post production treatment for better crystallinity. They proposed the oxidation of ferrous iron as means to remove metal ions from solution such as in acid mine drainage.

Upon fast addition of 0.4 M KOH base (10 mL/min) to the dissolved ferrous iron solution (0.012 M, pH=3), the pH rose to 11 and was maintained at that pH where a green rust II-type (GRII) compound precipitated. Simultaneously, air was sparged at a constant flow rate and oxidation took place as well as the transformation of the precipitates to magnetite. It was observed that the initial dark green precipitate (GRII) turned to a black one ($Fe_3O_4$) after 10 min contact time. Additional oxidation led this initially highly magnetic precipitate to change colour to dark brown with reduced magnetic responses. After 22 min of oxidation, the rate of protons released for pH adjustment became negligible and coincided with the end of oxidation or, in other words, the equilibrium condition between oxygen and the aqueous solution had been achieved.

### 2.2.3.2 Oxidation of Ferrous Hydroxide

Lin *et al.* [44] investigated the oxidation of ferrous hydroxide ([Fe(II)]=0.22 M) in a slightly basic 750 mL solution by sparging oxygen through a fritted-glass disk at a rate of 18.5 mL/min. An [Fe(II)] to [OH$^-$] molar ratio of 7:12 was selected yielding a white precipitate in suspension at pH equal to 8.2. At the onset of sparging, the white iron(II) hydroxide started to oxidize and changed color to green, then blue and ended as an orange-yellow slurry. Figure 3 shows a pH curve over time showing the evolution of pH (without pH adjustments) with ongoing oxidation from the onset of sparging at t=0.

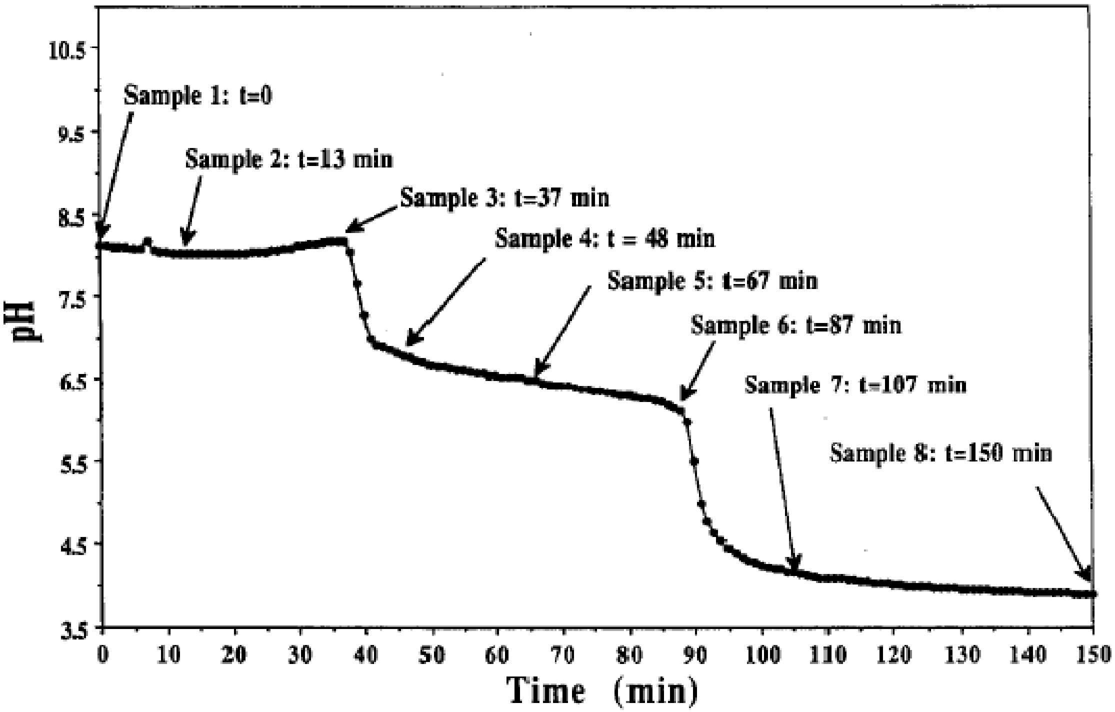

**Figure 3: Change in the pH of an Fe(OH)$_2$ solution undergoing oxidation over time (sample times are indicated) [44]**

Supporting XRD diffraction patterns of solids collected at each of the time intervals is shown in Figure 4.

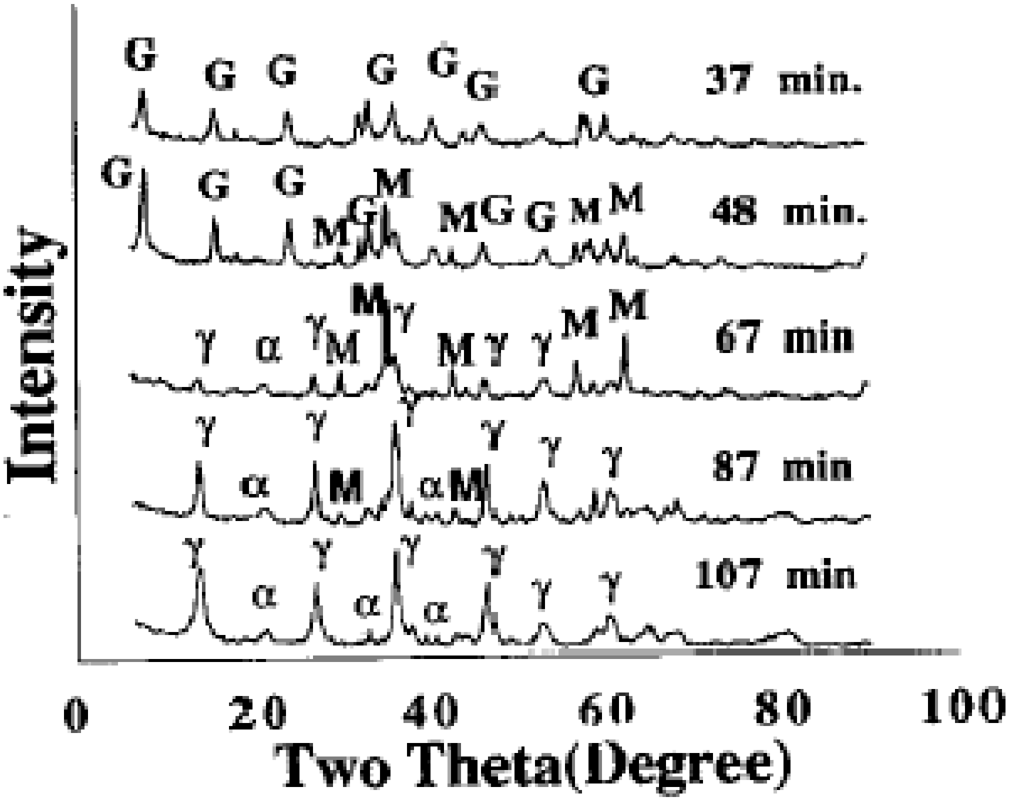

**Figure 4: X-ray diffraction pattern for samples withdrawn at times corresponding to those in Figure 3. The peaks are identified as: G, GRII; M, $Fe_3O_4$; α, α-FeOOH, and γ , γ-FeOOH [44]**

The authors show that oxidation of a slightly basic Fe(II) suspension from $FeSO_4$ media precipitates as a white, air sensitive $Fe(OH)_2$ solid. This precipitate suspension oxidizes to GRII at pH 8 during the first stage of oxidation of which the end is marked by a first pH drop (Figure 3). Green rust is said to form as Fe(II) oxidizes to Fe(III) and subsequently combines with Fe(II). This mixed-valence green complex, having a proposed empirical formula $[(Fe(II))_2(Fe(III))(OH^-)_4(O^{2-})]^+$, gets further oxidized at pH 6.2 to form $Fe_3O_4$ or y-FeOOH or mixture of both.

The rate of oxidation of Fe(II), or equally, the molar fraction of Fe(II) iron remaining in suspension over time (% Fe(II)) is plotted in Figure 5 and shows that there is a clearly constant rate of Fe(II) depletion during formation of GRII by the oxidation of iron(II) hydroxide (t=0-37 min) and continuing linear trend during GRII oxidation to ultimately form γ-FeOOH (t=37-107 min). The linearity of the plot suggests that either the reaction is zero order in terms of ferrous concentration or most likely that the reaction is controlled by oxygen mass transfer.

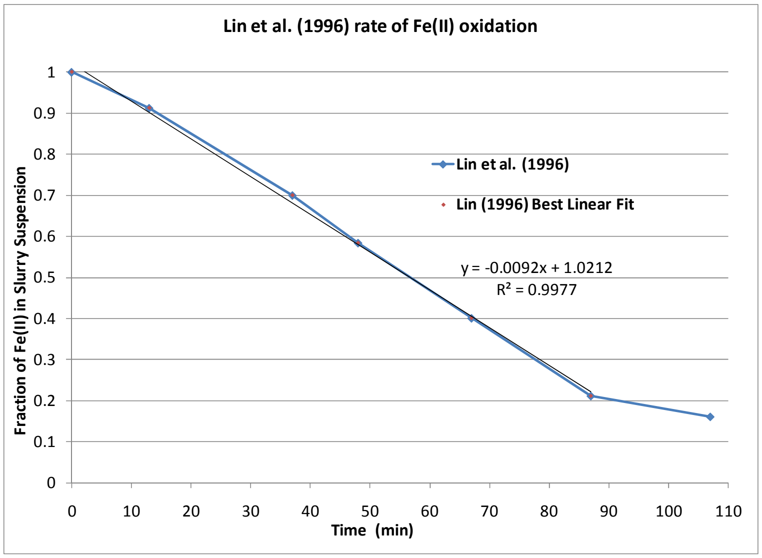

**Figure 5: Oxidation of Fe(II) slurry as a function of time with a drifting pH ([35])**

Finally it is worthy to mention the interesting work of Ruby *et al.* [45-46], who through measurements of ORP and pH were able to provide/monitor the pathway through the precipitation/oxidation/transformation of ferrous species to $Fe(OH)_2$ then to GRII and finally to FeOOH.

### 2.2.4 Effect of Fe(II) on As(V) Removal by Oxidation

Up to this point I have explored the oxidation behaviour of ferrous iron over a wide pH range and its subsequent conversion into various types of intermediate phases at constant or drifting pH. In this section, it is discussed how this relates to an arsenic removal system.

#### 2.2.4.1 The Effect of Fe(II) on As(V) Adsorption on Ferrihydrite

Reductive dissolution of iron, that is, the reduction of Fe(III) to Fe(II), is a mechanism by which arsenic associated with ferric iron may be released into the environment. Ferrous iron’s ability to inhibit bacterially driven dissimilatory iron reduction coupled with its ability to adsorb onto solid Fe(III) hydroxides possibly leading to a transformation of Fe(II) into a mixed iron phase prompted Mukiibi *et al.* [47] to investigate the effects of Fe(II) on adsorption of arsenate on the surface of amorphous ferric hydroxide (AFH or Ferrihydite). Firstly, they showed decreasing adsorption of arsenate on AFH in the absence of Fe(II) with increasing pH. At the same time they showed increasing uptake of Fe(II) onto AFH by adsorption in the absence of As(V) with increasing pH. Supported with adsorption isotherms, these results led them to conclude that sites available for $AsO_4^{3-}$ adsorption are not favorable for $Fe^{2+}$ adsorption. Next, the authors proved that at higher pH

(>7.5) part of the Fe(II) adsorbed irreversibly onto AFH either by simple chemisorption or through formation of a new phase at the surface. Another series of experiments was conducted in an attempt to see the effect of pre-equilibrating AFH with Fe(II) followed by addition of As(V) and vice-versa. According to the obtained results, the pre-adsorption of Fe(II) onto AFH was found to actually improve later arsenate adsorption. The same was observed for the opposite scenario and therefore Mukiibi *et al.* [47] suggested a cooperation between the two species upon sorption. Moreover, they observed a "darkening of the ferrihydrite to a blacker, more magnetite-like color" indicating the formation of a mixed iron oxide phase. Unfortunately no solids characterization was conducted to further verify this observation.

Similarly, De Klerk [8] investigated the 2-stage CCPTN of arsenic with added nickel (Fe/As=4, Ni/As=0.5). The results indicated that $Ni^{2+}$ does not compete for adsorption sites on ferrihydrite and suggested that there is a likely interaction of nickel with either ferric arsenate or ferrihydrite in the form of surface complexes creating a stabilizing effect against dissolution. Furthermore, constant pH 8 ageing data revealed the slow uptake of nickel by the coprecipitates thought to correspond to surface precipitation after initial complexation. Jia and Demopoulos [24] gathered analogous results for batch coprecipitation including nickel (Fe/As=4, Ni/As=1, pH=8) also indicating an enhanced uptake of As(V) and Ni itself with the formation of a nickel arsenate surface precipitate.

### 2.2.4.2 Adsorption of As(III,V) on Green Rust Intermediate Compounds

As previously mentioned in Section 2.2.3, with the presence of an oxidizing agent such as oxygen, ferrous hydroxide could partially oxidize and form a known intermediate mixed-valent iron(II,III) hydroxide with layered structure known as green rust. This compound has the general formula $Fe_y^{(II)}Fe_x^{(III)}(OH)_{3x+2y-2z}(SO_4)_z$ and consists of sheets of $Fe(II)OH_6$ where Fe(III) replaces some of the Fe(II) resulting in a positive layer charge [41]. That positive charge is countered by the inclusion of anions such as $Cl^-$ or $SO_4^{2-}$ and $CO_3^{2-}$ between the layers giving these green rusts their specific names GRI($Cl^-$), GRII($SO_4^{2-}$) and GRII($CO_3^{2-}$) respectively.

Green rust is known to be unstable in an oxidizing environment but its existence isn't ruled out in naturally occurring mildly reducing environments. Regardless, this compound is of interest for it is presumably prevalent at pH 8-8.2, which is the discharge pH in certain industrial As(V)-Fe(II,III) coprecipitation circuits as those employed by the U-milling industry in Northern

Saskatchewan. Unfortunately the literature available on the topic of adsorption of arsenic(V) onto green rust is limited and occasionally contradictory so the following presented discussion is considered rather tentative.

Jönsson and Sherman [48] conducted several experiments to investigate the adsorption of As(III) and As(V) onto secondary Fe(II) or mixed Fe(II)/Fe(III) phases such as siderite ($FeCO_3$), fougerite (carbonate green rust $[Fe(II)_4Fe(III)_2(OH)_{12}][CO_3CO_3{\cdot}2H_2O]$) and magnetite ($Fe_3O_4$) to explain the release of arsenic, when reductive dissolution of iron(III) hydroxides under anoxic conditions occurs. Their hypothesis was that if the adsorption of As(V) on these precipitates were weaker than that on original iron(III) hydroxides, the arsenic release into solution could be accounted for. According to the generated data, As(V) was found to adsorb strongly onto GR at pH<8 through a surface inner-sphere complex having a maximum arsenic sorption capacity of >3300 μmol $g^{-1}$. Compared to the adsorption capacity for sulphate and/or chloride, GR reported to be >1000 μmol $g^{-1}$ for arsenate at pH 7 [49], the authors attributed their higher sorption results to the formation of symplesite ($Fe(II)_3(AsO_4)_2{\cdot}8H_2O$) as a surface precipitate or through transformation of fougerite. Similar results were found for magnetite, where adsorption for As(V) was highest at pH<8. Normalization of the data for arsenic adsorption per gram of solid showed better performance for magnetite vs. fougerite. Moreover, Jönsson and Sherman reported the formation of symplesite as a pale blue-green coating onto black magnetite (confirmed by XRD) with increasing arsenate loading (As/Fe=0.55).

Refait *et al.* [50] investigated the effect of As(V) adsorption onto GRI($Cl^-$) and its effect on the subsequent transformation, growth and crystallinity of GRI into final Fe(III) compounds. Their experiments involved the oxidation of solutions containing 0.12 M Fe(II) and As(V) at different molar ratios (Fe/As=24, 12 and 4.8) through exposure to air by vigorous agitation. No pH adjustments were made. At lower arsenate concentrations (Fe/As=12, 24) two reaction stages are present as determined by ORP monitoring, suggesting the completion of $Fe(OH)_2$ oxidation into GRI($Cl^-$) at the first inflection point and the end of the latter intermediate product's oxidation at the second inflection point as seen in Figure 6. This is however not seen at the highest As(V) concentration (Fe/As=4.8), where formation of the intermediate product, GRI($Cl^-$), seems to have been inhibited. The authors also report a decrease in pH from ~8.5 down to 4.5-5 for lower arsenic concentrations and 5.9 for the highest [As]. Such pH drops have also been observed during other oxidation experiments not containing arsenic [44].

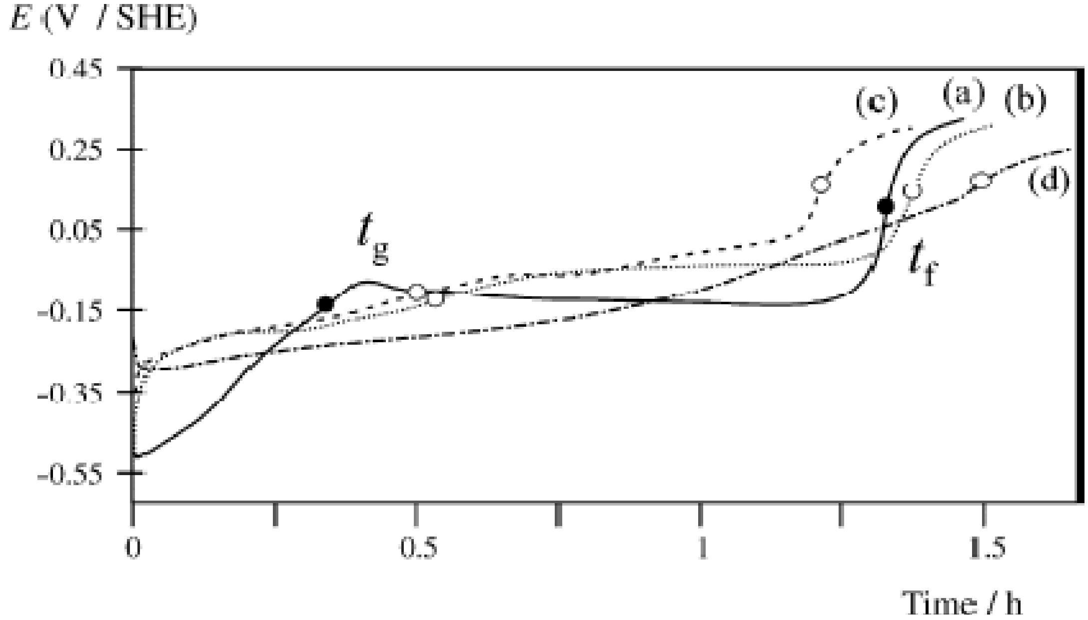

**Figure 6: Evolution with time of the potential during the oxidation of the Fe(II) compound precipitated from $FeCl_2 \cdot 4H_2O$, NaOH and $Na_2HAsO_4$: (a) curve obtained without $Na_2HAsO_4$, (b) curve obtained for Fe/As=24 (c) Fe/As= 12 and (d) Fe/As= 4.8 [50]**

The intermediate products were characterized at the end of the first oxidation stage ($t_g$ in Figure 6) and the final products were shown to have differences as confirmed by XRD, micro-Raman spectroscopy and FTIR. Table 1 summarizes the phases present for each experiment as characterized by the three techniques.

It was concluded that arsenates inhibited the growth and crystallization of GRI leading to a nano-crystalline or “amorphous” Fe(II-III) intermediate compound similar to GR [50]. It is proposed that this nano-crystalline product is formed as arsenate adsorbed onto clusters of $Fe(OH)_6$ octahedra thereby preventing them to form brucite-like sheets as seen in regular GR. Instead, these clusters aggregate trapping the anions and arsenate. Moreover, with increasing arsenate concentration, the final products changed from lepidocrocite to mixtures of ferrihydrite and feroxyhite to amorphous Fe(III) oxyhydroxides. It was also found that no reduction of As(V) to As(III) occurred.

**Table 1: Summary of the intermediate and final phases of oxidation of Fe(II) compounds precipitated from $FeCl_2$-$AsO_4$ solutions at Fe/As molar ratios equal to 24, 12 and 4.8 (Data taken from [50])**

| **Sample** | **Intermediate Products** | | **Final Products** | | |
|---|---|---|---|---|---|
| | **XRD*** | **Raman** | **XRD** | **Raman** | **FTIR** |
| No As added | N/A | Bands at 430 and 500 cm$^{-1}$ →**GRI(Cl$^-$)**<br>Bands at 238, 325 & 363 cm$^{-1}$ → **GRI(Cl$^-$)** | **γ-FeOOH** (Lepidocrocite) | **γ-FeOOH** (Lepidocrocite) | N/A |
| [As]=0.05 mol L$^{-1}$<br>Fe/As=24 | Most diffraction lines of **GRI(Cl$^-$)** are seen.<br>They are sharp and suggest a crystalline compound | Broader bands at 430 and 500 cm$^{-1}$ →**GRI(Cl$^-$)**<br>Bands at 250 and 384 cm$^{-1}$ → **γ-FeOOH** | γ-FeOOH + FeOOH (Ferrihydrite) OR δ-FeOOH (Feroxyhite) | N/A | N/A |
| [As]=0.01 mol L$^{-1}$<br>Fe/As=12 | **GRI(Cl$^-$)**<br>Diffraction lines more difficult to see | Broader bands at 430 and 500 cm$^{-1}$ →**GRI(Cl$^-$)**<br>Smaller bands for GRI disappear →**GR modified by arsenate** | **δ-FeOOH** + “6-line” FeOOH + γ-FeOOH | Typical **δ-FeOOH OR FeOOH** + peak for γ-FeOOH<br>As-O stretching mode at 840 cm$^{-1}$ | Broad O-H bands at 3370 cm$^{-1}$ typical of **FeOOH** + water O-H bending mode peak at 1625 cm$^{-1}$ + **$AsO_4^{3-}$** As-O stretching band at 800 cm$^{-1}$ |
| [As]=0.025 mol L$^{-1}$<br>Fe/As=4.8 | One broad hump between 20-60° 2θ → **amorphous** nanocrystalline compound | Broader bands at 430 and 500 cm$^{-1}$ →**GRI(Cl$^-$)**<br>**New bands** at 196, 280, 677 and 350 cm$^{-1}$ | **δ-FeOOH** | Shift in 2nd broad band towards left + shoulder at 320 cm$^{-1}$ suggests more **δ-FeOOH**<br>More intense **As-O mode** at 850 cm$^{-1}$ | **As-O** stretching region (~800 cm$^{-1}$) shows more intense peak than for [As]=0.01 mol L$^{-1}$. |

*Fe(II-III) intermediate compounds were not modified by ageing or oxidized after 15 days

Randall *et al.* [41] conducted a detailed study on the mechanism of As(V) adsorption on sulphate green rust (GRII($SO_4^{-2}$)) and its fate during oxidation at a constant pH of 7 (NaOH base used). Two modes of arsenic adsorption were considered namely one by addition of arsenic to pre-prepared GRII (As-GR) and the other by coprecipitation of As(V) and Fe(II) (As-GRCO), where both reactions were left to equilibrate for ~20 hours. In addition, for the sake of comparison, an experiment involving the adsorption of As(V) onto lepidocrocite (As-LEPID) was also conducted. The respective Fe/As molar ratios of these experiments were calculated by the present author to be 282 for As-GR and As-GRCO and 272 for As-LEPID (lepidocrocite molecular formula estimated as $FeOOH{\cdot}0.162H_2O$ based on Majzlan *et al.* [51]).

The results showed that As(V) adsorbs onto lepidocrocite as $(AsO_4)^{3-}$ through inner sphere complexes in a bidentate double-corner sharing arrangement. No evidence was found for single-edge sharing and monodentate complexes of $(AsO_4)^{3-}$. As(V) adsorption over the course of both reaction routes was very similar, where [As] were very low for the first 3-4 hours and subsequently dropped below detection limits. The authors reported that GR does not reduce As(V) to As(III) based on adsorption observations and conclusive EXAFS evidence.

XRD results (Figure 7) were similar for both cases where green rust peaks that were initially identifiable gradually disappeared after 6 hours. Characteristic lepidocrocite peaks began to show after ~4 hours and gradually became sharper suggesting an increase in crystallinity. However, their intensities are supposedly three times less than those recorded for a pure lepidocrocite XRD standard suggesting that the adsorption of As(V) hinders the process of crystallization. In the case of coprecipitation of As(V) with GRII, the GR peaks become more intense and hence GRII becomes more crystalline as it ages.

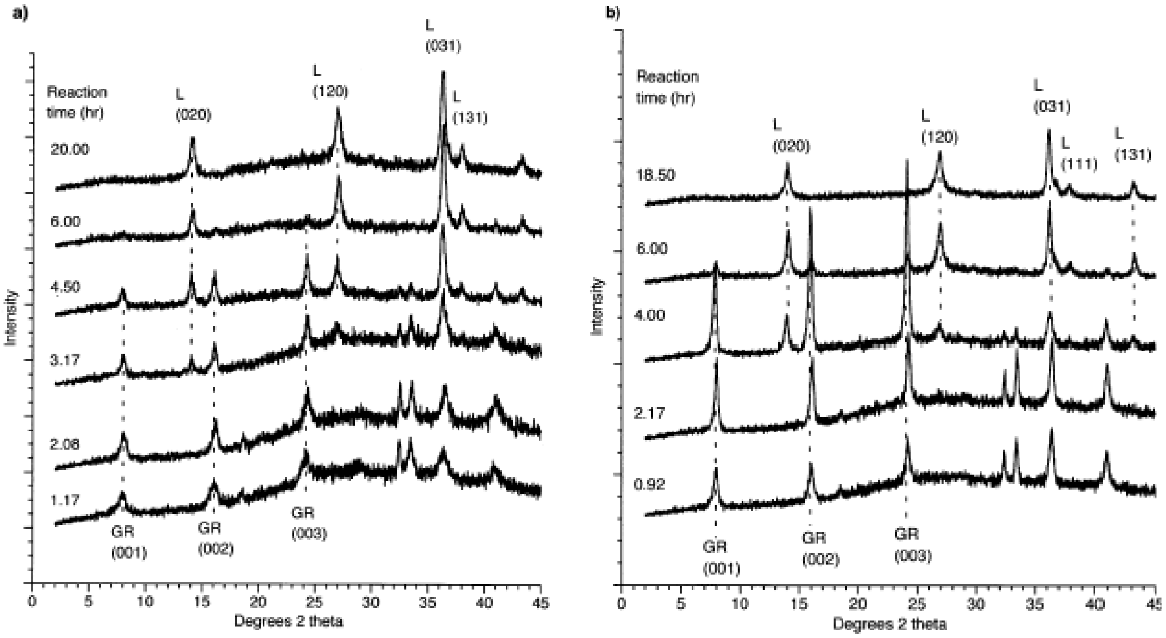

**Figure 7: (a) XRD results from the progressive oxidation of GR with adsorbed As(V) ('As-GR') to lepidocrocite at pH 7 (b) XRD results from the progressive oxidation at pH 7 of GR that was nucleated in the presence of As(V) ('As-GRCO') [41]**

Adsorption of arsenate onto GR during coprecipitation or adsorption onto pre-precipitated GR was shown to occur via single edge and double corner adsorption on Fe(II)$O_6$ octahedra (Figure 8). EXAFS results strongly suggested that As(V) remained adsorbed as surface complexes throughout the formation and oxidation of GRII. It was proven that As(V) would only adsorb on GRII even in the presence of lepidocrocite and that only once all of the GR was oxidized, As(V) would adsorb onto lepidocrocite through bidentate double corner sharing as seen in Figure 9. Moreover, the coordination environment observed for the final products of experiments As-GR and As-GRCO were identical to those of As-LEPID.

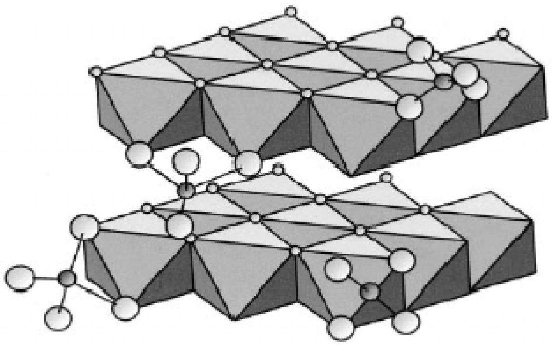

**Figure 8: Proposed inner-sphere surface complexes of $(AsO_4)^{3-}$ on GR showing both edge-sharing (1 Fe neighbor) and corner-sharing (2 Fe neighbors) arrangements [41]**

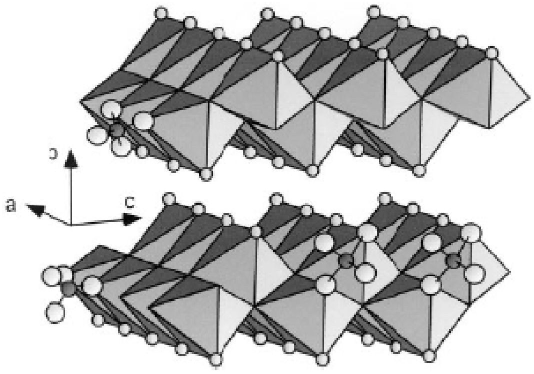

**Figure 9: Inferred inner sphere complexes of $(AsO_4)^{3-}$ on lepidocrocite based on EXAFS results [41]**

The authors concluded that arsenic is not reduced to arsenite by GR, that it adsorbs onto GR as surface complexes, that it is not incorporated into the GR bulk structure, and finally, that it does not exchange for negative sulphate anions present between the sheets of $Fe(II)(OH)_6$ for charge balance. The last two points differ from the findings of Refait *et al.* [50] as described above where aggregates of nano-crystalline GRI clusters incorporated arsenate anions. It must be noted however, that there were some substantial differences between the two research publications, notably the use of different ferrous salts ($FeCl_2$ vs. $FeSO_4$), a lower Fe/As molar (< 24), and a drifting pH vs. a constant pH during oxidation, which may have had an additional impact on the GR transformation. Nonetheless both research groups observed an impaired crystallization of the final products due to arsenate and that it did not reduce to the more toxic and mobile species arsenite.

Lin and Puls [49] carried out research on the possible remediation of arsenic (As(III) and As(V)) in contaminated soils and groundwater through natural attenuation (adsorption, desorption, reduction, oxidation, coprecipitation and dissolution of various iron hydroxides, clay minerals and feldspars) including the adsorption of arsenic on GR. Their rationale to investigate arsenic adsorption onto GR was based on evidence that green rust occurs naturally in soils and aquatic sediments. It is apparent that GR can be present in a reducing environment but will not persist in an oxidizing environment.

Table 2 contains the results of As(V) adsorption and desorption tests (competitive ligand exchange with $H_2PO_4^{1-}$ and $HPO_4^{2-}$ for 48 hrs) as well as the percent As(V) reduced to As(III) by three selected iron hydroxides, namely green rust, ,goethite and lepidocrocite. Clearly, GR performs equally if not better than both other iron hydroxides in terms of As(V) adsorption and desorption. GR, however, reduced ~5 % of the adsorbed arsenate into arsenite. Interestingly enough GR was found to oxidize As(III) to As(V) by ~75 % (data not shown) when using arsenite as the starting source of arsenic.

**Table 2: Arsenic adsorption, desorption and reduction by iron hydroxides [49]**

| | **As(V) adsorption** | **As(V) desorption** | **Reduction of As(V) on iron hydroxides** |
|---|---|---|---|
| ***Iron Hydroxides*** | % | % | % |
| Green Rust | 99.42 | 6.74 | 4.28 |
| Goethite | 99.10 | 7.04 | 2.97 |
| Lepidocrocite | 97.99 | 15.27 | 1.21 |

Lin and Puls [49] showed that by allowing GR to react with arsenic in reducing condition for prolonged time, GR transformed to parasymplesite [$Fe(II)_3(AsO_4)_2\cdot 8H_2O$]. They also managed to produce the mineral parasymplesite by introducing 200 mL of a 3 mM mixture of As(V) and As(III) to 200 mg of GR in a glove box for three months (back calculated Fe/As molar ratio of 1.7).

The review of the preceding research illustrates that GR and parasymplesite may play an important role in the control of arsenic mobility in intermediate oxidizing/reducing environments. Both phases were capable of removing arsenic from solution and hence must be taken into consideration as potential remediation mechanisms for dissolved arsenic in oxygen-depleted subsurface aqueous processes.

Finally it is worth mentioning the interesting work of Ruby *et al.*, who through measurements of ORP and pH were able to provide/monitor the pathway through the precipitation/oxidation/transformation of ferrous species to $Fe(OH)_2$ then to GRII and finally to FeOOH.

### 2.2.5 Ferrous Arsenate and its Solubility

It is well established that soluble As(V) can be controlled by coprecipitation with ferric iron via the formation of arsenic bearing phases such as ferric arsenate along with the adsorption of arsenate onto the highly reactive surface of ferric oxyhydroxides [22, 24, 31, 52]. Now begs the questions; what would occur if a slightly alkaline reducing environment was to contain significant amounts of ferrous iron and arsenate? Would we precipitate the respective ferrous arsenate? What are the specific conditions needed for such a phase to precipitate, remain stable and ultimately attribute to the removal of As(V)? The purpose of the following section is to answer some of these questions and introduce symplesite as a possible sink for arsenate [53].

In 2007, Johnston and Singer [54] mentioned that high levels of dissolved arsenic in reducing groundwaters are present due to the dissolution of iron oxides. An inconsistency exists, however, whereby the iron levels are not as high as anticipated from complete dissolution of Fe(III) oxides. It is suggested that a portion of the missing Fe(II) is either reoxidized or incorporated in Fe(II) phases such as ferrous sulfide, pyrite, siderite, green rust or vivianite [$Fe(II)_3(PO_4)_2 \cdot 8H_2O$]. With respect to the latter option, it is therefore conceivable that the arsenate analogue of vivianite, known as symplesite [$Fe(II)_3(AsO_4)_2 \cdot 8H_2O$], may form under particular conditions.

Johnston and Singer experimentally established a new solubility constant for symplesite, $pK_{SO}$, equal to 33.25. Moreover, they used geochemical modeling (PHREEQC-2) with geochemical data from Bangladesh and their new constant to suggest that some of the groundwaters are oversaturated with ferrous arsenate. Furthermore, the authors proposed a number of other environments in which symplesite could be precipitated to remove As(V) and remain stable such as in highly alkaline lakes and groundwaters. Finally, it was suggested that precipitation of symplesite in alkaline groundwater by addition of Fe(II) could replace conventional coprecipitation and adsorption of arsenate using Fe(III) that requires pH reduction.

Babechuk *et al.* [55] investigated the stability of the ferrous arsenate mineral, symplesite, in a reducing environment while in contact with an arsenate reducing bacterium (DAsRB). Their main goal was to elucidate the mechanism by which DAsRB can reduce and liberate aqueous species such as arsenite from stable ferrous arsenate. Their findings confirmed an initial release of reduced arsenite by up to 9.8 % of total available arsenic from ferrous arsenate and similar release of Fe(II) corresponding to 11.8 %. This release conforms to the peak in active bacterial biomass production used to quantify bacterial growth. Final sampling showed a slight drop in total arsenite release as well as a decrease in soluble Fe(II) and suggested the onset of a removal mechanism. The proposed mechanism was that of the precipitation of ferrous arsenite mineral onto organic exudates, which provided a new surface for sorption and precipitation. This observation was supported by SEM and TEM imaging and as well with X-ray absorption spectroscopy (XANES and EXAFS).

### 2.2.6 Industrial Considerations

As briefly mentioned in Section 2.2.2.3, the rate of oxidation of ferrous iron is subjected to the limitations of gas-liquid mass transfer kinetics and more specifically, mass transfer coefficients. The latter is considered as a measure of the rate of mass transfer. This coefficient becomes imperative in the design of the process to ensure the reaction occurs efficiently. It determines the size of the equipment, the speed of the agitation, the required gas flow rate and so on. Ultimately, the mass transfer coefficient is directly related to the power consumption and therefore the cost of the operation all together [56].

Less important for this thesis but crucial in the industry is the power consumption in continuous co-precipitation neutralization circuits for the mixing of slurries from the tailings and raffinate solution containing a significant solids fraction. Formerly, tanks where outfitted with gas sparging devices to decrease the power consumption due to agitation [38] and unfortunately not intended for the in situ oxidation of ferrous containing waste waters [57].

## *2.3 Summary*

This first part of this chapter gave an overview of the widely applied arsenic removal process in the industry known as coprecipitation. The effects of process parameters on production and stability of coprecipitates, such as Fe(III)/As(V) molar ratio, type of base, batch vs. continuous operation, and staging were discussed and the nature of the Fe(III)-As(V) coprecipitate was shown to consist of ferric arsenate and arsenical ferrihydrite.

In the second part of the review, the rate of oxidation of ferrous iron with oxygen over a wide range of pH was examined followed by a review of results from research involving the oxidation of ferrous hydroxide after an initial pH near or above 8 was reached. At this pH, it was shown that an intermediate phase known as green rust (GR) forms that further oxidizes at constant rate indicative of gas-liquid mass transfer control. Depending on the rate of oxidation, influenced by gas flow rate, different final products can be achieved ranging from magnetite to lepidocrocite. Arsenic(V) was found to adsorb onto the intermediate compound (GR) through inner-sphere complexes as long as the intermediate phase was still present, after which As(V) was picked up by ferric oxyhydroxides. During oxidation of ferrous containing phases, arsenic was found to limit the crystallinity of the final oxidation products and it was generally not reduced to its more toxic species arsenite.

# 3 Experimental Methods

This section contains standard information on the experimental work conducted throughout this thesis such as the chemicals used, the procedures and characterizations methods.

## 3.1 Chemicals

The chemicals, their grades and additional information, used throughout the course of the research are listed in Table 3. All solutions were prepared with deionized water, which was produced with the use of a Biolab 2200 reverse osmosis system.

**Table 3: List of chemicals used**

| Type | Chemical name | Formula | Assay/Grade | Supplier |
|---|---|---|---|---|
| **Salts** | Iron(III) sulphate hydrate | $Fe_2(SO_4)_3 \cdot xH_2O$ | 21.6 % Fe(III)/ 97 % | Sigma-Aldrich |
| | Iron(II) sulphate heptahydrate | $FeSO_4 \cdot 7H_2O$ | 20.1 % Fe(II)/ ReagentPlus®, ≥99 % | Sigma-Aldrich |
| | Manganous Sulphate | $MnSO_4 \cdot H_2O$ | ACS | Fisher Chemical |
| **Oxides** | Arsenic(V) oxide hydrate | $As_2O_5 \cdot xH_2O$ | 53-61 % As(V) | Sigma-Aldrich |
| | Calcium Oxide Powder | $CaO$ | Technical | Fisher Chemical |
| **Acids** | Hydrochloric Acid | $HCl$ | 36.5-38 % / Reagent ACS | Fisher Chemical |
| | Nitric Acid | $HNO_3$ | TraceMetal Grade | Fisher Chemical |
| | Sulphuric Acid | $H_2SO_4$ | 95-98 % / ACS-Pur | Fisher Chemical |
| | O-Phosphoric Acid | $H_3PO_4$ | 85 % / Certified ACS | Fisher Chemical |
| **Bases** | Sodium Hydroxide | $NaOH$ | 50 % w/w Certified | Fisher Chemical |
| **Titrant** | Potassium Dichromate | $K_2Cr_2O_7$ | N/10 ACS/EP/USP | Ricca Chemical |
| **Indicator** | Diphenylamine Sulfonic Acid Sodium Slat | $C_6H_5NHC_6H_4$-4-$SO_3Na$ | ACS | Fisher Chemical |

## 3.2 Continuous Coprecipitation (CCPTN)

The continuous circuit used to investigate the removal of As(V) in simulated acidic waste solution by coprecipitation with iron sulphate and lime neutralization was previously built and described by De Klerk [8]. De Klerk's research has shown that for most effective As(V) removal and retention during ageing, a two-reactor configuration, where the first reactor is set to a pH of four and the second maintained at a pH of eight, is preferred. As a result, the 2-stage circuit shown in Figure 10 was selected to perform all subsequent CCPTN tests.

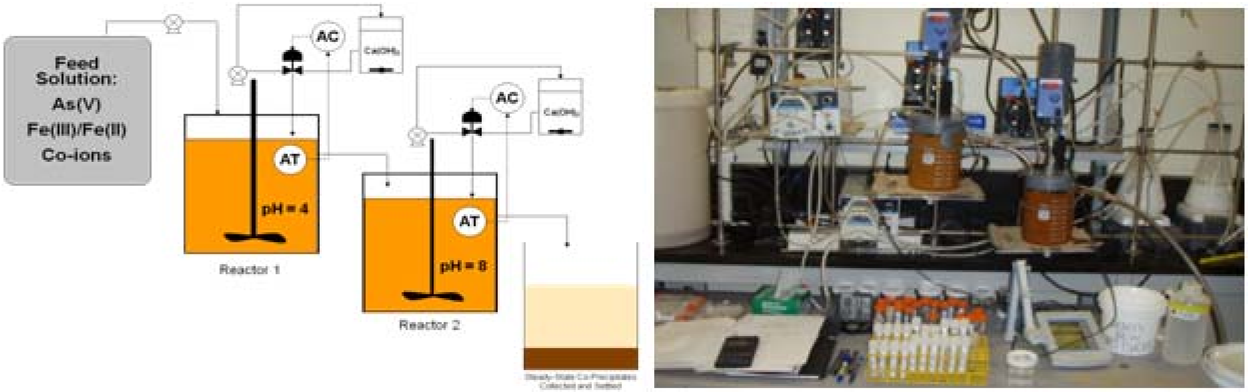

**Figure 10: Schematic and actual appearance of a 2-stage continuous coprecipitation reactor set-up**

This section presents a rundown of most aspects involved in operating a CCPTN test. It begins with a summary of the type of equipment used followed by the solution and reactor preparation steps. After that the start-up of the circuit and the post production procedure is described.

### 3.2.1 Continuous Coprecipitation Equipment

The CCPTN circuit, as depicted schematically in Figure 10, consists of the following equipment:

**Table 4: List of equipment for the CCPTN circuit**

| Equipment | Description |
|---|---|
| Masterflex variable speed peristaltic pumps A) and B) | A) Feeds simulated effluent into Reactor 1 at constant rate of 27.5mL/min<br>B) Circulates base circuits for Reactors 1 & 2 |
| Reactors | 2 x 2L glass beakers customized with discharge spouts (h=13.5cm, d=12.6cm, V=1650mL) furnished with CPVC 4-walled baffles (h=14.5cm, w=1.0cm, t=3mm) |
| Agitators | 2 x IKA RW20 overhead mixer equipped with Lightning A310 impeller (3 blade pitched, d=6.3cm) |
| Base circuit | 2 x 2L Erlenmeyerkolben flasks with magnetic stirring sealed with rubber plug adapted with circuit tubing |
| Base pump and controller | Etatron DLX/B pH (diaphragm positive displacement) unit with an industrial self-cleaning Cole-Parmer pH electrode (2-point calibration) |
| pH and ORP data logger | Consort Multichannel R305 Controller with Cole-Parmer pH electrode and Accumet Platinum Ag/AgCl ORP combination electrode. Data logging software pyConsort |
| Flow controllers | Matheson flow controller Model 3270 with mass flow transducer |

The equipment assembly is secured onto a wall grid and has been upgraded and maintained to a consistent and high standard over the course of this work.

*Data Logging Software pyConsort:*

In an attempt to accurately monitor the pH and ORP of hydrolysis, oxidation and precipitation experiments, electrodes with BNC connectors were wired into two controllers units (Consort R305) along with an RS-232 serial port cable. Philippe Tétreault-Pinard wrote the software called "pyConsort" using the programming language Python (version 2.5), which enables the computer to communicate with the controllers and acquire data. In addition, a graphical user interface (GUI) with timer and time display that allows the user to easily start/stop recording data from two Consort R305's with two channels of data was designed. The data are automatically saved in a user defined and located CSV file and are graphically displayed live as they are being acquired. The open source code for this software is available in Appendix Section 8.7 along with a screen shot.

### 3.2.2 Feed Solution Preparation

Feed solutions were prepared from separate arsenic and iron stock solutions by dissolving 100 g of reagent grade arsenic pentoxide (Sigma-Aldrich) and 500 g reagent grade ferrous- and/or ferric sulphate (Sigma-Aldrich) into four liters deionized water respectively. To prevent premature iron hydrolysis, 86 g of reagent grade sulphuric acid (98 %, Fisher Scientific) was added per 500 g of iron-sulphate media. The stock solutions were analyzed for total iron and total arsenic concentration using ICP-OES. Ferrous concentration was determined using a modified potassium dichromate titration procedure (See Section 3.4.3). Based on the results obtained, calculated volumes of stock solutions were diluted with deionized water to predetermined feed volumes. The subsequent final feed solution was analyzed for As(V) and total Fe using ICP-OES and ferrous concentration by titration.

### 3.2.3 Reactor Preparation and Start-up

The circuit preparation was initiated once all equipment was thoroughly cleaned. See the sub-headings for detailed accounts on separate circuit sections.

*Reactors:* Reactors were filled with DI water and pH adjusted to 1.5 using 0.5 M $H_2SO_4$. Next, baffles were inserted and fastened and the impellers were centered and positioned 2 cm above the bottom of the reactors. Lastly all pH & ORP electrodes were calibrated and mounted on the air tight lids and any additional holes were plugged. Agitators were set to 1000 rpm.

*Base addition:* Calculated amounts of CaO powder were added and dissolved into two 2.0 L flaks with DI water to create 1 M $Ca(OH)_2$. The alkaline solutions were magnetically stirred and continuously pumped in a circuit connected to the base controllers. The latter were calibrated and their pH set points adjusted to pH 4 and 8 for Reactors 1 & 2 respectively.

*Data Logging:* After all electrodes were calibrated and mounted in the reactors, the pyConsort software was opened and new filename was created.

*Feed pump:* The feed solution peristaltic pump rate was adjusted using a 250 mL graduated cylinder until the flow rate was as close as possible to 27.5 mL/min. This flow rate was chosen to provide a fixed mean retention time ($\tau$) of 60 minutes per reactor.

Once all circuit sections appeared ready for launching, a final review of a checklist is made and any last minute anomalies were corrected. Finally, both the stopwatch and data logging software were started, and simultaneously the feed began to pump into Reactor 1. For the first 6.5 hours ($6.5\tau$) unsteady state solids were collected at the exit of Reactor 2. The attainment of steady-state was validated previously by De Klerk [8]. Beyond 6.5 $\tau$, steady state (SS) solids were collected in a separate bucket. During the course of SS operation, each reactor was regularly sampled to monitor residual arsenic and co-ion concentrations. The sample manipulation was conducted as described in Section 3.4.1.

As mentioned above, the ORP and pH in each reactor was monitored and it was observed that the pH never fluctuated by more than ± 0.5 pH units when using slaked lime for neutralization.

### 3.2.4 Post-Production Handling and Accelerated Ageing

The steady state coprecipitates were left to settle in the collection bucket and sealed. Pre-ageing of production products at room temperature began at this point and continued as is with periodic sampling for a duration of 12 weeks post production. Subsequently, the samples were manipulated and stored as described ahead.

Following pre-ageing, the steady state (SS) products were re-suspended into a slurry with a large impeller and siphoned into a 4 L graduated cylinder. The solids were left to settle for 24 hours after which half of the volume of liquid over of the settled solids was removed resulting in an approximate solid/liquid ratio of 1/25. The remaining solids and solution were mixed and three equal parts of slurry (~750 mL) were transferred into HDPP Nalgene wide mouth bottles. Bottles marked with "A" were shelved at ambient temperature (~22 °C) whereas bottles marked "B" and "C" were placed into 40 °C and 70 °C temperature controlled baths respectively to simulate accelerated ageing.

## 3.3 Batch Experiments

A significant number of tests were conducted using a single closed reactor in batch mode. All tests of this sort were designated as batch experiments. The two main types of batch experiments conducted were hydrolysis and oxidation batch experiments.

### 3.3.1 Hydrolysis

The starting solution was prepared by weighing out calculated amounts of ferrous and/or ferric sulphate media dissolved in 1.5 L of pH adjusted DI water (unless otherwise stated, pH≈1.5, $H_2SO_4$ or HCl) into a 2 L beaker with baffles to achieve the desired total iron concentration of 74.74 mmol/L (4174 mg/L). When applicable, a calculated amount of $As_2O_5$ was fully dissolved overnight in a 100 mL volumetric flask placed in a heated ultrasonic bath. This solution was later added to the Fe(II) solution in the reactor prior to base addition. Separately, a 0.5 M $Ca(OH)_2$ base solution (unless otherwise stated) was prepared by dissolving CaO powder in DI water. Subsequently, the impeller and calibrated pH and ORP electrodes were submerged into the reactor and held into place through corresponding openings in the reactor lid. The impeller was inserted in the agitator (500 rpm) and the whole assemblage was secured to the laboratory wall grid. Base was then added as described in each specific section along with the generated results.

### 3.3.2 Oxidation

These experiments involved the use of different types of impellers, gases, agitation speeds and pH set points in a reactor containing identical starting solutions (Table 12 in Section 6). Solutions were prepared in a 2 L reactor by dissolving calculated amounts of ferrous sulphate in 1650 mL DI water to yield an iron concentration of 74.74 mmol/L (4174 mg/L) and, in later experiments, the addition of dissolved $As_2O_5$ to yield an Fe/As molar ratio of 4 and 1.65 for pH 8 Oxidation Experiments OEAs-1 and 2 respectively. The reactor was equipped with baffles, calibrated pH and ORP electrodes as well as a base pump and controller when applicable. A gas tank was connected to a gas flow controller (Matheson Model 3270), which supplied a constant regulated flow of gas (air or pure oxygen) to the reactor via a tube attached to a simple L-shaped aluminum rod with a 2 mm aperture positioned directly underneath the impeller and fixed firmly onto the reactor's lid through a rubber plug.

The starting pH of the solution was approximately 1.5 unless otherwise noted. Base was added automatically using the pH controller with a pH set point of 8 and was added as either 0.5 M $Ca(OH)_2$ or 0.5 M NaOH (OE8-9, OEAs-1) and in one case 1 M NaOH (OEAs-2). In the case of experiments OEAs-1 & 2, NaOH was added at a constant flow rate up to pH 8 before being manually added to maintain that pH for a duration of one hour as well as during oxidation at constant pH 8.

When applicable, the pH of the solution was ramped up to pH 8 within 20 minutes before the onset of oxidation by gas sparging. After the targeted pH was achieved the gas flow controller was switched on such that oxidation could commence. During that time, automatic base addition continued to maintain the select pH set point. For drift oxidation experiments OEDrift-1 & 2, ten minutes after addition of ferrous sulphate, a calculated amount of NaOH base ($[Fe(II)]/[OH^-] = 0.58$) was added to solution at once thereby immediately increasing the pH to 8.6 and 8.4 respectively. The pH adjusted solution was left to equilibrate for an additional 10 minutes prior to the onset of air sparging where no further pH adjustments were made.

## 3.4 Analysis and Characterization Methods

In this thesis, solid samples produced by the addition of calcium hydroxide base ($Ca(OH)_2$) to iron sulphate media ($Fe_2(SO_4)_3$ or $FeSO_4$) formed a byproduct known as gypsum ($CaSO_4 \cdot 2H_2O$). In order to be able to characterize the solids, the gypsum needed to be dissolved or "washed" in pH adjusted DI water after which the solids were rinsed, filtered and dried in a 40 °C oven.

### 3.4.1 Sampling

CCPTN and batch experiment slurry samples were drawn out of the agitated reactors with 10 mL syringes. A slurry sample was then centrifuged and the supernatant was filtered using 0.02 μm Whatman Anatop or 0.2 μm MCE Fisherbrand syringe filters. The resulting filtrate solution was acidified using three drops of tracemetal grade nitric acid (Fisher Scientific).

Long term ageing samples as well as pH and Oxidation Reduction Potential (ORP) measurements were taken periodically in the following manner: Similar to the case of industrial tailings management facilities, where the neutralized coprecipitates are dumped and stored in a tailings pond, the produced coprecipitates were left to settle underneath a layer of water. In as such, the pH and ORP of the liquid over settled ageing coprecipitates was recorded first. Subsequently, the contents of the samples was agitated at 500 rpm during which pH and ORP measurements were recorded over a two minute period and a 10 mL sample aliquot was taken. The samples were centrifuged and their supernatants were drawn out with syringes and filtered and acidified.

### 3.4.2 Elemental Analysis

Arsenic analysis for production solution samples and samples containing less than 500 µg/L As(V) was done using a Flow Injection Metal Hydride Spectrometer (Perkin Elmer Analyst 100 AAS equipped with a FIAS-400 Hydride generator). Most accelerated ageing As(V) samples, samples with As(V) concentration greater than 0.5 mg/L and total iron measurements were analyzed using a Thermo Jarrell Ash Trace Scan ICP-OES.

### 3.4.3 Ferrous Iron Titration

To determine the Fe(II) concentration in slurry or filtrate samples, a modified potassium dichromate titration method was used. The procedure consisted of the following steps: Firstly, 50 to 100 mL of deionized water was added in a 250 mL beaker containing a magnetic bar for stirring. Next, a known volume of filtered sample is pipetted into the beaker followed by addition of 20 mL concentrated HCl and 25 mL of prepared mixed acid (15 % v/v $H_3PO_4$, 15 % v/v $H_2SO_4$, 65 g/L $MnSO_4$). In the case of a slurry sample however, the sample is first introduced into the HCl to quickly digest the solids followed by addition of the deionized water and mixed acid. The solution is hastily agitated and a few drops of dissolved sodium diphenylamine sulphonate indicator are added. Subsequently, 0.01 N potassium dichromate held in a 100 mL dispensing burette was added drop wise to the solution until it turned from grey to purple at the titration point. Finally, the concentration of Fe(II) is calculated based on the volume of titrant dispensed over the volume of sample using Equation (9):

$$[Fe(II)] = MW_{Fe} \times N_{K_2Cr_2O_7} \times \left(\frac{Vol_{Titrant}}{Vol_{Sample}}\right) \tag{9}$$

Where [Fe(II)] is given in g/L, $MW_{Fe}$ is the molar mass of iron and $N_{K_2Cr_2O_7}$ is the titrant normality.

### 3.4.4 X-Ray Diffraction

X-Ray Diffraction was conducted on the solids using a Philips PW 1710 diffractometer equipped with a copper target (Cu $K\alpha_1$ radiation, $\lambda$= 1.54060 Å), a crystal graphite monochromator and scintillation detector. Scanning was performed at 40 kV and 20 mA with a step size of 0.1 degrees held for three seconds within an interval of five to 100 degrees two theta.

### 3.4.5 Raman Spectroscopy

Raman spectra were generated using a Renishaw inVia Raman microscope with a 633nm red laser. Typically, a 50 x low working distance lens was used at a laser power of 10 % to generate eight acquisitions of 35 seconds each.

### 3.4.6 BET Surface Area

The surface area of the CCPTN precipitates was measured by BET analysis. Samples were degassed at 30 °C overnight by nitrogen gas. Subsequently multi-point BET readings were taken using a Micromeritics TriStar Surface Area and Porosity Analyzer.

### 3.4.7 Secondary Electron Microscopy

For surface imaging, a Philips XL30 FEG-SEM with an Everheart Thornley secondary electron detector was used. Solids were placed on sample holders with double sided carbon tape and coated with a thin layer of gold/palladium. For imaging, a beam strength of 5 keV was used which was ramped up to 20KeV for EDS (Energy-dispersive X-ray spectroscopy by EDAX) analysis.

# 4 Results and Discussion - Continuous Coprecipitation (CCPTN)

In this chapter, the continuous two-stage (pH 4 and pH 8) co-precipitation work is described. The material is divided into two sections, one of which is concerned with all aspects of “Production” of the fresh coprecipitates and the other with the “Long Term Stability” of the products.

## 4.1 Production

In these experiments, a high fixed initial As(V) concentration (targeted: 1400 mg/L) was used. Such high concentrations are encountered in uranium milling effluents generated from the processing of arsenic-rich ores in Northern Saskatchewan. Furthermore, the Fe/As molar ratio was set to four, as is commonly practiced in industrial coprecipitation circuits. Iron was added in the form of iron(II,III) sulphates at various Fe(II)/Fe(III) ratios to explore the effect of substituting Fe(II) for part of Fe(III). The neutralizing agent used was slaked lime (2.8 w/v or 0.5 M unless otherwise stated) $Ca(OH)_2$, in order to be consistent with industrial coprecipitation practices [3-4, 6, 22].

A summary of the relevant experiments together with their respective feed solution compositions and CCPTN effluent concentrations is given in Table 5. The tests performed by this author are labelled RD. For comparison/reproducibility purposes the data from two tests, labelled RP, previously carried out by De Klerk [8] using the same CCPTN circuit are also included.

**Table 5: Summary of feed solution concentrations, true molar ratios for Fe(III) and Fe(II) over As(V) plus average residual steady state production arsenic concentrations in all CCPTN experiments**

| **Experimental Conditions** | | **Concentration (mg/L)** | | | | **Molar Ratios** | | | **Av. SS Prod. [As] mg/L** | |
|---|---|---|---|---|---|---|---|---|---|---|
| | | **[$Fe^{3+}$]** | **[$Fe^{2+}$]** | **[$Fe]_{tot}$** | **[As]** | **$Fe^{2+}/Fe^{3+}$** | **$Fe^{3+}$/As** | **$[Fe]_{tot}$/As** | **R1** | **R2** |
| RP5 | 2-Stage, 0.5 M $Ca(OH)_2$ | 4295.00 | 0.00 | 4295.00 | 1418.00 | 0.00 | 4.06 | 4.06 | 0.024 | 0.008 |
| RD5 | 2-Stage, 1 M $Ca(OH)_2$ | 4188.40 | 0.00 | 4188.40 | 1034.89 | 0.00 | 5.43 | 5.43 | 0.009 | 0.010 |
| RP12 | 2-Stage, 0.5 M $Ca(OH)_2$ | 3131.00 | 1050.00 | 4181.00 | 1399.00 | 0.34 | 3.00 | 4.01 | 0.079 | 0.182 |
| RD6 | 2-Stage, 0.5 M $Ca(OH)_2$ | 3103.16 | 1083.4 | 4186.56 | 1106.40 | 0.33 | 3.81 | 5.08 | 0.051 | 0.041 |
| RD7 | 2-Stage, 0.5 M $Ca(OH)_2$ | 2272.09 | 2272.09 | 4544.18 | 1351.45 | 1.00 | 2.26 | 4.51 | 0.122 | 0.106 |
| RD8 | 2-Stage, 0.5 M $Ca(OH)_2$ | 1074.63 | 3223.88 | 4298.51 | 1543.25 | 3.00 | 0.93 | 3.74 | n/a | 0.148 |

Figure 11 compares the residual arsenic steady-state (SS) concentrations from the various CCPTN campaigns. As it can be seen there is a systematic tendency for the [As] to increase with increasing fraction of ferrous iron in the feed as indicated by RD6, 7 & 8 notwithstanding the behaviour of experiment RP12. Overall, the resultant residual arsenic concentrations from all experiments are below the effluent discharge regulation limit of 1 mg/L [20]. In other words, even with an Fe(III)/As(V) molar ratio of one (Test RD8) surprisingly a very low arsenic concentration was obtained (<0.2 mg/L). By comparison, batch experiments involving neutralization of equimolar $Fe(SO_4)_{1.5}$-As(V) solutions with NaOH to final pH 8 yielded anywhere between 100 and 700 mg/L As(V) in solution depending on the initial concentration [58] for otherwise short retention times between 1 and 24 hours. Although as already mentioned in the Literature Review chapter, it is now well established that the use of lime leads to lower residual arsenic concentration than NaOH, nevertheless the contrasting big difference (at least 3 orders of magnitude) must reflect to a great extent the beneficial role of excess ferrous iron present in RD8.

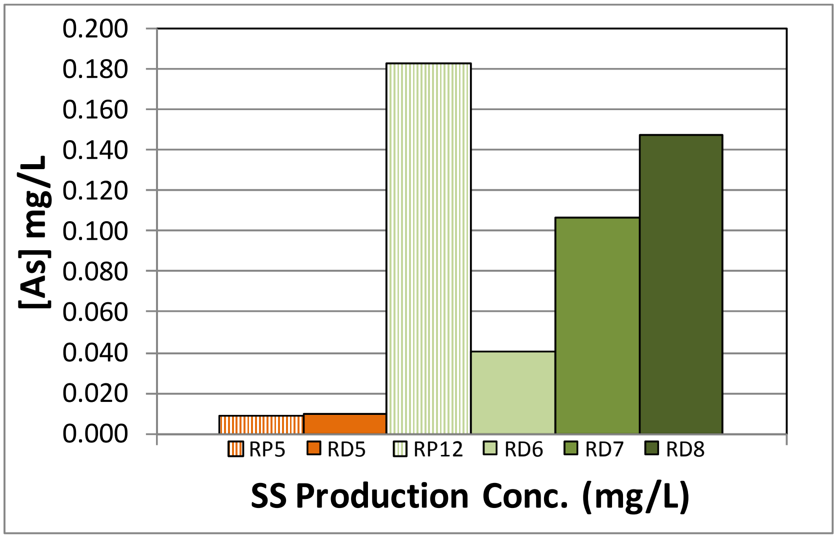

**Figure 11: Bar graph showing the residual arsenic SS production concentration (Reactor 2)**

### 4.1.1 Reproducibility

The coprecipitate filtrate solution (pH=8) at the exit of the 2-stage continuous circuit during SS operation contained essentially the same residual arsenic levels for repeat experiments RP5 and RD5 with 8 and 10 µg/L respectively. On the other hand the two repeat experiments involving mixed Fe(II)/Fe(III) media (Tests RP12 vs. RD6) were observed to register some difference: 0.04 vs. 0.18 mg/L. On a first reading this might appear as large but considering that analysis of such low concentrations involves a higher measurement noise on one hand and on the other that Test RD6 had a higher actual Fe/As molar ratio than Test RP12, 5 vs. 4 (or Fe(III)/As(V) 3.8 vs. 3), which is known to improve coprecipitation performance [2, 21] then the observed difference can be at least partly rationalized.

### 4.1.2 Coprecipitate Production Analysis

During the CCPTN ramp up to SS, samples were periodically taken from Reactors 1 & 2 (as described in Section 3.4.1) in order to monitor the removal of arsenic from solution and simultaneously follow the dissolved Fe(II) concentration as a function of time. For example, Figure 12 (A) shows the [Fe(II)] in Reactor 1 (pH=4) over the course of the CCPTN experiments with increasing ferrous content. Not shown are the curves for dissolved [Fe(II)] in Reactor 2 (pH=8) as these data points were all very low or below detection limits due to the precipitation of ferrous iron at pH>7.5 (See Chapter 5). As the ferrous content in Reactor 1 became more significant, notably for RD8, the [Fe(II)] in solution at SS did not reach the target value. This could be attributed to the co-precipitation of ferrous iron with ferric iron and arsenate as will be shown in Chapter 5. Moreover, it should be mentioned that this drop in soluble [Fe(II)] in Reactor 1 (notably for RD8) was not due to oxidation at pH 4. As discussed in Chapter 6 the oxidation of ferrous iron at pH 4 due to air entrainment is extremely slow to account for the observed drop.

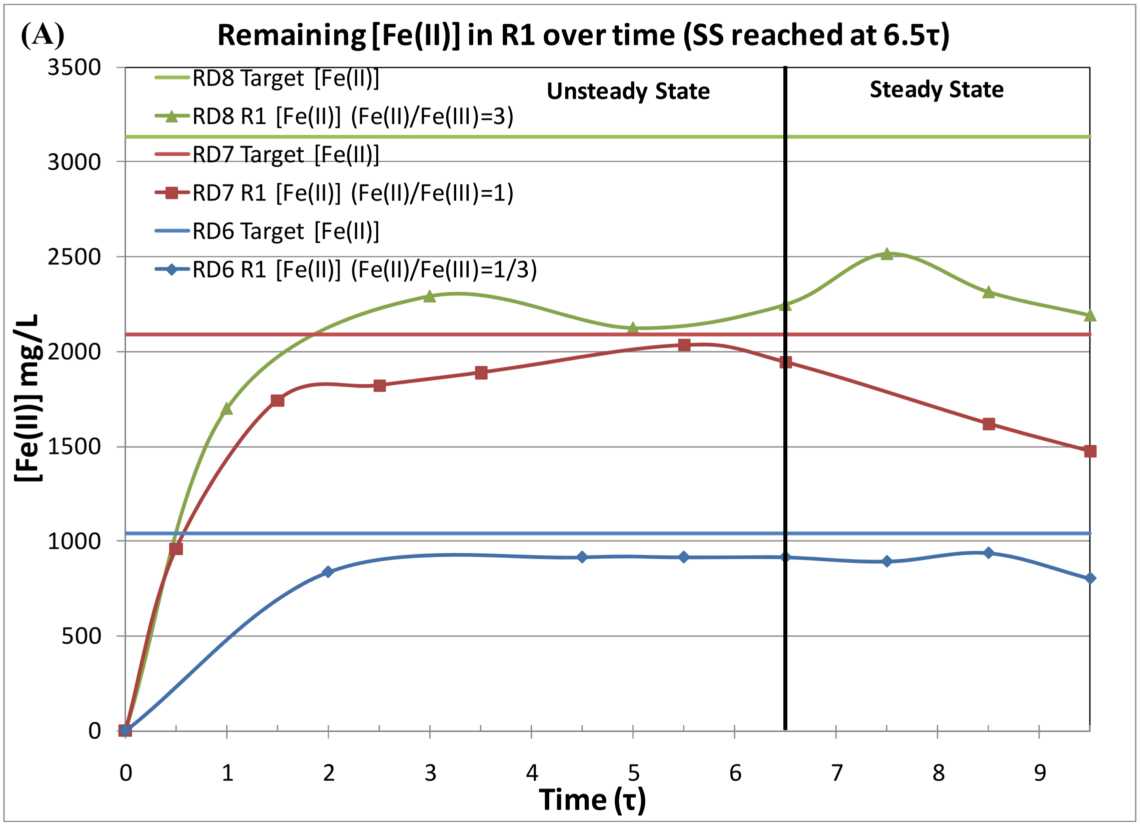

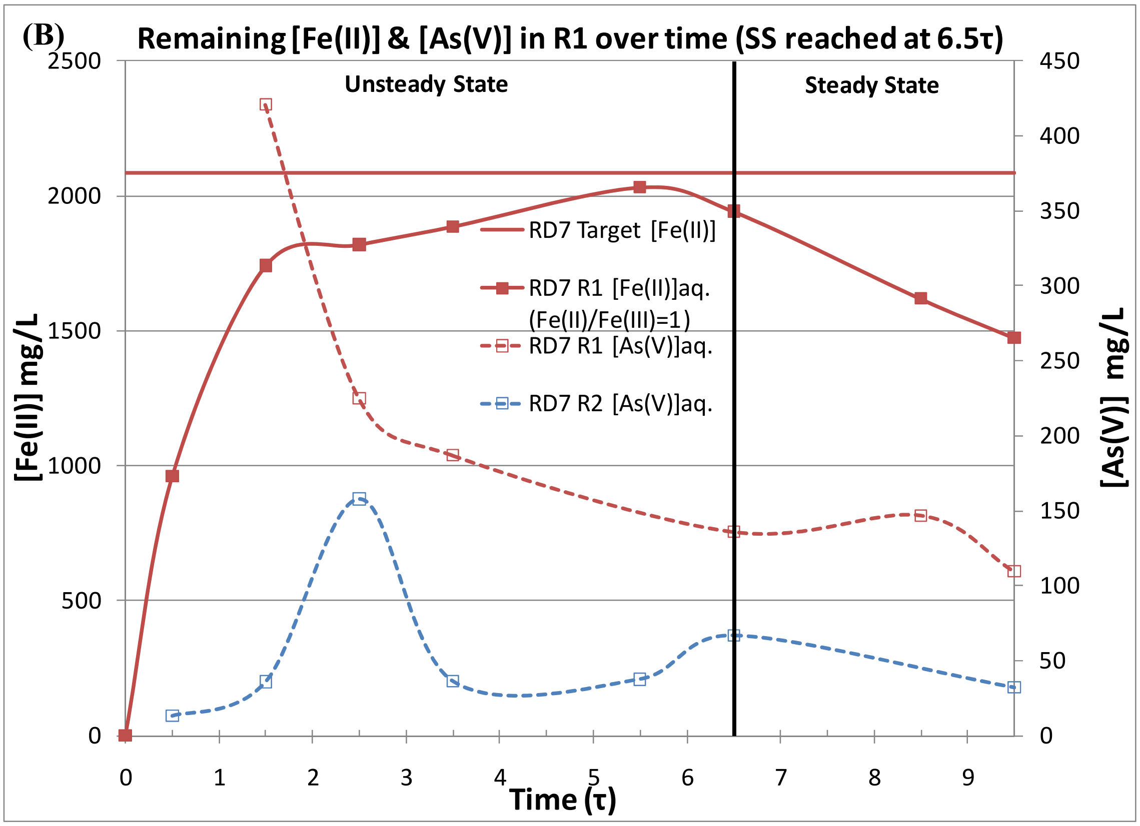

**Figure 12: Remaining dissolved [Fe(II)] in Reactor 1 during CCPTN experiments with increasing ferrous to ferric fractions (A), Dissolved [Fe(II)] & [As(V)] for exp. RD7 (Fe(II)/Fe(III) molar ratio =1) (B)**

Figure 12 (B) shows how dissolved [As] concentration in Reactor 1 of RD7 (Fe(II)/Fe(III)= 1 and Fe(III)/As(V)=2.3) gradually decreased and stabilized as the steady state regime was reached. Here we should note, as explained in Chapter 3, that the attainment of steady state was verified previously via tracer tests. Of the three tests reported in Figure 12 (A), two look to have attained reasonable steady state apart from Test RD7, which showed some deviation from SS in terms of iron(II) concentration but to be reasonable in terms of arsenic concentration. For all practical purposes the operation can be considered to have reached steady-state.

## *4.2 Long Term Stability Testing*

### 4.2.1 Reproducibility and General Trends

The produced coprecipitated solids were subjected to long term ageing tests at 20, 40 and 70 °C. Before the detailed ageing/stability data is presented as a function of time they are compared with data generated in a previous study by De Klerk [8] to evaluate their reproducibility as well as among themselves to establish the general trends. This comparison/evaluation can be made with the aid of Figure 13. This graph shows the levels of released arsenic (mg/L) after 223 days of ageing at 20, 40 and 70 °C for the case of Fe(II)/Fe(III)/As(V)=0/4/1 (comparison of campaigns RD5 and RP5 [8]) and Fe(II)/Fe(III)/As(V)=1/3/1 (comparison of campaign RD6 and RP12 [8]) under two pH conditions, namely drifting pH and constant pH=8. The arsenic concentrations were obtained by linear interpolation between the two closest data points encompassing the chosen ageing time. This ageing time (223 days) was chosen as it represented stable drifting pH, i.e. attainment of practical equilibrium.

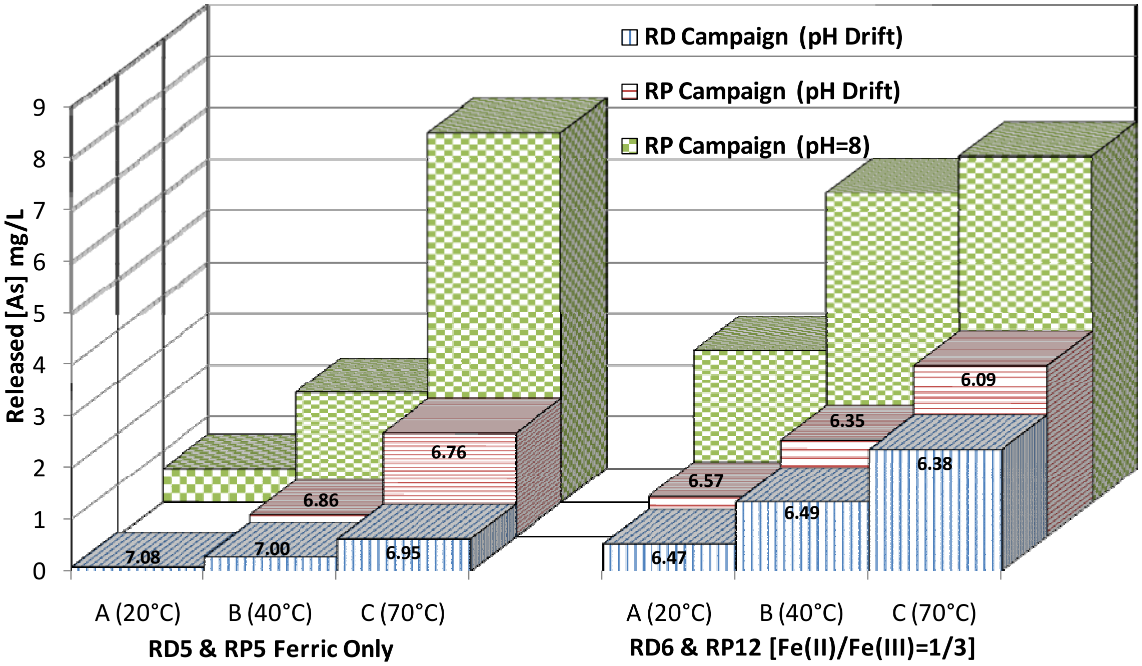

**Figure 13: Summary of released [As] (mg/L) for 2-stage replicate CCPTN experiments after 223 days ageing at various temperatures. The corresponding final pH for the drifting experiments is given. Chequered and lined columns represent constant pH=8 and drifting pH experiments respectively**

The pH drift ageing replicate experiments generally have comparable levels of released arsenic with the exception of RD5 C and RP5 C pH Drift which showed a more significant concentration difference, namely 0.62 vs. 2.01 mg/L respectively. Once again, the effect of slightly different Fe/As molar ratio between the two campaigns (Table 5) may be the origin, at least partly, of this difference. Lastly, but very significantly, the pH of replicate experiments were all within ± 0.3 pH units of one another, another indicator of good reproducibility.

In terms of trends, the following can be noted: the increased release of arsenic with increasing temperature; The lower arsenic release with pH drifting as opposed to constant pH ageing; the higher arsenic release when ferrous is substituted for part of ferric (however, according to the data of Test RD6 A (20 °C) the released arsenic concentration is still < 1 mg/L but the “equilibrium” pH is lower in this case, namely 6.47 vs. 7.08 indicating that ferric iron provides a higher “buffering” effect than ferrous iron). These trends are further elucidated and discussed in the following sections.

## 4.2.2 Coprecipitate Ageing/Stability Behaviour

### 4.2.2.1 Constant pH vs. Drifting pH Ageing

In Figure 14 and Figure 15, ageing data from coprecipitates produced with different Fe(II)/Fe(III)/As(V) ratios are compared for two ageing conditions: constant pH and drifting pH. It must be mentioned that the presented ageing data was collected following 12 week pre-ageing at ambient temperature before the slurry was split into three batches for ageing at different temperatures. The procedure is detailed in Chapter 3. Figure 14 summarizes the ageing results, that is, the release of As(V) into solution over time, for experiments RD5 & RP5 pH Drift as well RP5 pH=8 (Fe(II)/Fe(III)/As(V)=0/4/1) at two ageing temperatures, 20 and 40 °C. Figure 15 does the same for experiments RD6 & RP12 pH Drift and RP12 pH=8 (Fe(II)/Fe(III)/As(V)=1/3/1) (Note: the data at 70 °C is available in Appendix Section 8.1 as well as tables containing all data including additional recent data points not shown in the figures). First it can be noted that for non-ferrous iron containing aged CCPTs (Figure 14), ageing at room temperature at constant pH for three years resulted in excellent stability with only 1.15 mg/L As(V) released back into solution. RD5 A shows that even lower [As] is achieved when the pH was allowed to drift during ageing (no pH adjustments, Figure 14). Thus at 20 °C, there was only 0.14 mg/L As(V) released when the drifting pH stabilized at 7.09. Moreover the drifting pH approach allowed for faster attainment of pseudoequilibrium than the constant pH approach. This is important as the drifting pH more closely reflects real tailings disposal environments. This systematic difference between drifting and constant pH ageing is also valid at all ageing temperatures for both RP5 and RP12 experiments and is further discussed later. Where available, both RP and RD campaigns aged at drifting pH showed similar arsenic retention over time, specifically RP5 B & RD5 B pH Drift. In all cases, raising the ageing temperature increased the rate of As(V) release and the final [As]. For example, the last three data points for RD6 pH Drift A, B & C were all relatively steady at average concentrations of 0.64, 1.25 and 2.66 mg/L.

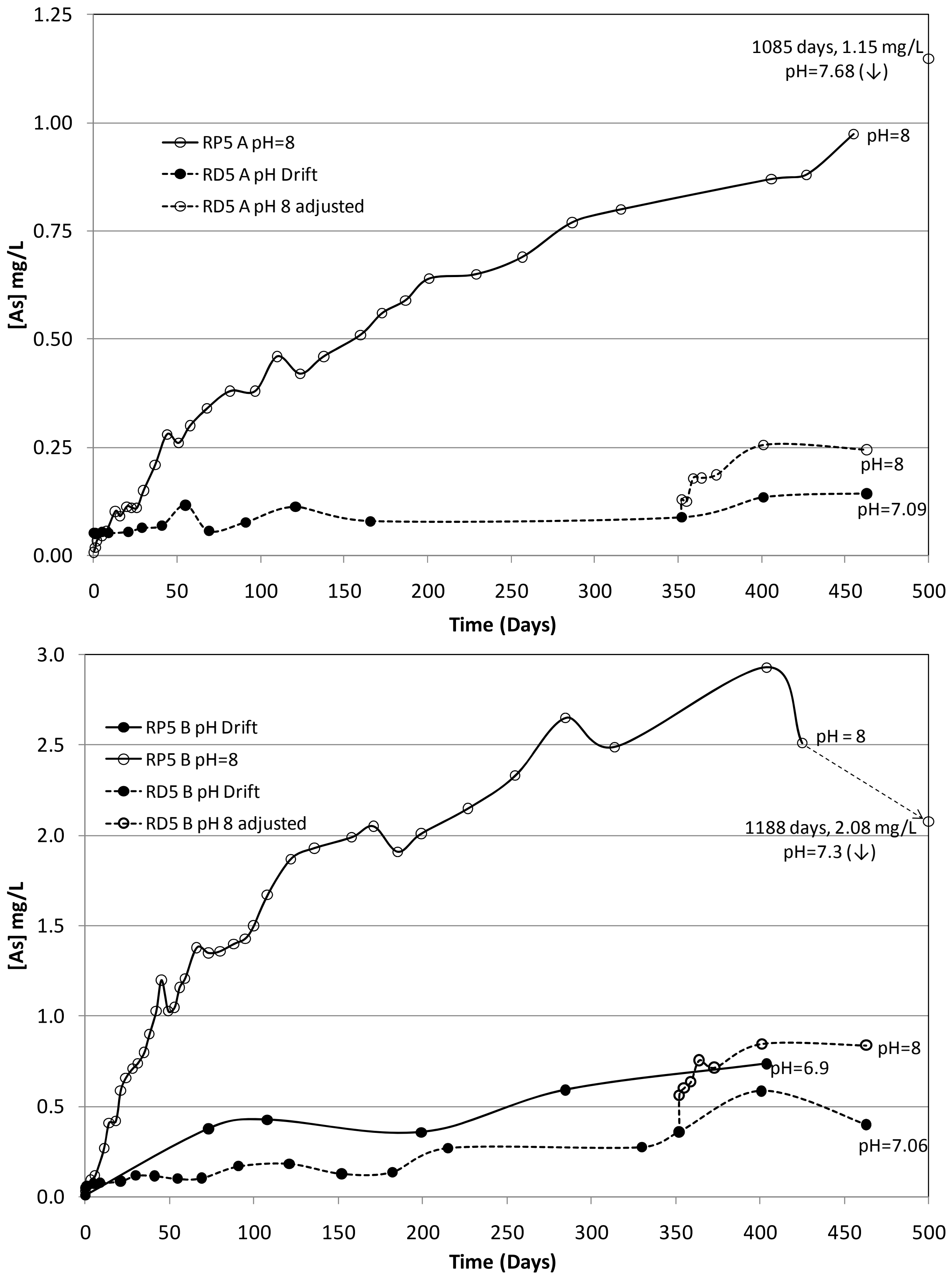

**Figure 14: Long term ageing data-comparison between RD5 and RP5 [8] for room temperature (top) and accelerated ageing at 40 ºC (bottom). Note: solids from RD5 had been pre-aged in their final coprecipitation liquor at room temperature for 12 weeks; t=0 represents the extension of ageing following solids concentration by reducing by half the liquor volume (S/L=1/25). "pH adjusted" involved splitting of the ageing slurry in two halfs with one of them continuing on free pH drift while the other was regularly adjusted to pH 8**

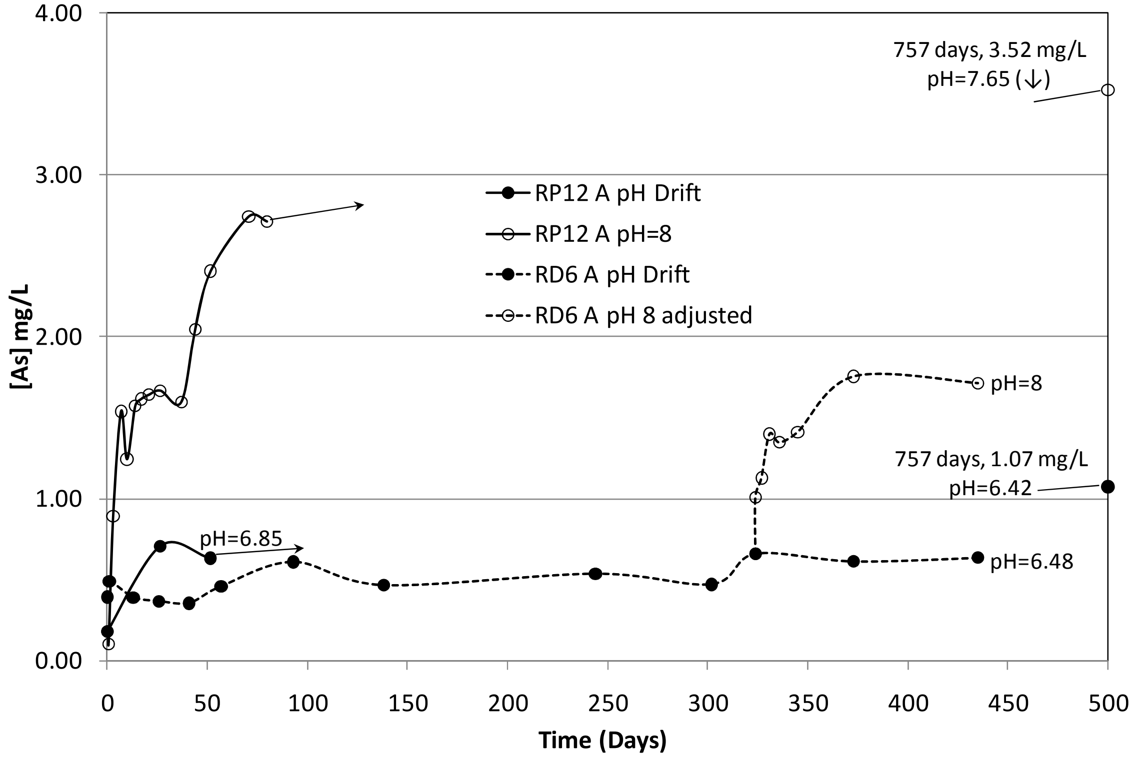

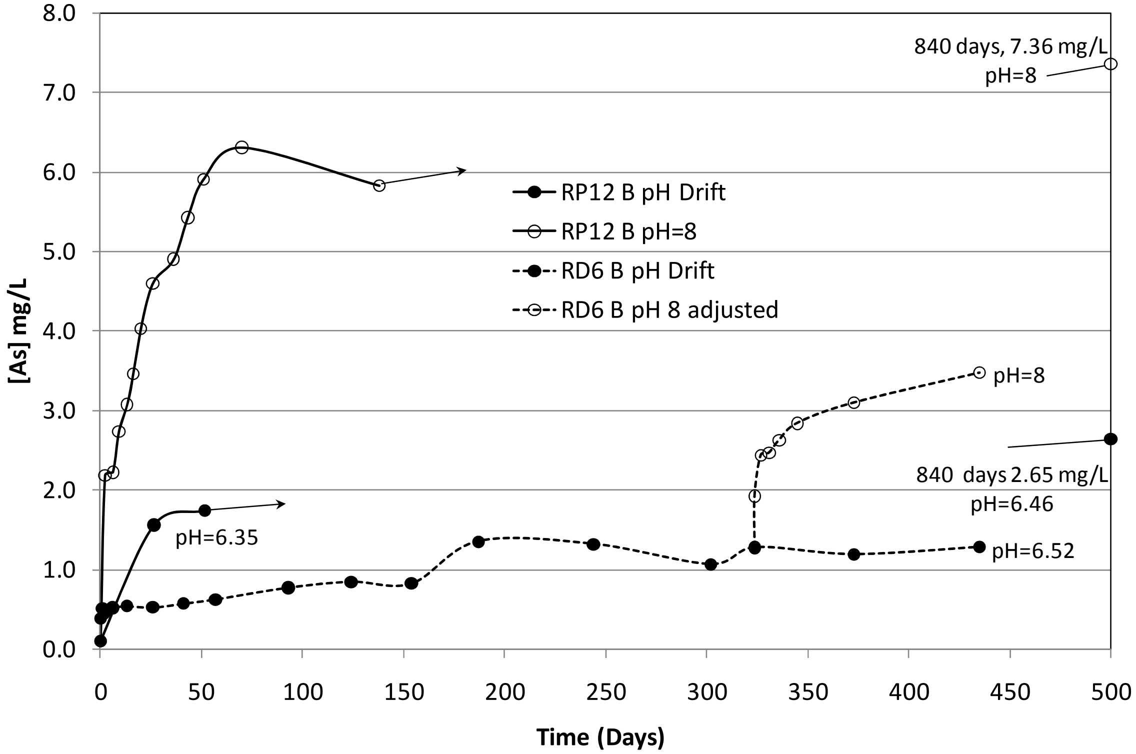

**Figure 15: Long term ageing data-comparison between RD6 and RP12 [8] for room temperature (top) and accelerated ageing at 40ºC (bottom). Note: solids from RD6 had been pre-aged in their final coprecipitation liquor at room temperature for 12 weeks; t=0 represents the extension of ageing following solids concentration by reducing by half the liquor volume (S/L=1/25). "pH adjusted" involved splitting of the ageing slurry in two halfs with one of them continuing on free pH drift while the other was regularly adjusted to pH 8**

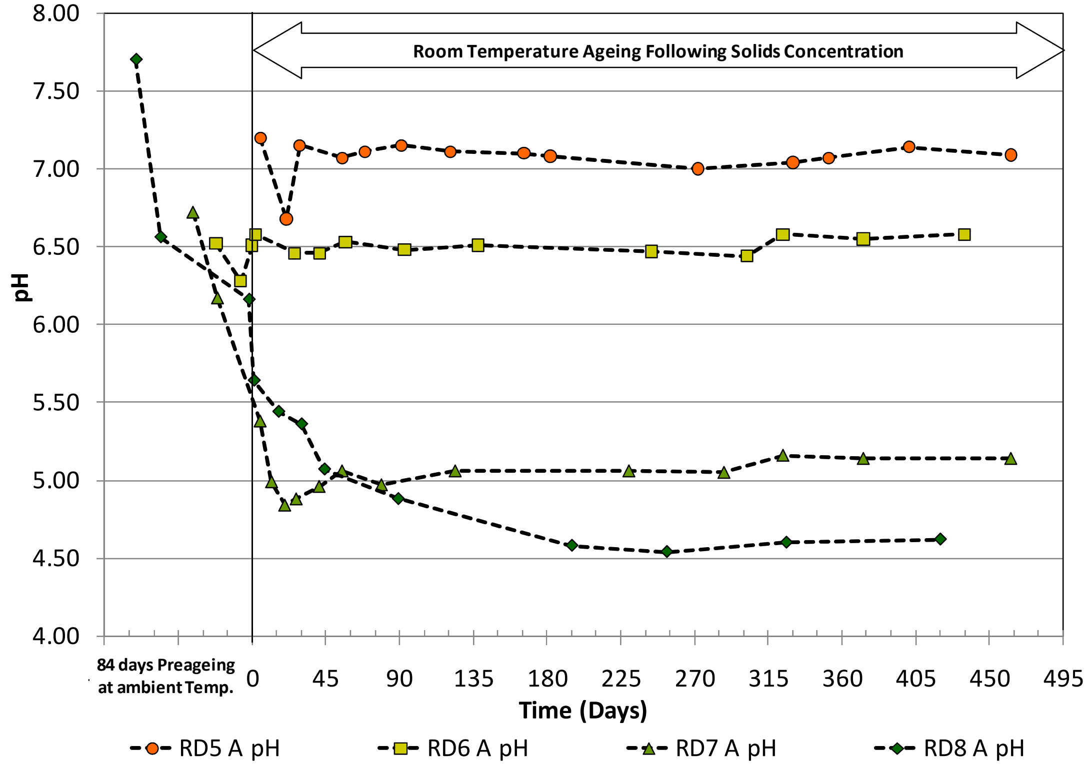

**Figure 16: Drift pH variation of CCPTN experiments aged at room temperature**

#### 4.2.2.2 Response to pH Adjustment/Regulation during Drifting pH Ageing

As seen above, the pH drifted from the initial discharge value of 8 down to 7 (Figure 14) or 6.5 (Figure 15). It was decided after pseudoequilibrium was reached (after about 320 days of ageing) to split the aged slurries into two batches with one of them continuing its pH drifting ageing while the other adjusted (with slaked lime) to pH 8 thereafter keeping it at that pH via frequent pH adjustment. The ageing data from this splitting/mid-way pH adjustment is plotted on Figure 14 and Figure 15. It can be seen that after about 100 days, the newly pH 8 adjusted data stabilized at values much lower than the values of arsenic released from the constant pH 8 tests. Thus from the data of Figure 14 corresponding to Fe(III)/As(V)=5, the respective values are: 0.24 vs. ~1 mg/L As(V) at 20 °C and 0.84 vs. ~2.25 mg/L As(V) at 40 °C. Similar observations can be made for the data of Figure 15. This implies that some unidentified transformations occurred during ageing to render the coprecipitates more stable (a finding first observed by Jia and Demopoulos [24]). In that case the coprecipitates were produced in batch reactors as opposed to being produced in continuous reactors in the current work, and hence by extrapolation, similar behaviour can be predicted for the industrially generated tailings.

#### 4.2.2.3 The Effect of Increasing Ferrous Fraction Substitution

The data of Figure 13, Figure 14 and Figure 15 already presented evidence that replacement of part of ferric iron by ferrous iron while the total Fe/As(V) molar ratio is kept constant leads to increased arsenic release. Here, this trend is quantified by comparing the ageing data from 4 tests. Thus in addition to the first two experiments, RD5 & 6, two other CCPTN experiments with increasing ferrous fraction, RD7 & 8, were conducted. The ageing results for each individual experiment, with multiple curves showing the effects of pH drift ageing at various temperatures, are presented in Figure 57 that can be found in Appendix Section 8.1. Only a sample of data (the 20 °C ageing data) is presented here in Figure 17 so the effect of increasing ferrous substitution on arsenic release can be evaluated/discussed. The data plotted in Figure 17 comprise two ageing periods: 84 days ageing in the CCPTN production slurry followed by ageing at double S/L ratio at room temperature always (t=0). The [As(V)] release data during the initial (84 days) preageing period is given in µg/L. As it can be seen, RD5 & 6 exhibit gradually increasing and uninterrupted [As] profiles during preageing. However, RD7 & RD8 exhibit rather irregular [As] profiles during preageing. In other words the higher the amount of ferrous substitution the more erratic the data are. A possible explanation for this behaviour is the transformation of the ferrous-containing coprecipitates due to oxidation. Ferrous iron may precipitate as ferrous arsenate (symplesite) in addition to ferrous hydroxide and/or green rust (GRII) as discussed in Chapter 2 and 5. Ferrous hydroxide is very easily oxidized when contacted with air. Although the steady state collection buckets were sealed and in between sampling the solids were left to settle, the top of the surface of the settled solids containing iron(II) bearing hydroxides was slowly becoming orange and thicker with time. This provides evidence of some oxidation of iron(II) hydroxide (due to the reopening of the bucket and agitation of the slurry for each new sample) to form for example iron(III) oxyhydroxides. These erratic As(V) concentration profiles were extended into the regular ageing (post t=0) period. These fluctuations were more pronounced at higher initial [Fe(II)] and higher ageing temperatures (refer to Figure 57 in Appendix 8.1). After 420 days (in addition to the pre-aging time of 12 weeks) or more of pH drifting ageing, no true equilibrium appears to have been achieved with the exception perhaps of the ferrous-free test (RD5). In other words the presence of ferrous prolongs the attainment of equilibrium; this being so due to its reactive nature that causes transformations to occur by its oxidation. Iron concentration (not shown) was consistently found to be minimal (<1 mg/L) or below detection limits throughout the whole ageing period thereby indicating full precipitation and retention with the solids of all ferrous iron.

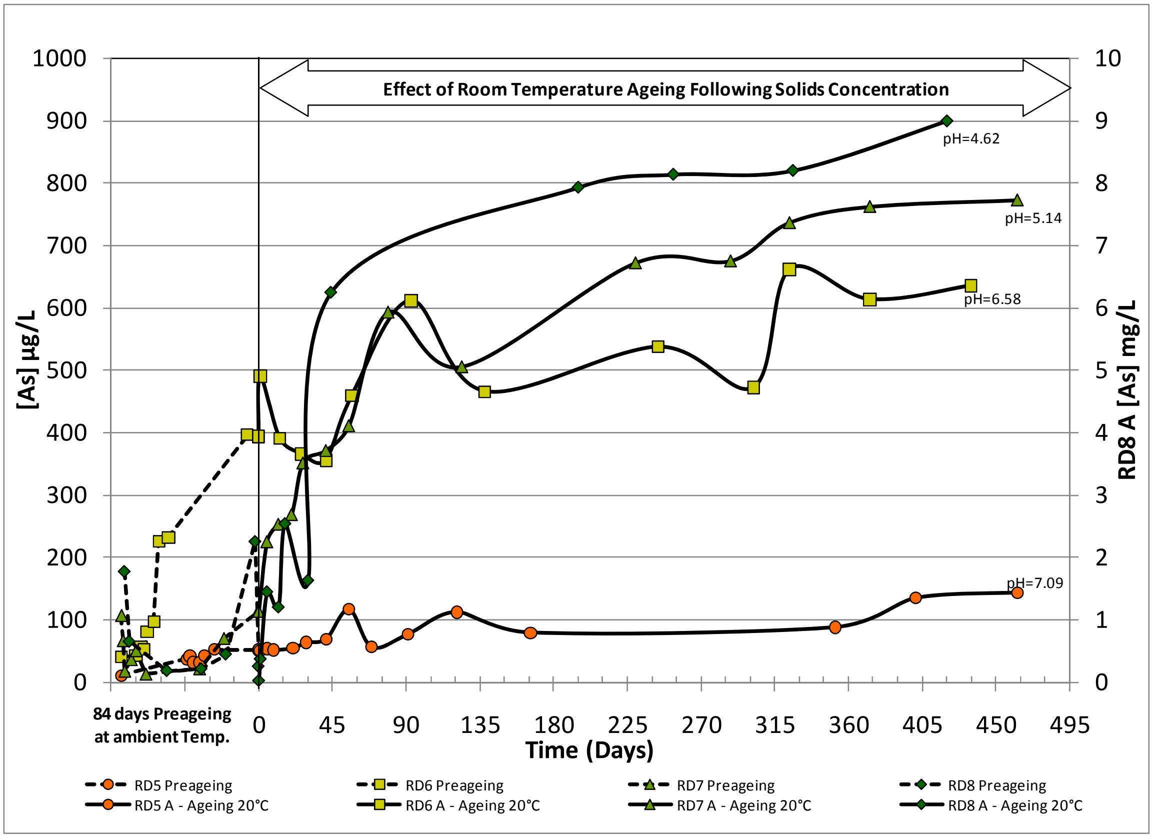

**Figure 17: Comparison of long term "drift" stability curves of experiments RD5, 6, 7 & 8 at 20°C. RD5 contains no addition of ferrous sulphate while RD6, 7 & 8 contain increasing amount ferrous; there was a 84 day pre-ageing at room temperature; time zero signifies the beginning of ageing following solids concentration (S/L=1/25)**

A summary of the final (almost stable-pseudoequilibrium) data from all ageing tests (Figure 57 in Appendix Section 8.1) is presented in Table 6 and Figure 18.

**Table 6: Final ageing/pseudo-equilibrium data**

| Exp. | Fe(II)/Fe(III) | Time (Days) | (A) 20 °C | | (B) 40 °C | | (C) 70 °C | |
|---|---|---|---|---|---|---|---|---|
| | | | [As] mg/L | pH | [As] mg/L | pH | [As] mg/L | pH |
| RD5 | 0/4 | 463 | 0.14 | 7.09 | 0.40 | 7.06 | 1.25 | 7.09 |
| RD6 | 1/3 | 435 | 0.64 | 6.58 | 1.28 | 6.52 | 2.66 | 6.48 |
| RD7 | 2/2 | 463 | 0.77 | 5.14 | 3.02 | 5.12 | 7.83 | 5.14 |
| RD8 | 3/1 | 420 | 9.00 | 4.62 | 16.91 | 4.04 | 4.86 | 4.12 |

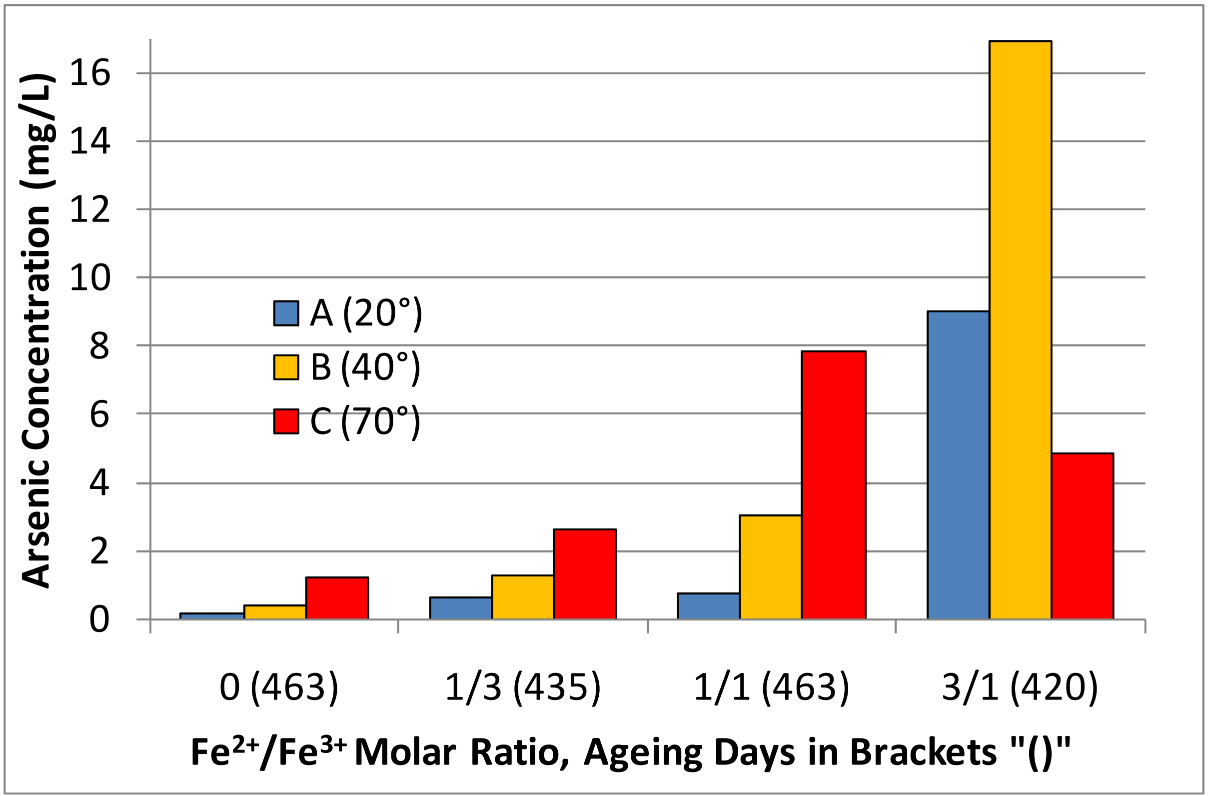

**Figure 18: The effect of $Fe^{2+}/Fe^{3+}$ molar ratio and ageing temperature on arsenic pseudoequilibrium levels**

From these data the following observations can be made: (1) With increasing ferrous fraction the attainment of equilibrium was prolonged due to apparent phase transformations involving partial oxidation of the precipitated ferrous-bearing compounds. (2) With increasing ferrous a lower stable pH was reached. This was more evident at Fe(II)/Fe(III)=1 or higher (at Fe(tot)/As(V)=4). (3) At Fe(II)/Fe(III)=1 and Fe(III)/As(V)=2 (conditions corresponding to Test RD7) the resultant coprecipitate was stable as less than 1 mg/L arsenic was released after 463 days. It is interesting to note that mid-way adjustment and control of pH to 8 (data shown in Figure 57 in the Appendix Section 8.1) the arsenic concentration increased and stabilized at ~2 mg/L (Test RD7), i.e. very modest indeed. This was the first time that such long ageing data was presented showing stability at Fe(III)/As(V)<3. This may be another indirect evidence of the enhanced retention of arsenate by other than simple adsorption mechanism on ferrihydrite, such as ferric arsenate as shown by Chen *et al.* [7] for pH<7 and probably ferrous arsenate (symplesite) or arsenate adsorption on green rust. (4) With the exception of the RD8 test the arsenic release increased as the temperature of ageing increased. In the case of RD8, ageing at 70 °C resulted in lower arsenic release than ageing at 20 or 40 °C. This unexpected behaviour is discussed in the next section.

#### 4.2.2.4 Ferrous-rich Coprecipitate Ageing at 70 °C

As noted in the previous section with increasing ferrous content erratic arsenic release data was recorded causing a delay in the attainment of apparent equilibrium (pseudoequilibrium). Such behaviour was related to partial (at least) oxidation of the ferrous-containing phases. In this context among the collected stability data the case of ageing at 70 °C for RD8 C test (Fe(II)/Fe(III)/As(V)=3/1/1) is of particular interest. The relevant data are presented in Figure 19. As it can be seen during the early stages of ageing at 70 °C (following the 12 week preageing), [As] reached a maximum measured soluble level of 19.87 mg/L after only 12 days followed by a decrease down to 7.11 mg/L at the 30 day mark. From there, [As] increased again to 18.21 mg/L after 75 days to decrease consistently thereafter reaching 4.86 mg/L after 420 days. At the same time the free drifting pH following its initial dip down to 3.3 had climbed up after that eventually stabilizing around 4.1. This behaviour is attributed to conversion of an initially formed ferrous containing phase (ferrous hydroxide and(?) ferrous arsenate) by oxidation over time to green rust and/or iron(III) hydroxide or ferric arsenate. The oxidation of a ferrous phase potentially able to fix arsenic [41, 49-50] would naturally result in an increase in soluble arsenic. It is plausible that over time, the released arsenic can be picked up (via adsorption) again by the new iron(III) hydroxide formed through oxidation or through crystallization (promoted by the elevated temperature) of symplesite or scorodite as discussed in the latter case by Le Berre *et al.* [59]. In terms of the possible arsenic pick up by the newly formed ferric hydroxide (ferrihydrite), Randall *et al.* [41] showed that arsenic may only be picked up by the in-situ formed iron(III) phase after all the “metastable” or “intermediate” phase, in their case GRII, is oxidized. Finally, given that the ageing of CPTs took place in static capped bottles and that they were only stirred enough to uniformly mix the slurry during sampling, it is likely that oxidation was controlled through slow gas-liquid mass transfer kinetics.

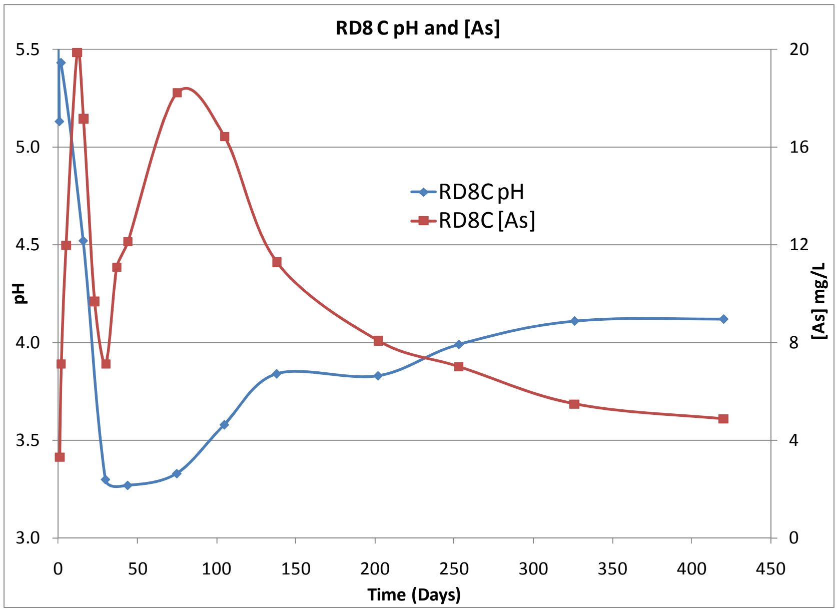

**Figure 19: RD8 C (70 °C) ageing results showing the release of [As] over time and the associated pH profile (Fe(II)/Fe(III)/As(V)=3/1/1)**

## 4.2.3 Characterization of Aged Coprecipitates

Several of the aged coprecipitates were subjected to various characterization techniques in an effort to identify phases and substantiate to the extent possible the transformations mentioned in the previous section. Such characterization is rather challenging because of the instability of ferrous phases especially when they are separated and dried prior to analysis. A list of the aged products characterized along with their specific conditions is provided in Table 7.

**Table 7: Summary of ageing coprecipitates subjected to characterization**

| **Exp.** | **RD5** | | | **RD6** | | | **RD7** | | | **RD8** | | |
|---|---|---|---|---|---|---|---|---|---|---|---|---|
| **Ageing Temp.** | 20°C (A) | 40°C (B) | 70°C (C) | 20°C (A) | 40°C (B) | 70°C (C) | 20°C (A) | 40°C (B) | 70°C (C) | 20°C (A) | 40°C (B) | 70°C (C) |
| **Age** | 272 | 272 | 279 | 244 | 244 | 251 | 230 | 230 | 237 | 195 | 195 | 202 |
| **pH** | 7.00 | 7.08 | 6.94 | 6.47 | 6.54 | 6.30 | 5.06 | 5.23 | 5.00 | 4.58 | 4.02 | 3.83 |
| **[As]** | 0.08 | 0.27 | 0.72 | 0.54 | 1.32 | 2.42 | 0.67 | 3.21 | 8.71 | 7.94 | 16.96 | 8.07 |

### 4.2.3.1 XRD Analysis

XRD analysis revealed only broad peaks matching the 2-line ferrihydrite-FH (34 and 61° 2θ [52]) at lower temperature and lower ferrous fraction. Starting at 40 °C, other peaks were evident which were clearly matched at 70 °C to those of 6-line FH (Figure 20). According to the 70 °C patterns reported in Figure 20 the 6-line FH has best developed in the RD8 product which contained the majority of iron as ferrous (Fe(II)/Fe(III)/As(V)=3/1/1). In the other end lies RD5 with the least signs of evolution to 6-line FH. No arsenate phases could be detected.

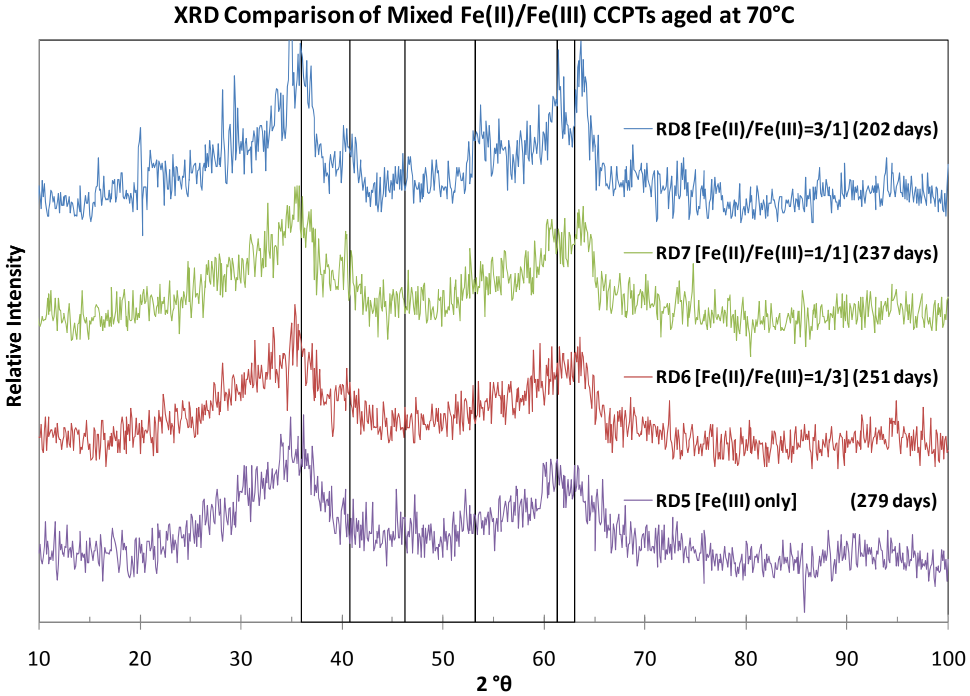

**Figure 20: XRD patterns for CPTs aged at 70 °C. An increased ferrous fraction results in the formation of 6-line ferrihydrite (Black lines represent 6-line FH peaks taken from JCPDS Card# 00-029-0712)**

### 4.2.3.2 RAMAN Spectroscopy

Since characterization via XRD was limited to crystalline compounds and the present study did not confirm the presence of arsenate in the samples, RAMAN spectroscopy was employed to distinguish among the ageing products. For the scope of this thesis, it will suffice to just focus on the features of arsenate. Figure 21 shows the differences in spectra between poorly crystalline FA and arsenical FH (Fe/As=4, pH8) prepared by the method of Jia *et al.* [31]. Additionally, the Raman spectra of crystalline atmospheric scorodite (SD) and plain FH standards are included. The arsenate region lies roughly between 808 and 927 cm$^{-1}$ [60] and several bands for similar products have been recorded [31, 50, 61-62]. It can be clearly seen that plain FH does not contain any bands in that region, yet the scan for As-FH contains a shoulder related to the characteristic As-O stretching vibration region. The bands for arsenate are even more defined in the poorly crystalline FA standard, which are well aligned with the sharp bands of crystalline scorodite. Figure 22 compares the Raman spectra of the 70 °C aged CCPTN products with increasing initial ferrous to ferric fraction. Each spectrum shows a shoulder in the arsenate region defined above but with some distinguishing features among them. The biggest difference can be seen between the ferrous-free product (RD5) and the ferrous-rich (RD8) product with the other two lying between these two end-members. While it is tempting on a first examination to relate the exhibited shoulder (arsenate fingerprint) to that of As-FH standard the observed differences among the four products points out to a more complex mineralogical makeup that cannot be resolved in the present work. Additional spectra can be found in the Appendix Section 8.1.

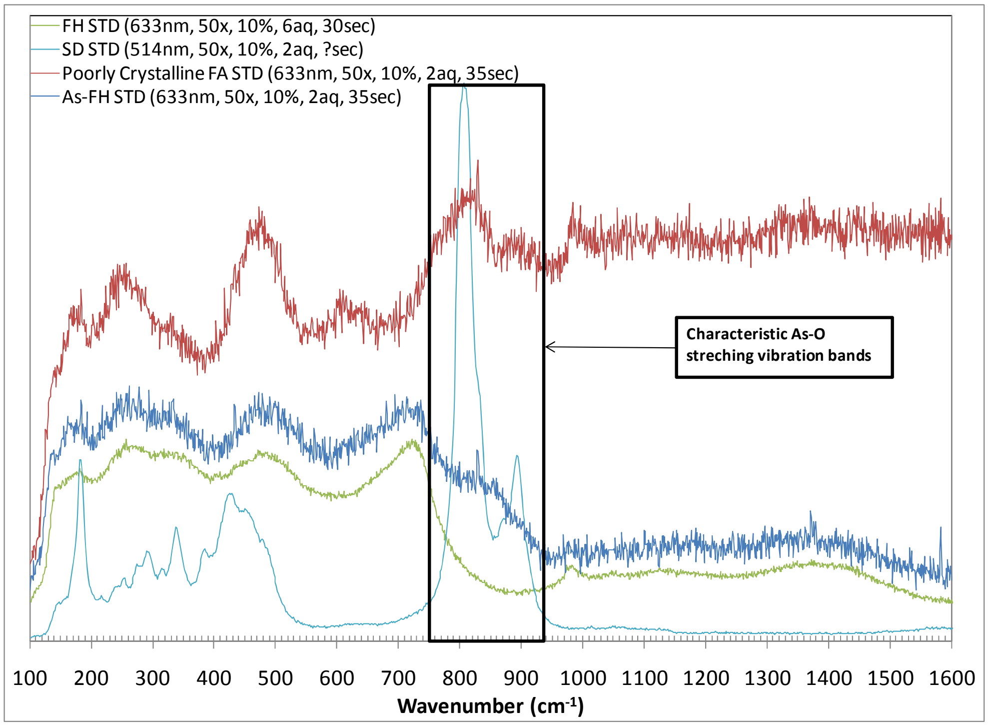

**Figure 21: Raman spectra of reference compounds: FH= Ferrihydrite, As-FH= Arsenical Ferrihydrite, FA= Ferric Arsenate, SD = Scorodite**

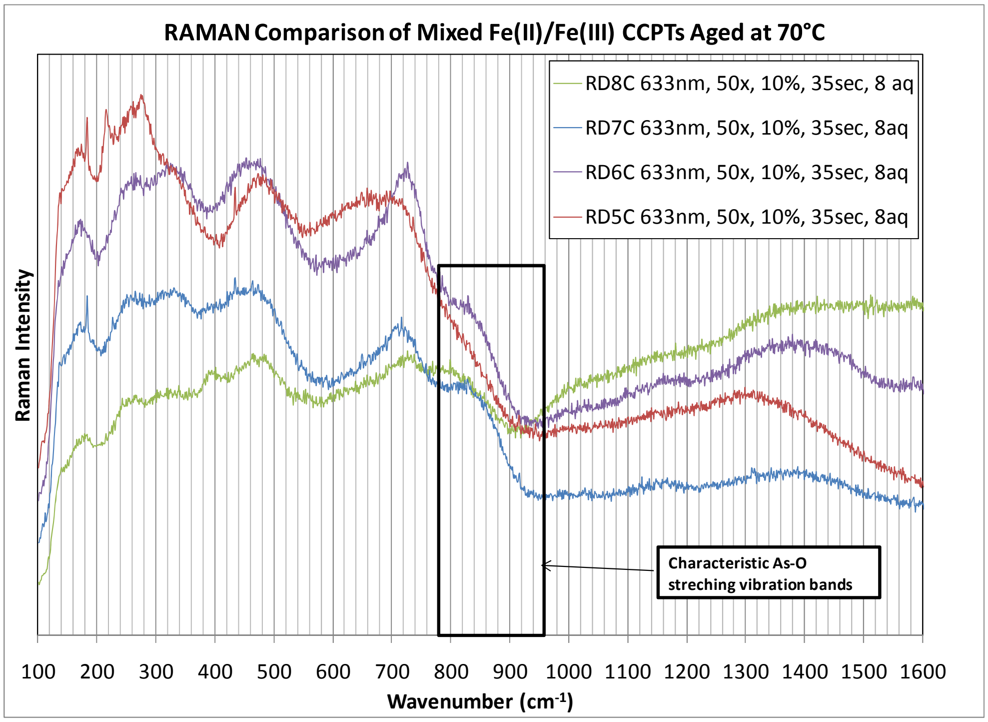

**Figure 22: Raman spectra for 70°C aged CCPTN products with increasing initial ferrous to ferric fraction**

### 4.2.3.3 BET Surface Area

The BET surface area (s.a.) analysis for aged CCPTs is provided in Table 8. From the results, the following was deduced:

1. All coprecipitates were characterized by large surface areas indicative of poorly crystalline/amorphous precipitates produced via a predominantly homogeneous nucleation process [63].
2. It seems that the ferrous-free CCPTs (RP5 A and RD5 A) have a much lower surface area than the CCPTs produced in the presence of ferrous iron.
3. Ageing at increasing temperature typically increases the BET surface area; similar observations were made by De Klerk [8].

For comparison, it is mentioned that typical BET s.a. measurements for FH are in the range of 241-280 $m^2/g$ [22, 30, 64-65] and for arsenical FH and coprecipitated iron(III) with arsenate both at Fe/As molar ratios equal to 4 & pH=4 are 266 $m^2/g$ and 250 $m^2/g$ respectively [22]. The s.a. measurements of the aged CCPTN products range between 43 and 282 $m^2/g$ (Table 8). Measurements for hydrothermal scorodite synthesized at 160 °C by the McGill Hydrometallurgy group has a specific surface area of 7.57 $m^2/g$. The latter serves to compare the relatively low s.a. of a highly crystalline product versus that of amorphous 2-line FH and aged CCPTN products.

**Table 8: BET surface area analysis for aged CPTs**

| **Experiment** | | **RP5** | **RD5** | **RP12** | **RD6** | **RD7** | **RD8** |
|---|---|---|---|---|---|---|---|
| **Conditions** | | **$Fe^{3+}$ only** | **$Fe^{3+}$ only** | **$Fe^{2+}/Fe^{3+}$ 1/3** | **$Fe^{2+}/Fe^{3+}$ 1/3** | **$Fe^{2+}/Fe^{3+}$ 2/2** | **$Fe^{2+}/Fe^{3+}$ 3/1** |
| **Surface Area ($m^2/g$)** | **Ageing A** | 29.10* | 42.91 | 144.76* | 189.23 | 192.61 | 153.42 |
| | **Ageing B** | 73.00 | 259.39 | n/a | 251.64 | 200.69 | 162.36 |
| | **Ageing C** | 178.83 | 244.96 | n/a | 282.23 | 205.78 | 181.95 |

*production samples (no ageing) at 20 °C

### 4.2.3.4 SEM Imaging

High magnification images were taken for RD6 & 8 solids aged at 20 & 70 °C (Figures 23-26).

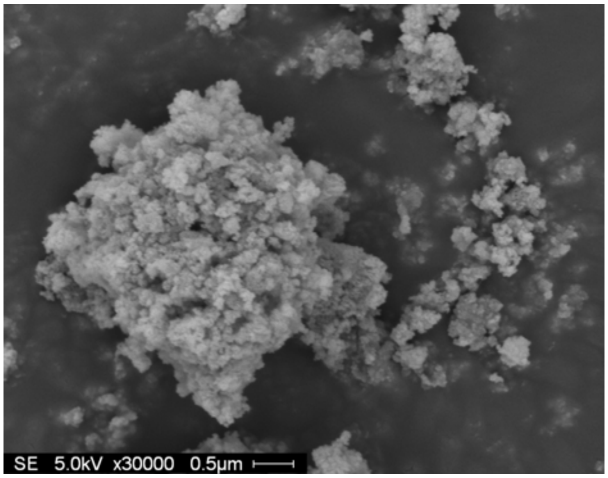

**Figure 23: RD6 A product aged 244 days (BET=189.23)**

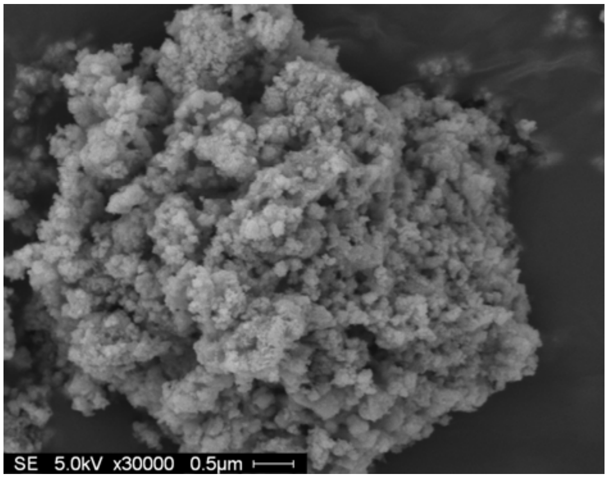

**Figure 24: RD6 C product aged 251 days (BET =282.23)**

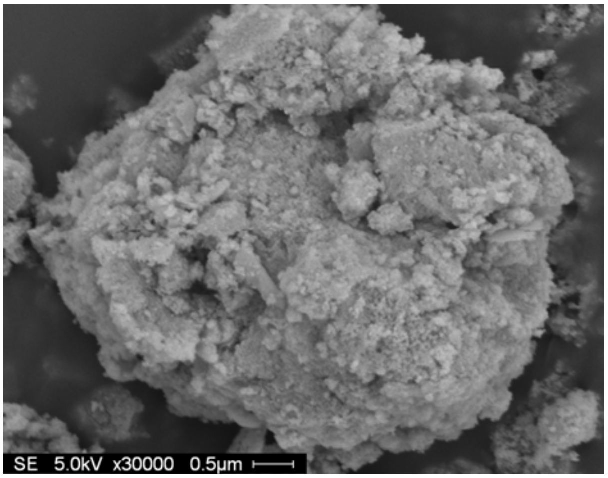

**Figure 25: RD8 A product aged 195 days (BET=153.42)**

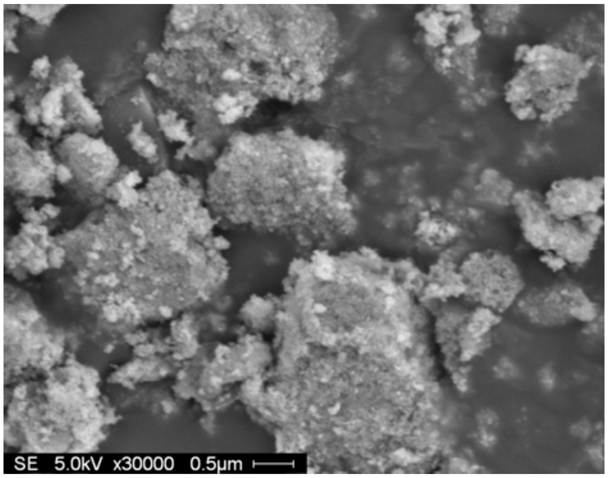

**Figure 26: RD8 C product aged 202 days (BET=181.95)**

SEM scanning of the samples generally showed large agglomerates of nanosized particles (not resolved). Although samples were lightly ground to break large chunks, the surface details between small and big agglomerates were consistent. Typically, higher surface area measurements go in hand with samples that are more porous. When comparing the surface topography of RD6 A with RD6 C, the latter appears to be spongier, which would be in line with the increase in BET s.a. measurements between the two (Table 8). Spot EDS analysis (not shown) confirmed the presence of arsenic, iron and oxygen.

## 4.3 Partial Conclusions

A 2-stage (pH4, pH8) lime neutralization continuous coprecipitation (CCPTN) circuit was used to study the removal of high arsenic(V) concentrations (1400 mg/L) from acidic sulphate effluent waters containing various ratios of ferrous to ferric at Fe(total)/As molar ratio equal to 4. The CCPTN process was shown to generate reproducible results on separate occasions. The substitution of ferrous for ferric iron resulted in an increase of arsenic concentration in the CCPTN process effluent but this was still below the 1 mg/L limit even with Fe(II)/Fe(III)=3 and Fe(III)/As(V)=1. By comparison arsenic levels from isomolar Fe(III)-As(V) solutions in the absence of ferrous were at least three orders of magnitude higher showing that excess iron above the stoichiometric ratio one contributed to effective arsenic retention/precipitation even when present as ferrous.

Long term ageing of the coprecipitates at various temperatures showed slow release of arsenic reaching apparent (pseudo) equilibrium after a few months of equilibration. Ageing under drifting pH conditions led to lower arsenic release than pH-controlled ageing. The reached pseudoequilibrium pH had the tendency to be lower with increasing ferrous fraction and increasing temperature. A pH adjustment to 8 following ageing near pseudoequilibrium resulted in much lower arsenic level than the corresponding one reached by constant pH 8 ageing from the beginning. At Fe(II)/Fe(III)=1 and Fe(III)/As(V)=2 the pseudoequilibrium arsenic release level following mid-way pH adjustment/ageing to pH 8 was only 1.9 mg/L. The retention of arsenic in the presence of ferrous may be achieved via a combination of paths including a precursor to ferrous arsenate (symplesite), arsenate adsorption on green rust, and re-adsorption of arsenate on ferrihydrite (ferric hydroxide) produced during ageing by partial oxidation of ferrous hydroxide. XRD and Raman analysis done on aged products could not detect a ferrous-containing phase. XRD analysis of aged CCPTN products showed that an increase of initial ferrous content and increasing ageing temperature promoted the formation of 6-line FH as opposed to the ferrous-free products that were better matched with the 2-line FH variety. BET analysis coupled with SEM surface imaging showed the CCPTs to consist of aggregates of large (50-300 $m^2/g$) surface area.

# 5 Results and Discussion – Hydrolysis Studies

In order to shed light on the continuous coprecipitation of arsenate in mixed ferrous-ferric sulphate media, additional studies were undertaken focusing on the hydrolytic and oxidation chemistry of ferrous sulphate in the absence and presence of arsenate. In particular in these studies first (discussed in this Chapter) the precipitation behaviour of Fe(II) alone (onset of metal hydroxide formation e.g. precipitation) or with Fe(III) (co-precipitation of Fe(III) along ferric hydroxide/ferrihydrite) or with As(V) as a function of pH was determined. This was followed by studying the oxidation (discussed in the next Chapter) of the resultant hydrolyzed slurry at pH 4, 6, and 8[1] in order to evaluate how arsenic precipitation and release is affected. Some preliminary characterization of the post-hydrolysis oxidation products was also carried out and reported.

## *5.1 Hydrolytic Precipitation Iron Only*

### 5.1.1 Single and Mixed Fe(II) and Fe(III) Sulphate Open Air Hydrolysis - High RPM

#### 5.1.1.1 Single Iron Solutions

In this series of tests, $Ca(OH)_2$ base was gradually added manually into the precipitation reactor filled with either $FeSO_4$ or $Fe(SO_4)_{1.5}$ containing solutions (0.075 M or 4174 mg/L Fe) to pH 4 and maintained at that pH for one hour before finally raising and maintaining the pH at 8 for an additional hour. Slurry samples were taken at regular pH intervals (and after constant pH upholding), centrifuged immediately followed by filtration using 0.02 μm syringe filters. The filtrate was analyzed for its total iron concentration using ICP. Figure 27 summarizes the results of the two hydrolysis experiments, where one contained only ferrous and the other only ferric iron. On the same Figure the predicted solubility of iron according to OLI Environmental Simulation Program (ESP V-8.0.60) is plotted for the two iron hydroxides for comparison purposes.

---

[1] Additional experiments performed at initial pH 11.5 were performed with results similar to those obtained at pH 8. These data are reported in the Appendix Section 8.3.

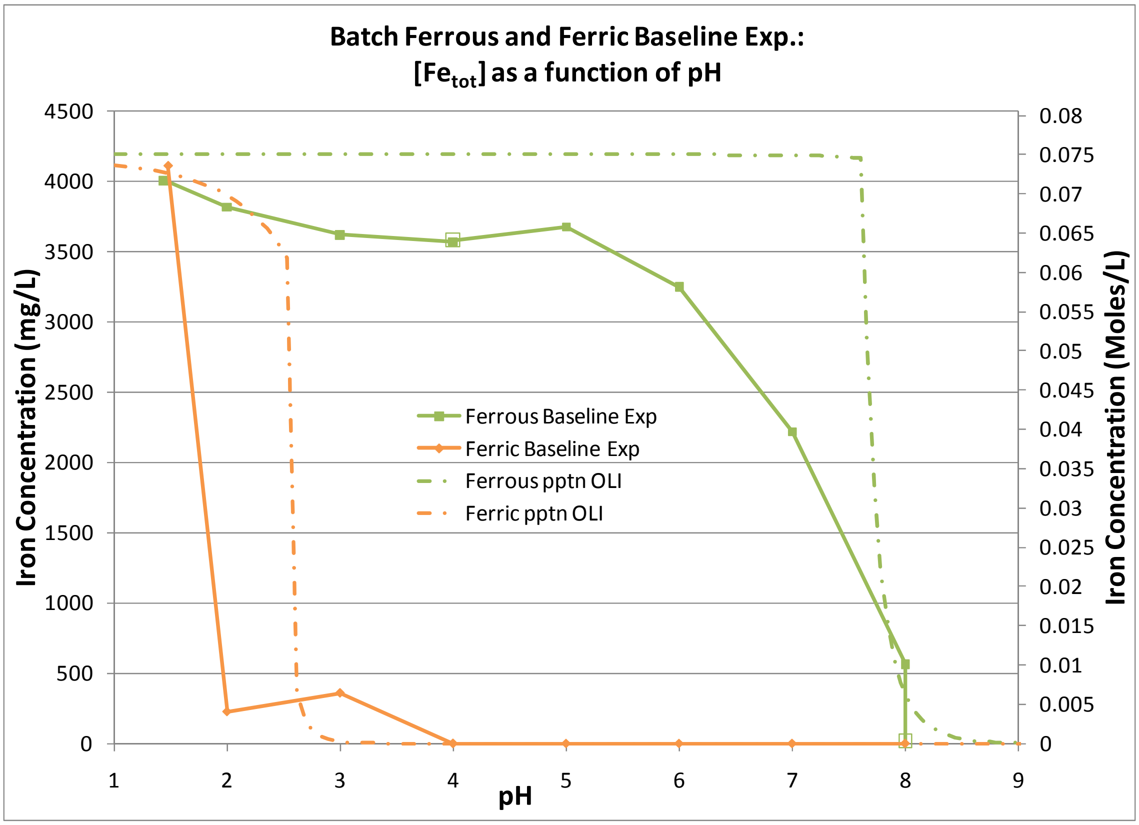

**Figure 27: Fe(II) and Fe(III) hydrolytic precipitation. Solid lines represent Fe(II) and Fe(III) precipitation as a function of pH. Dotted lines represents OLI (simulation software for aqueous chemistry) predicted precipitation curves. Large empty markers denote [Fe] after 1 hour at given pH (4 or 8)**

It can be seen that the start of ferric iron precipitation occurred between pH values 1.5 and 2, during which the total iron concentration dropped significantly (~90 %). There exists a discrepancy of approximately one pH unit between the simulation and the experimental values. The origin of the discrepancy is not known although it is conceivable that errors with the thermodynamic data used by OLI including complexation and activity effects may be responsible. At pH 4 and beyond it is clear that all Fe(III) has precipitated. Similarly, for Fe(II) at pH 8 most of the iron (82 %) is precipitated out of solution further dropping down to 20 mg/L after 1 hour retention at that pH represented by the second data point at pH 8. However, it can be seen that dissolved Fe(II) begins to precipitate at much lower pH right from the onset of pH increase (~10 % between pH 1.5 and 5) and more dramatically so between pH 5 to 8. By contrast the OLI simulation predicts a sharp drop in concentration between pH 7.5 and 8. It is suspected that oxidation contributed to this “pre-mature” level of iron precipitation. It must be noted that this experiment was conducted at ambient conditions and that while an attempt was made at limiting oxidation, it was not enough to completely prevent it. It is believed that the combination of inevitable exposure to air at the surface of the reactor and air entrainment due to relatively high agitation (1000 rpm) promoted the slow ferrous oxidation above pH 5 over time.

### 5.1.1.2 Mixed Fe(II) and Fe(III) Solutions

Similarly to Section 5.1.1.1, an equal parts mixed solution of Fe(II) and Fe(III) was prepared in a batch reactor. Using $Ca(OH)_2$ the pH of the solution was slowly raised from its initial pH=1.4 to 8 with two 1 hour constant pH periods at pH 4 and 8. Figure 28 shows the obtained results. This time there was very good agreement between the experimental and OLI predicted Fe(III) solubility data.

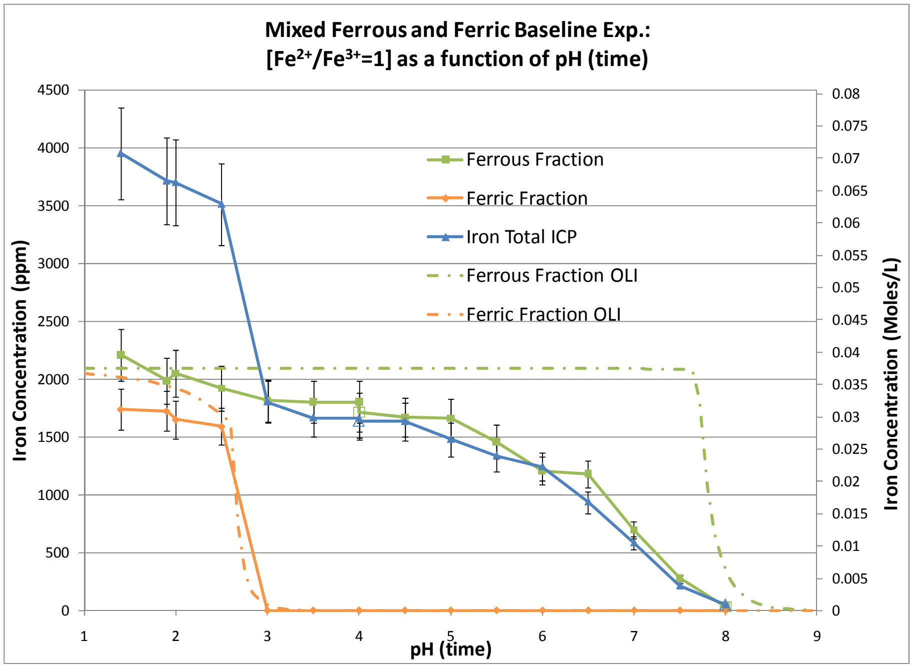

**Figure 28: Experimental hydrolysis curves for a mixed Fe(II,III) solution together with OLI simulated precipitation curves. Large empty markers denote [Fe] after 1 hour at given pH. 10 % error bars are displayed**

However, it is seen again that the Fe(II) concentration dropped significantly prior to its theoretical precipitation point predicted by OLI (as shown by the broken line in Figure 28). Moreover it is evident that the “pre-mature” precipitation of Fe(II) is more extensive this time than in the single solution (refer to data in Figure 27). Thus at pH 5 there was ~20 % Fe(II) precipitated in the mixed system (Figure 28) but only 10 % in the single iron (II) solution (Figure 27). The corresponding precipitation levels at pH 7 are ~67 % (mixed system) vs. ~45 % (single system). This enhanced precipitation of ferrous could have been due to its adsorption onto precipitated iron(III) hydroxide beyond pH 3 [36]. Alternatively the formation of a mixed ferrous-ferric hydroxide phase like green rust cannot be ruled out. Since, however, the ferrous concentration was only half in the mixed system with reference to the one of the single system it is also possible (at least in part) the difference in % values to be eliminated if the absolute amount of ferrous precipitated is considered. Most likely coprecipitation but more importantly adsorption have contributed to this "pre-mature" ferrous precipitation. The oxidation of ferrous species is known to be favoured at higher pH as deduced from the data of Figure 28 [39].

### 5.1.2 Single Fe(II) Hydrolysis Under Restricted (No Open Air) Atmosphere - Low RPM

#### 5.1.2.1 Nitrogen Sparging Test

In order to prevent oxidation new measures were adopted in a new series of hydrolysis experiments. The same reactor as before was outfitted with a sparging device through which nitrogen gas was supplied to prevent oxidation as done in other ferrous-related studies [42-44, 66-67]. An arbitrary $N_2$ flow rate was selected and a constant rate of base addition was employed (3.347 mL/min) this time using 0.56 M NaOH instead of $Ca(OH)_2$. The agitation speed was reduced to 500 rpm (from 1000 rpm) which, based on observations made with a water filled reactor, minimized the entrainment of air from the surface into the reactor. No acid was added to the reactor before the start of base addition ($pH_{ini}$= 3.64). The results obtained, much more satisfying this time, are shown in Figure 29. The evolution of pH and $E_h$ with time is reported in Figure 59 in Appendix Section 8.2.

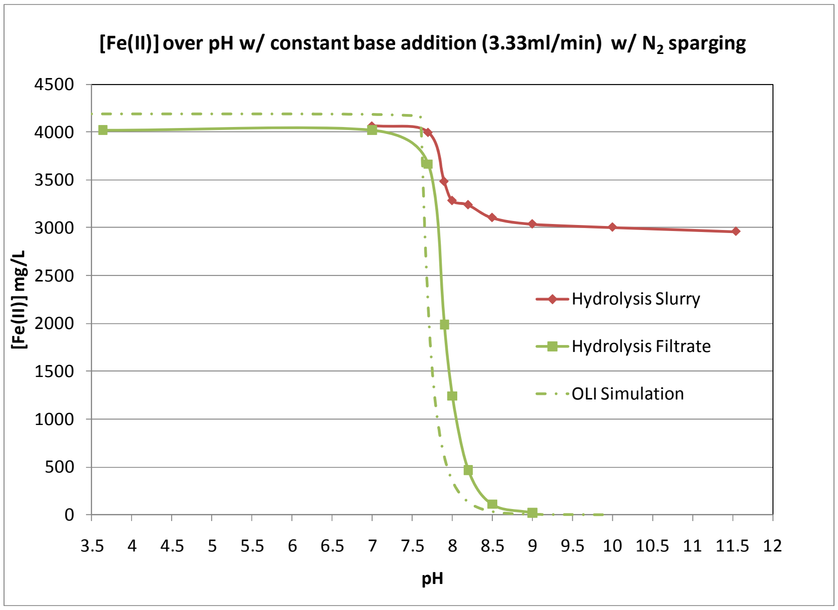

**Figure 29: Fe(II) hydrolytic precipitation with constant 0.56M NaOH base addition, 500 rpm agitation and $N_2$ sparging to minimize oxidation. Solid lines represent filtrate and slurry Fe(II) concentrations respectively. Dotted line represents OLI predicted precipitation curve**

There is a good correlation between the OLI predicted and the filtrate experimental ferrous concentration values. In addition to the solution (filtrate), slurry samples were also analysed for Fe(II) as a function of pH. It can be seen that the total [Fe(II)] (slurry titration) drops from ~4000 mg/L to ~3000 mg/L between pH 7.5 and 9. In other words, ~15 % of Fe(II) was oxidized (despite sparging with $N_2$) between pH 7.5 and 8 increasing to 25 % when the pH reached 9 thereafter remaining constant. Based on literature reports (unable to validate in this work) it is possible that this partial oxidation due to air infiltration to have led to the formation of a mixed valence Fe(II,III) hydroxide phase known as green rust [68]. It may be concluded that ferrous hydroxide forms as predicted by OLI, i.e. essentially all ferrous precipitating out of solution over the narrow pH zone of 7.5 to 8.5 as long as no ferric or air is present to enhance the precipitation of ferrous by either co-precipitation with ferric or oxidation (in either adsorbed or green rust form).

#### 5.1.2.2 No Nitrogen Sparging

The test described by Figure 29 was repeated but this time without $N_2$ sparging to verify if it were the nitrogen or the reduced agitation speed that resulted in less oxidation than the earlier experiment of Figure 27. The results from the new test are compared to those obtained with nitrogen sparging in Figure 30. As it can be seen almost identical results were obtained with and without $N_2$ sparging. These data serve also as proof of the good experimental reproducibility associated with the data of this work. In light of the identical data, it can be concluded that at agitation speeds of 500 rpm or less, nitrogen sparging does not provide additional protection against oxidation during the hydrolysis of Fe(II) in the particular laboratory reactor. Hence unless otherwise stated all subsequent tests were carried with the same reactor setup and 500 rpm agitation without resorting to use of nitrogen.

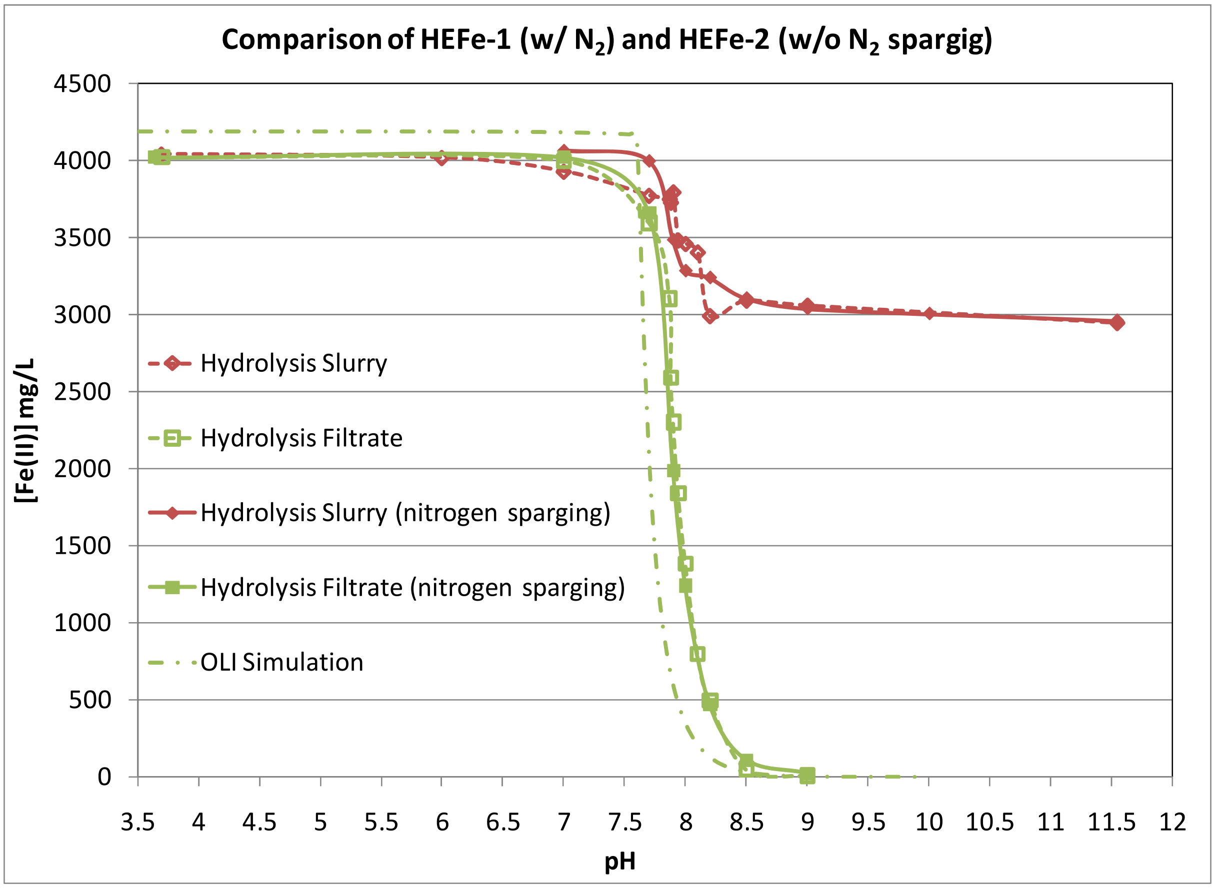

**Figure 30: Fe(II) hydrolytic precipitation with constant 0.56 M NaOH base addition and 500 rpm agitation. Solid lines represent data obtained with $N_2$ gas sparging. Broken lines represent data obtained without $N_2$ gas sparging. Dotted line represents OLI predicted precipitation curve**

### 5.1.2.3 Empirical Kinetic Equations

It must be noted that plotting the hydrolysis filtrate [Fe(II)] vs. time (reminder: base was being added at a constant feed rate) generated a linear curve with excellent $R^2$ score, which in the case of both aforementioned hydrolysis tests the slopes or rate of ferrous precipitation, represented by Equations (10) & (11), are remarkably similar (where y is expressed in mg/L Fe(II) units and x in min):

Hydrolysis of Fe(II) with $N_2$ sparging. Filtrate [Fe(II)] vs. time:

$$y = -38.147x + 4445.8 \qquad \text{where } R^2 = 0.9966 \tag{10}$$

Hydrolysis of Fe(II) without $N_2$. Filtrate [Fe(II)] vs. time:

$$y = -41.233x + 4454.1 \qquad \text{where } R^2 = 0.9961 \tag{11}$$

## 5.2 Ferrous Hydrolysis in the Presence of Arsenic(V)

In this section, hydrolysis experiments similar to the previous section are described this time involving solutions containing ferrous sulphate and arsenic(V) (added as arsenic pentoxide) at two molar ratios, namely Fe(II)/As(V) equal to 4 (Test ID HEAs-1) and 1.65 (HEAs-2). The first one was selected as it is the standard Fe/As molar ratio prescribed for effective coprecipitation of arsenic with iron(III). The second one represents the stoichiometric ratio of ferrous arsenate, also known as symplesite (increased by 10 % to compensate for the partial oxidation of ferrous as described in the previous section). The relevant data from the two tests are summarized in Table 9.

**Table 9: Conditions and data for experiments HEAs-1 &2 involving hydrolysis of Fe(II)-As(V) solutions**

| Exp. | Targeted Fe/As molar ratio | Actual Fe/As molar ratio | Base Concentration | Base flow rate (mL/min) | % Fe(II) oxidized in slurry at pH 8 | Time to reach pH 8 (min) |
|---|---|---|---|---|---|---|
| HEAs-1 | 4 | 3.91 | 1 M NaOH | 1.915 | 11.7 | 87.5 |
| HEAs-2 | 1.65 | 1.49 | 1 M NaOH | 0.884 | 15.8 | 322 |

### 5.2.1 Hydrolysis of Fe(II)/As(V)= 4 Solution up to pH 11.5

Figure 31 shows the solution Fe(II), Fe(total) and As(V) concentration curves as a function of increasing pH as well as the Fe(II) concentration of the resultant slurry. Comparison of the curves for iron in solution (filtrate), namely Fe(II) by titration and Fe(total) by ICP, gives comparable profiles establishing that most of the dissolved iron was in fact present as ferrous iron. The slight discrepancy is partly due to experimental error and partly due to some minor fraction of ferrous oxidation. This was determined to be 11.7 % at pH 8 (data in Table 9). The presence of the bulk (~90 %) of iron as ferrous even after precipitation is confirmed with the slurry Fe(II) concentration data of Figure 31. In contrast to the precipitation behaviour of ferrous in the absence of arsenic that was well simulated with OLI (Figure 30), a different response was observed in the presence of arsenic. In the latter case, as seen in Figure 31, ferrous precipitated at much lower pH apparently in concert with arsenic(V).

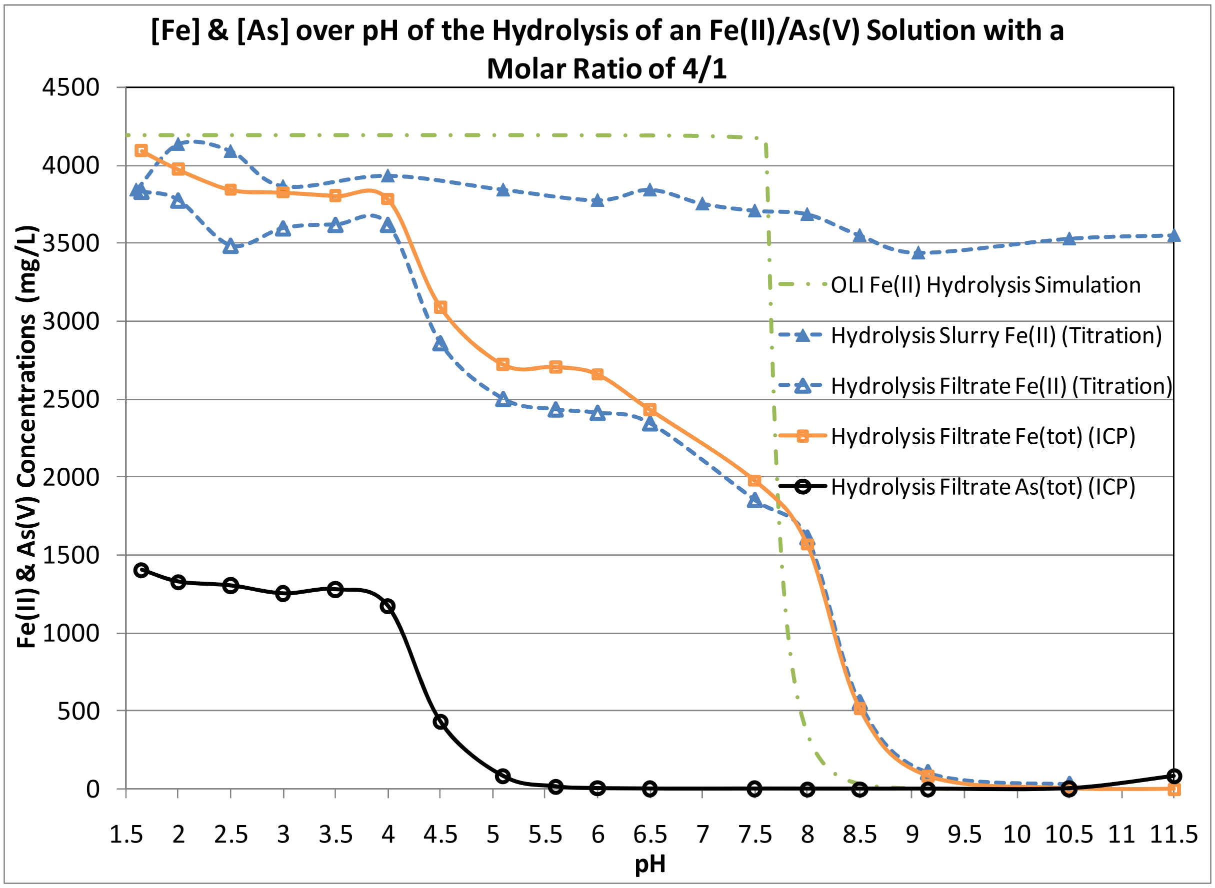

**Figure 31: Hydrolysis of an Fe(II) and As(V) containing solution at a molar ratio of Fe(II)/As(V)=4. Dotted lines show results obtained via Fe(II) titration and solid lines represent total iron analysis using ICP. Filled symbols denote slurry samples while open symbols are for filtered samples (0.2 µm)**

According to the data plotted in Figure 31, As(V) started to precipitate significantly at pH passed 4 and had almost been completely removed from solution after pH 5.5, thereafter remaining out of solution (<0.2 mg/L As(V) over the pH range 7 to 9 (refer to Table 10)) before starting to redissolve at pH> 10.5. By comparison, Fe(II) also followed a similar pattern of removal from solution up to pH 6-6.5 suggesting the precipitation of a ferrous arsenate compound. This is further evident with the data of Table 10. It can be seen that in the pH region 4 to 6.5 the precipitated Fe(II)/As(V) molar ratio was hovering around 1.5, the stoichiometric ratio of ferrous arsenate: $Fe_3(AsO_4)_2$. At pH> 6.5 the remaining soluble ferrous started precipitating and was completely removed from solution past pH 9. The two precipitation events could also be inferred from the pH and ORP curves shown in Figure 32. During constant base addition, distinct inflection points were detected at pH values of 4 and 7 accompanied with complementary ORP inflections[2].

---

[2] Upon reaching pH 11.5 the precipitated slurry was subjected to oxidation via air sparging with pH and ORP decreasing and increasing respectively as shown on Figure 32. The response of arsenic to this oxidation "treatment" is discussed in the Appendix Section 8.3.

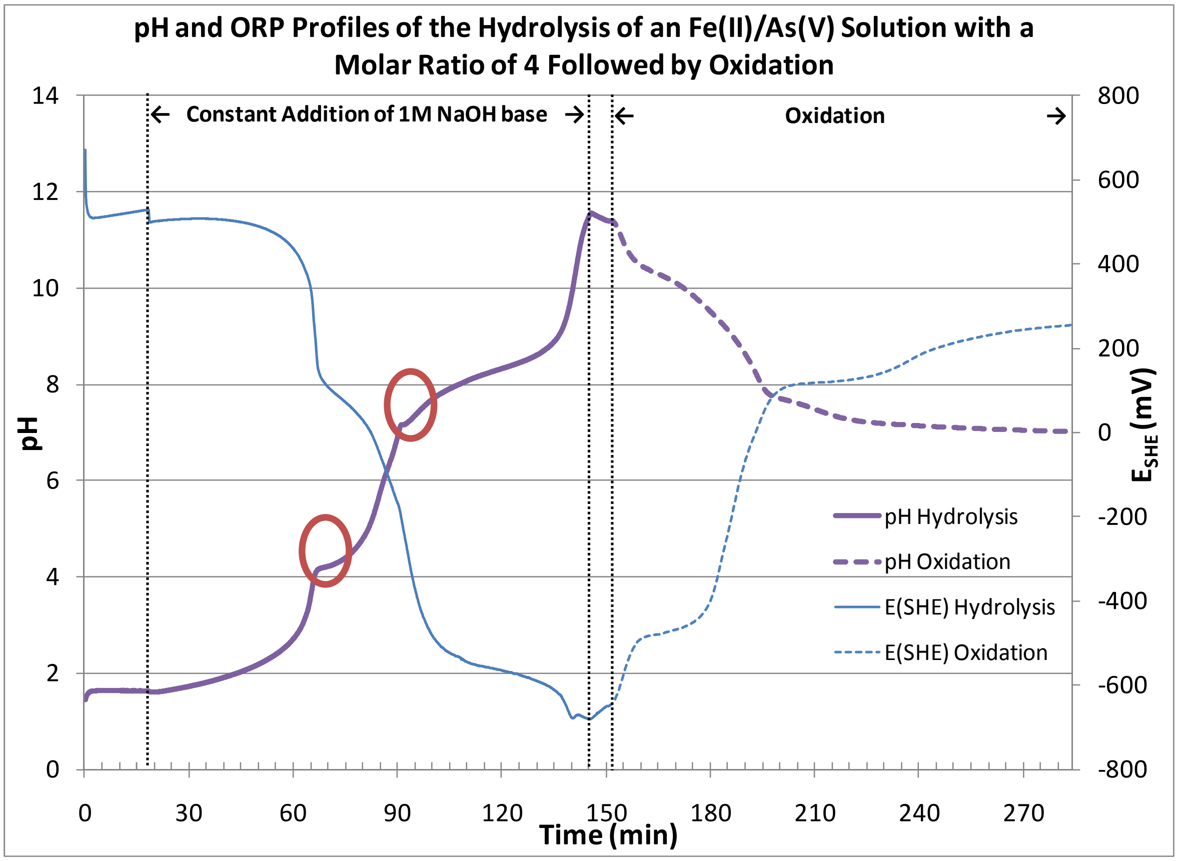

**Figure 32: pH and ORP profiles for the hydrolysis of a solution with an Fe(II)/As(V) molar ratio of 4 with constant 1 M NaOH addition (1.914 mL/min) followed by air oxidation (pH Drift) at 500rpm**

**Table 10: Arsenic concentration in solution and molar ratio of precipitated Fe(II) and As(V) as a function of pH (same conditions as in Figure 32)**

| pH | [As] (mg/L) | Molar Ratio ($[Fe_{ini}]-[Fe_{pH}])/([As_{ini}]-[As_{pH}]$) |
|---|---|---|
| 1.65 | 1404.72 | 0 |
| 2 | 1328.84 | 2.13 |
| 2.5 | 1303.92 | 3.32 |
| 3 | 1252.96 | 2.36 |
| 3.5 | 1279.26 | 3.09 |
| **4** | 1171.49 | **1.79** |
| 4.5 | 430.34 | **1.38** |
| 5.1 | 80.80 | **1.39** |
| 5.6 | 14.86 | **1.34** |
| 6 | 3.39 | **1.37** |
| **6.5** | 0.72 | **1.59** |
| 7.5 | 0.24 | 2.02 |
| 8 | 0.10 | 2.41 |
| 8.5 | 0.03 | 3.41 |
| 9.15 | 0.09 | 3.83 |
| 10.5 | 3.02 | 3.91 |
| 11.5 | 81.21 | 4.15 |

The proposed precipitation of ferrous arsenate over the pH region 4 to 6.5 is supported further when the work of Johnston and Singer [54] is being considered. These authors precipitated symplesite (ferrous arsenate) by raising the pH of an acidic solution (pH=4.5) containing Fe(II) and As(V) at a molar ratio of 2. After drop wise addition of KOH base up to pH 7, the authors noticed the appearance of a white precipitate, which upon analysis gave an Fe-As stoichiometry equal to 1.5 as per Equation (12):

$$3\ \mathrm{Fe}^{2+} + 2\mathrm{HAsO}_4^{2-} \rightarrow \mathrm{Fe}_3(\mathrm{AsO}_4)_{2\,(s)} + 2\mathrm{H}^+ \qquad (12)$$

### 5.2.2 Hydrolysis of Fe(II)/As(V)= 1.65 Solution up to pH 11.3

The targeted Fe/As molar ratio of 1.65 represents the stoichiometric molar ratio (with a 10 % excess ferrous) required to precipitate a ferrous arsenate compound known as symplesite [54]. The solution containing iron in its reduced state, Fe(II), together with arsenic(V) was hydrolyzed by slow constant addition of 1 M NaOH base (0.884 mL/min)[3].

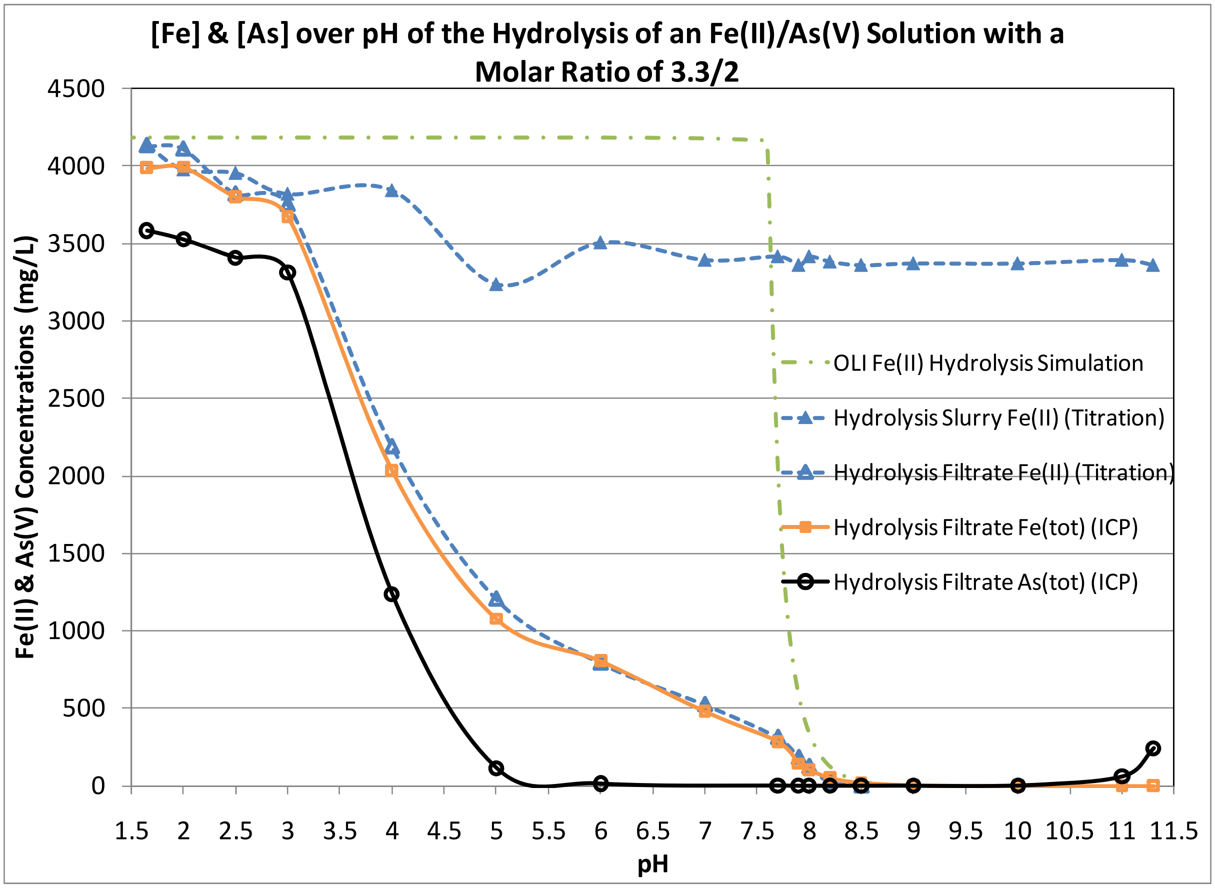

**Figure 33: Hydrolysis of an Fe(II) and As(V) containing solution at a molar ratio of Fe(II)/As(V)=3.3/2 (=1.65). Dotted lines show results obtained via Fe(II) titration and solid lines represent total iron analysis using ICP. Filled symbols denote slurry samples while open symbols are for filtered samples (0.2 µm)**

---

[3] In order to limit the oxidation of ferrous iron, the reactor was once again stirred at 500 rpm and outfitted with a nitrogen sparger and sealed as best as possible with rubber plugs and parafilm wax paper, the latter precaution not used in Section 5.2.1.

The Fe(II) (solution and slurry), Fe(total) and As(V) concentration profiles are shown in Figure 33. The As(V) concentration dropped significantly between pH 3 and 5. At the same time the total iron and ferrous iron in solution, which have identical profiles denoting that essentially all dissolved iron was in fact ferrous, were also significantly decreasing in concentration. This behaviour differs from that of ferrous-only solutions (see Figure 30), thereby indicating once again that arsenic precipitated out from solution with ferrous iron.

**Table 11: Arsenic concentration in solution and molar ratio of precipitated Fe(II) and As(V) as a function of pH (same conditions as in Figure 33)**

| pH | [As] mg/L | Molar Ratio of $([Fe_{ini}]-[Fe_{pH}])/([As_{ini}]-[As_{pH}])$ |
|---|---|---|
| 1.65 | 3583.22 | 0 |
| 2.5 | 3409.05 | 1.44 |
| 3 | 3314.24 | **1.56** |
| 4 | 1235.85 | 1.12 |
| 5 | 114.11 | 1.13 |
| 6 | 13.23 | 1.20 |
| 7 | 0 | 1.31 |
| 7.7 | 0.60 | 1.39 |
| 7.9 | 0.09 | 1.44 |
| 8 | 0 | 1.45 |
| 8.2 | 0.18 | 1.47 |
| 8.5 | 0.02 | 1.49 |
| 9 | 0.04 | 1.49 |
| 10 | 1.71 | 1.49 |
| 11 | 60.09 | 1.52 |
| 11.3 | 242.83 | 1.60 |

Table 11 summarizes the arsenic concentration in solution as well as the molar ratio of precipitated Fe(II) and As(V) at various pH values. First, comparison of the soluble As(V) concentration data with that of the Fe(II)/As(V)=4 test (Table 10) reveals slightly higher values with the lower Fe(II)/As(V) (=1.65) ratio. For example at pH 5 and 6 the corresponding values for high and low ratio were: 81 vs. 114 and 3.4 vs. 13 mg/L As(V) and this despite the slower hydrolysis rate, hence longer retention time adopted in the second test with Fe(II)/As(V)=1.65. This may be a manifestation of the solubility product relationship ($K_{sp}=[Fe(II)]^3[AsO_4]^2$) that predicts lower arsenic concentration for higher ferrous concentration. What is puzzling, however, is the recorded molar ratio of precipitated ferrous and arsenate. Thus according to the presented data in Table 11, in the range up to pH 3 that represents low arsenic precipitation (~7 % at pH 3), the molar ratio coincides with that of the symplesite phase ($Fe_3(AsO_4)_2 \cdot 8H_2O$). However, beyond pH 3, where drastic arsenic precipitation took place, this ratio fell down to approximately 1.15 which is much lower than the anticipated 1.5 ratio corresponding to ferrous arsenate. This may suggest the formation of an Fe/As=~1 compound. But this cannot be ferric arsenate as at least 85% of the precipitated iron was in the ferrous state (refer to data in Figure 33). Alternatively, a metastable Fe/As=~1 ferrous arsenate may be thought to have formed such as $FeHAsO_4$. This though is unlikely since a slower hydrolysis rate was employed that should have led to the most stable ferrous arsenate compound. Moreover, similar to the Fe(II)/As(V)=4 system the ORP and pH profiles (shown in Figure 34) do nonetheless also display inflection points at pH 3.41 and 7.64 (compare with Figure 32). Therefore, despite the observed discrepancy with the precipitated ferrous/arsenate ratio it would be safe to conclude that ferrous arsenate is again the predominant form by which arsenic was removed from solution.

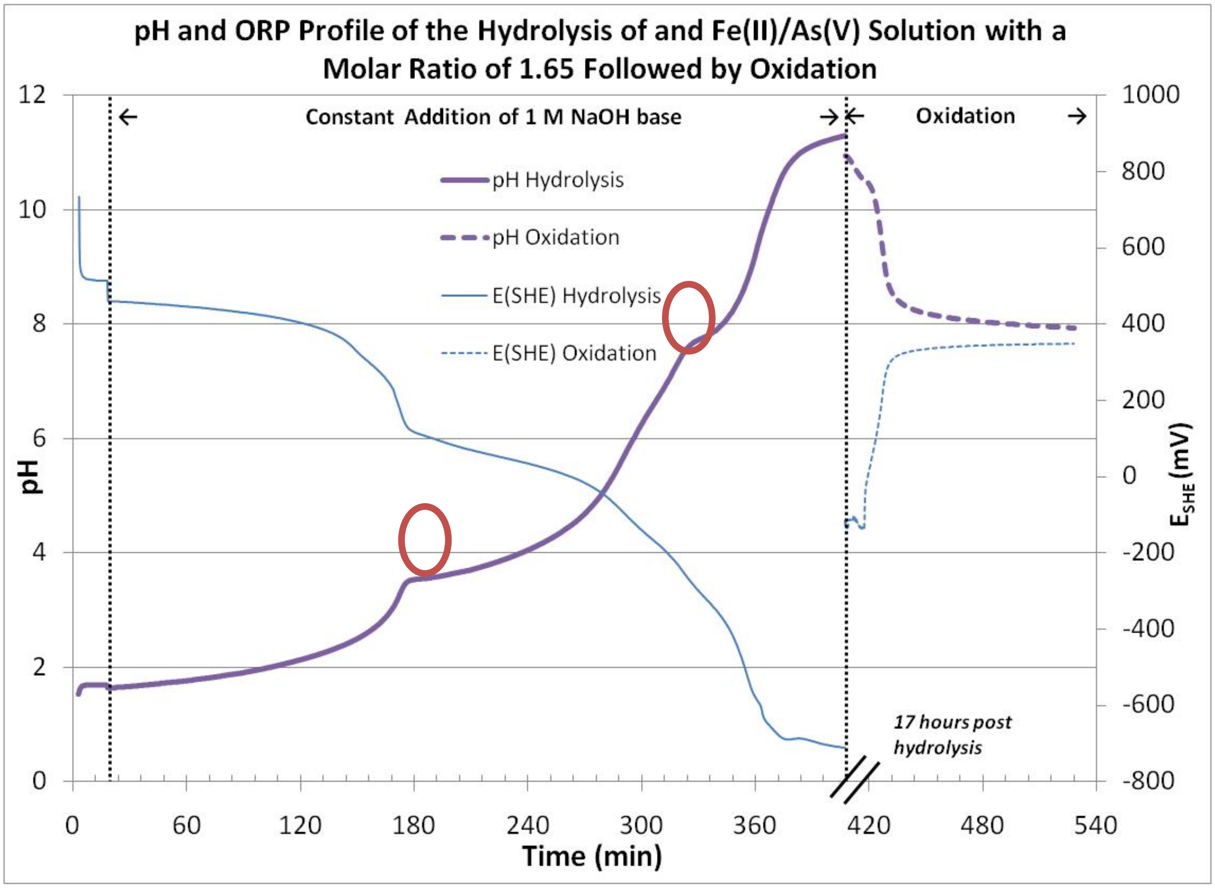

**Figure 34: pH and $E_{SHE}$ profiles for the hydrolysis of a solution with an Fe(II)/As(V) molar ratio of 4 with constant 1 M NaOH addition (0.884 mL/min) and $N_2$ sparging followed by air oxidation (pH Drift) at 500rpm**

## 5.3 Partial Conclusions

Hydrolytic precipitation of ferrous (~4000 mg/L) alone or with arsenate (Fe(II)/As(V)= 1.65 or 4) was carried out via gradual increase of pH. The major findings from this work are:

- As a result of air infiltration promoted by vigorous agitation, a significant part of ferrous oxidized to ferric. However, upon reduction of agitation speed to 500 rpm and proper cover of the reactor the amount of ferrous oxidation was limited to ~10-15 %.

- In the absence of ferric iron or arsenate, ferrous was found to precipitate as ferrous hydroxide mimicking very close theoretical predictions made with the OLI software, namely, essentially all ferrous precipitating out of solution over the narrow pH zone of 7.5 to 8.5. Titration of the ferrous content of solution and slurry gave almost identical results confirming that the bulk of iron reports to precipitate as ferrous.

- In the presence of ferric iron evidence was found of "pre-mature" removal of ferrous from solution at much lower pH than theoretically predicted for ferrous hydroxide. This enhanced precipitation of ferrous could have been due to its adsorption onto precipitated iron(III) hydroxide beyond pH 3 or the formation of a mixed ferrous-ferric hydroxide phase, like green rust (GR II) but this could not be resolved.

- In the case of Fe(II)-As(V) solutions, ferrous arsenate ($Fe_2(AsO_4)_3$) was found to precipitate at pH higher than 3 with the remaining arsenic concentration in solution dropping below 1 mg/L over the pH region 6.5 to 9. This was true for both Fe(II)/As(V) ratios tried, namely 1.65 and 4. In the latter case the excess ferrous precipitated at pH 7 or higher apparently as hydroxide. Beyond pH 10, arsenic was being released back into solution.

# 6 Results and Discussion - Oxidation Studies

In the previous chapter evidence was presented of some oxidation of ferrous iron during its hydrolytic precipitation due to air infiltration. But oxidation may be deliberately applied in an actual coprecipitation system if it involves a lot of ferrous iron. Hence it is of interest to study the oxidation chemistry of ferrous iron in the context of an iron-arsenate coprecipitation process. To this end multiple oxidation experiments (OE) were conducted. These involved the use of different types of impellers, gases, agitation speeds, bases and pH set points in a reactor containing identical starting solutions (See Table 12). The goal of these experiments was to show how these conditions influence the oxidation of total (soluble and precipitated) Fe(II) in the reactor. Subsequently, oxidation experiments containing variable molar fractions of As(V) were carried out to study the coprecipitation behaviour of arsenate during oxidation of Fe(II) to Fe(III). The procedure adopted involved first neutralization of the acidic solution (initial pH ~1.5) containing ferrous iron (~4174 mg/L) either in the absence or presence of arsenic (V) to a target pH value, namely, 4, 6, 8 and 11.5 similar to the hydrolysis tests described in the previous chapter followed by oxidation. In most tests the pH was kept constant during oxidation but some tests were also run at drifting pH during oxidation. All the details are summarized in Table 12. As a result of the adopted procedure, oxidation in most conditions tested involved essentially precipitated ferrous (and not soluble) either as hydroxide or ferrous arsenate/hydroxide slurry.

**Table 12: Summary of oxidation experiments (OE) providing the oxidation conditions and the resulting linear trends of the decreasing total [Fe(II)] over time during gas sparging. Also included in this table are the linear trends of the oxidation of hydrolysis (pH>11.3) experiments (HE) presented in Chapter 5**

| Experiment $OEpH_{ox}$-# | Gas, Flowrate (mL/min) | Impeller Type 5BF / 3BP* | Agitation (rpm) | pH initial | Oxidation pH Set pt./Actual | Base | Linear Equation | R² |
|---|---|---|---|---|---|---|---|---|
| *Oxidation Experiment pH=4, 6 (REACTOR 1)* | | | | | | | | |
| OE4-1 | Air, 500 | 5BF | 1000-2400 | ~3.7 | 4 | 0.5 M $Ca(OH)_2$ | na | na |
| OE4-2 | Oxygen, 500 | 5BF | 1000-2400 | ~3.7 | 4/4.06 | 0.5 M $Ca(OH)_2$ | na | na |
| OE4-3 | Oxygen, 500 | 5BF | 750 | 2.55 | 4/3.78 | 0.5 M $Ca(OH)_2$ | y = -0.90x + 4285.2 | 0.941 |
| OE6-1 | Air, 300 | 5BF | 750 | 3.77 | 6/5.17 | 0.5 M Ca(OH)2 | $y_{in.}$ = -54.19x + 5523.6<br>$y_{f.}$ = -111.56x + 7734.5 | 0.994<br>0.983 |
| *Oxidation Experiment pH=8 (REACTOR 2)* | | | | | | | | |
| OE8-1 | Air, 500 | 5BF | 1000 | 3.70 | 8/7.67 | 0.5 M $Ca(OH)_2$ | na | na |
| OE8-2 | Air, 500 | 5BF | 2000 | 3.70 | 8/7.76 | 0.5 M $Ca(OH)_2$ | y = -242.48x + 762.7 | 0.983 |
| OE8-3 | Air, 300 | 5BF | 750 | 1.58 | 8/8.18 | 0.5 M $Ca(OH)_2$ | y = -88.12x + 2952.9 | 0.951 |
| OE8-4 | Oxygen, 300 | 5BF | 750 | 1.68 | 8/6.59 | 0.5 M $Ca(OH)_2$ | y = -914.33x + 3354.9 | 0.997 |
| OE8-5 | None | 5BF | 750 | 1.32 | 8/7.95 | 0.5 M $Ca(OH)_2$ | y = -12.49x + 3202.6 | 0.925 |
| OE8-6 | Air, 300 | 5BF | 1000 | 1.32 | 8/8.05 | 0.5 M $Ca(OH)_2$ | y = -126.12x + 2484.1 | 0.992 |
| OE8-7 | Air, 300 | 5BF | 500 | 1.47 | 8/8.19 | 0.5 M $Ca(OH)_2$ | y = -29.91x + 3100 | 0.995 |
| OE8-8 | Air, 300 | 3BP | 1000 | 1.5 | 8/8.13 | 0.5 M $Ca(OH)_2$ | y = -38.13x + 3242.2 | 0.977 |
| OE8-9 | Air, 300 | 5BF | 750 | 1.58 | 8/7.77 | 0.5 M NaOH | y = -159.88x + 2740.5 | 0.997 |
| OEDrift-1 | Air, 300 | 5BF | 700-740 | 8.6 | Drift $pH_{F.}$ = 4.37 | 50 w/w NaOH | y = -177.24x + 7319.6 | 0.998 |
| OEDrift-2 | Air, 300 | 5BF | 721 | 8.4 | Drift $pH_{F.}$ = 4.48 | 50 w/w NaOH | y = -198.65x + 7930.8 | 0.997 |
| OEAs-1 Fe/As=3.52 | Air, 300 | 5BF | 500<br>750 | 1.51 | 8/7.88 | 0.56 M NaOH (3.39 mL/min) | $y_{500}$= -51.38 x + 2989.6<br>$y_{750}$= -104.99x + 3487 | 0.999<br>0.997 |
| OEAs-2 Fe/As=1.68 | Air, 300 | 5BF | 500<br>750 | 1.48 | 8/7.94 | 1 M NaOH (1.88 mL/min) | $y_{500}$= -75.95x + 3507.1<br>$y_{750}$= -166.42x + 4354 | 1.000<br>0.986 |
| *Post Hydrolysis Oxidation (pH Drift)* | | | | | | | | |
| HEFe-1 | Air, 300 | 5BF | 500 | 11.54 | Drift $pH_{F.}$ = 11.30 | 0.56 M NaOH (3.34 mL/min) | y = -39.82x + 2903.4 | 0.990 |
| HEFe-2 | Air, 300 | 5BF | 500 | 11.54 | Drift $pH_{F.}$ = 11.09 | 0.56 M NaOH (3.08 mL/min) | y = -29.78x + 2957.8 | 0.996 |
| HEAs-1 Fe/As=3.91 | Air, 300 | 5BF | 500<br>750 | 11.3 | Drift $pH_{F.}$ = 7.95 | 1 M NaOH (0.88 mL/min) | $y_{500}$= -40.21x + 3350.7<br>$y_{750}$= -194.28x + 4881 | 0.991<br>0.998 |
| HEAs-2 Fe/As=1.49 | Air, 300 | 5BF | 500 | 11.5 | Drift $pH_{F.}$ = 7.02 | 1 M NaOH (1.91 mL/min) | y = -656.74x + 3551.7 | 1.000 |

* 5BF = Five Blade Flat impeller; 3BP = Three Blade Pitched impeller

## *6.1 Analysis of a Typical Oxidation Experiment at Constant pH*

Before the effects of the various process parameters on ferrous hydroxide/arsenate oxidation are presented it is considered appropriate to describe/analyze in detail one of these tests. The test chosen for description is OE-8-7 that involved oxidation of ferrous hydroxide at constant pH 8.

As can be seen in Figure 35, the automated controlled constant base (0.5 M $Ca(OH)_2$) addition to the starting solution to raise the pH from 1.47 to 8 took 20 minutes. This ramp-up to pH 8 was equivalent to a hydrolysis test as described in the previous chapter, which resulted in the bulk of ferrous iron to precipitate as ferrous hydroxide (refer to Figure 30). The reactors were covered by a lid containing a rubber o-ring, however no nitrogen sparging was used or any other measures to limit air infiltration. Upon reaching pH 8, oxidation was started via constant flowrate air sparging. The average pH between the onset of air sparging and the end of oxidation (later determined by titration) for this test was 8.19. The start of oxidation was marked by a slight simultaneous drop in pH and increase in $E_{SHE}$. The end of total (involving soluble and precipitated forms) Fe(II) oxidation was marked by an increase in ORP and the total stabilization of pH signalling no further reaction and consequently the discontinuation of automatic base addition.

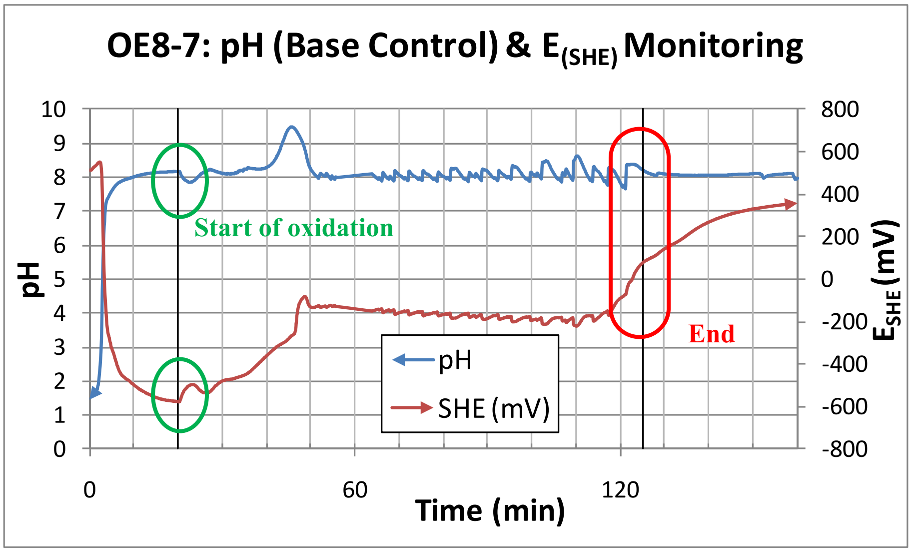

**Figure 35: Variation of pH and $E_{SHE}$(mV) during oxidation test OE8-7. Vertical lines denote the start and end of Fe(II) oxidation**

The corresponding oxidation curve for the conversion of ferrous to ferric upon air sparging at pH 8 is shown in Figure 36. The ferrous concentration data were obtained by titrating slurry samples for total (soluble and precipitated) Fe(II) at different time intervals. The starting Fe(II) concentration was 4233 mg/L and dropped to approximately 3100 mg/L (~14 % drop) over the course of the 20 minute ramp-up to pH 8. This significant loss in ferrous iron, observed to range between 14-35 % for most experiments, likely represents the portion of Fe(II) that was oxidized (by air infiltration as no air sparging had been provided in this part of the experiment) to form a green precipitate known as green rust [44]. Green rust is a mixed valence iron compound with the typical formula $Fe(II)_4Fe(III)_2(OH)_{12}SO_4 \cdot nH_2O$ [68]. The bulk of the remaining ferrous just before air sparging commenced, can be thought to be in the form of precipitated ferrous hydroxide, judging from the data presented in the previous chapter (Figure 30). Nonetheless there is a clearly linear oxidation of slurry Fe(II)[4] with time (constant rate): $y = -29.91x + 3100$ ($R^2 = 0.995$) true for all tests (refer to Table 12). The linear plot suggests that the oxidation of ferrous is most likely controlled by oxygen mass transfer at the gas/liquid interface. This is confirmed in the next section.

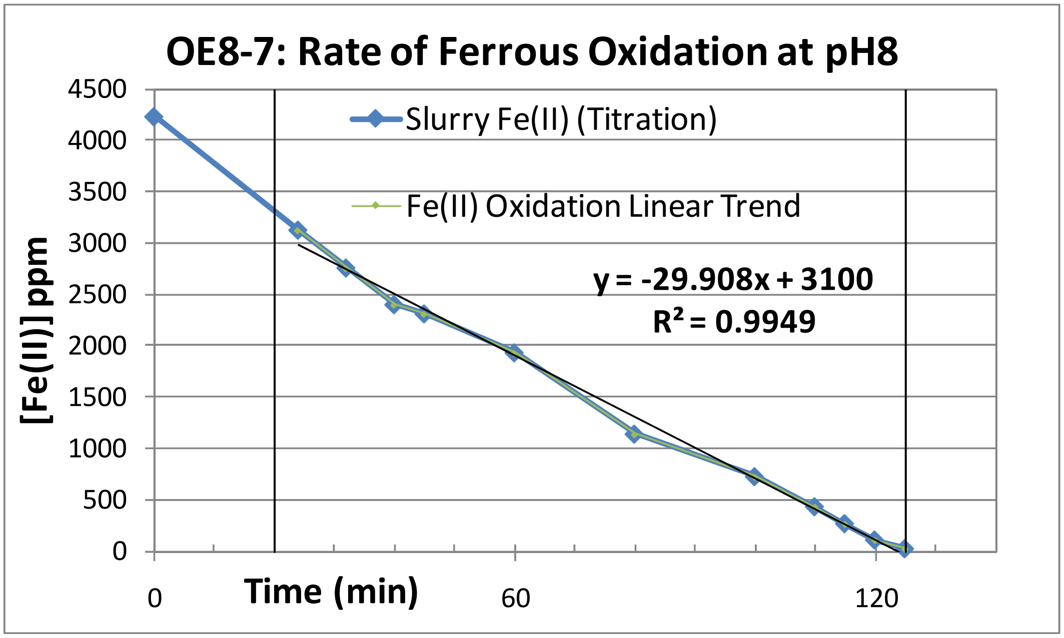

**Figure 36 Linear conversion plot representing the oxidation of total Fe(II) by gas sparging at pH 8. Conditions were as follows: 500 rpm agitation, 300 mL/min air flow rate, 5BF impeller, 0.5 M $Ca(OH)_2$, constant pH 8 oxidation**

During the oxidation experiments, color changes were recorded that are consistent with those observed by Lin *et al.* [44] going from green, dark green, blue, greenish-yellow to finally orange-yellow. These color changes most likely reflect gradual formation and transformation of ferrous hydroxide and green rust to ultimately some form of poorly crystalline FeOOH [44].This type of transformation sequence may also be inferred from the $E_h$ variations during the experiment

---

[4] Given the propensity of ferrous to undergo spontaneous oxidation especially if products are removed from solution, measures were taken to carefully preserve collected samples prior to analysis by titration. Thus, slurry samples collected in test tubes were never kept longer than 24 hrs in a 4 °C fridge before Fe(II) analysis by titration.

(Figure 35). Thus in terms of $E_h$ it is interesting to note that precipitation of ferrous during the ramp-up period resulted in a dramatic drop of $E_h$ from ~500 mV at pH ~1.5 to -500 mV at pH ~8. This was followed upon air sparging to an increase of $E_h$ to -200 mV plateau until oxidation was complete thereafter increasing gradually to near 400 mV. These $E_h$ changes are consistent with the oxidation pathways determined by Ruby *et al.* [45] as depicted in the $E_h$-pH diagram of Figure 37. When plotting the experimental pH and $E_h$ values (pH8, -490 mV) of OE8-7 just before the start of oxidation (see Figure 35) onto Figure 37, the point falls exactly on the intersection of the lines (3), (4) and (8) representing the equilibrium conditions of the couples $Fe^{2+}$/GRII, $Fe^{2+}/Fe(OH)_2$, $Fe(OH)_2$/GRII respectively. This shows that these species are in equilibrium as predicted by this Pourbaix diagram [45]. During oxidation between times 20-50 min, it is interpreted that $Fe(OH)_2$ oxidized to form GRII. Throughout this time, the $E_h$ and pH values drifted across the GRII equilibrium region bound by equilibrium lines (3), (6) and (8). Subsequently, between times 50-115 min, the pH was forced to remain constant at pH 8 and the corresponding $E_h$ was ~ -170 mV. This point lands on line (6), corresponding to the equilibrium couple GRII/γ-FeOOH thereby confirming the species present during oxidation are indeed GRII and lepidocrocite, with the former slowly oxidizing into the latter final product. The end product of oxidation, lepidocrocite, was confirmed via XRD analysis.

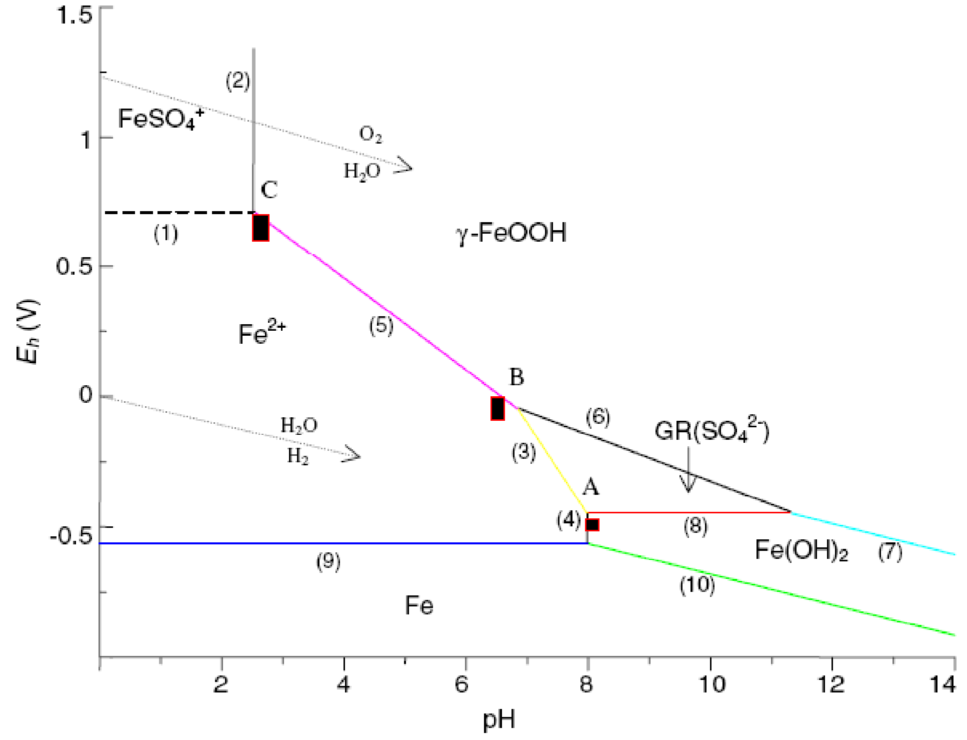

**Figure 37: $E_h$-pH diagram taken from Ruby *et al.* [45] explaining the variation of potential with pH as a result of the precipitation/oxidation of different iron oxy-hydroxide species**

For additional information about the interaction between the Pourbaix diagram and $E_h$ and pH curves consult Appendix Section 8.4.

## 6.2 Effects of Agitation Speed, Impeller Type, Gas Type, Base and pH

As reported in the previous section, the oxidation of precipitated ferrous (either as ferrous hydroxide or green rust or a mixture of the two) followed constant rate kinetics indicative of oxygen mass transfer control. To obtain further insight into the kinetics of the oxidation process several experiments were carried out following a similar procedure with the one described in the previous section. All tests generated linear kinetic equations as summarized in Table 12. The effect of the various parameters is discussed with the help of linear plots of these equations as presented in Figure 38.

### 6.2.1 Kinetic Plots

Figure 38 compares the rates of ferrous oxidation (as a qualitative measure) of matching experiments having one changed variable. As anticipated from the literature review presented in Chapter 2, using pure oxygen over air, increasing agitation speed, increasing pH and changing from a three blade pitched impeller (axial type) to a five blade flat impeller (radial type, specifically designed to enhance gas-liquid mass transfer [69]), all improved the rate of ferrous oxidation.

It was also found that using a more potent base for pH control, such as 0.5 M NaOH versus 0.5 M $Ca(OH)_2$, increased the oxidation rate (sodium hydroxide exhibits a strong concentration gradient immediately after being contacted in a solution whereas slaked lime has a slower rate of dissolution [8]). It should be mentioned however that base addition using NaOH was done manually whereas $Ca(OH)_2$ was done automatically. Furthermore, it was found that the presence of arsenic as well as increasing the fraction of arsenic to ferrous iron in the starting solution accelerated oxidation, a rather unexpected result. Although this may have to do with the complexation of ferrous with arsenate anions below $pH<7$ [70] further work would need to be undertaken to provide a better understanding-explanation for this effect.

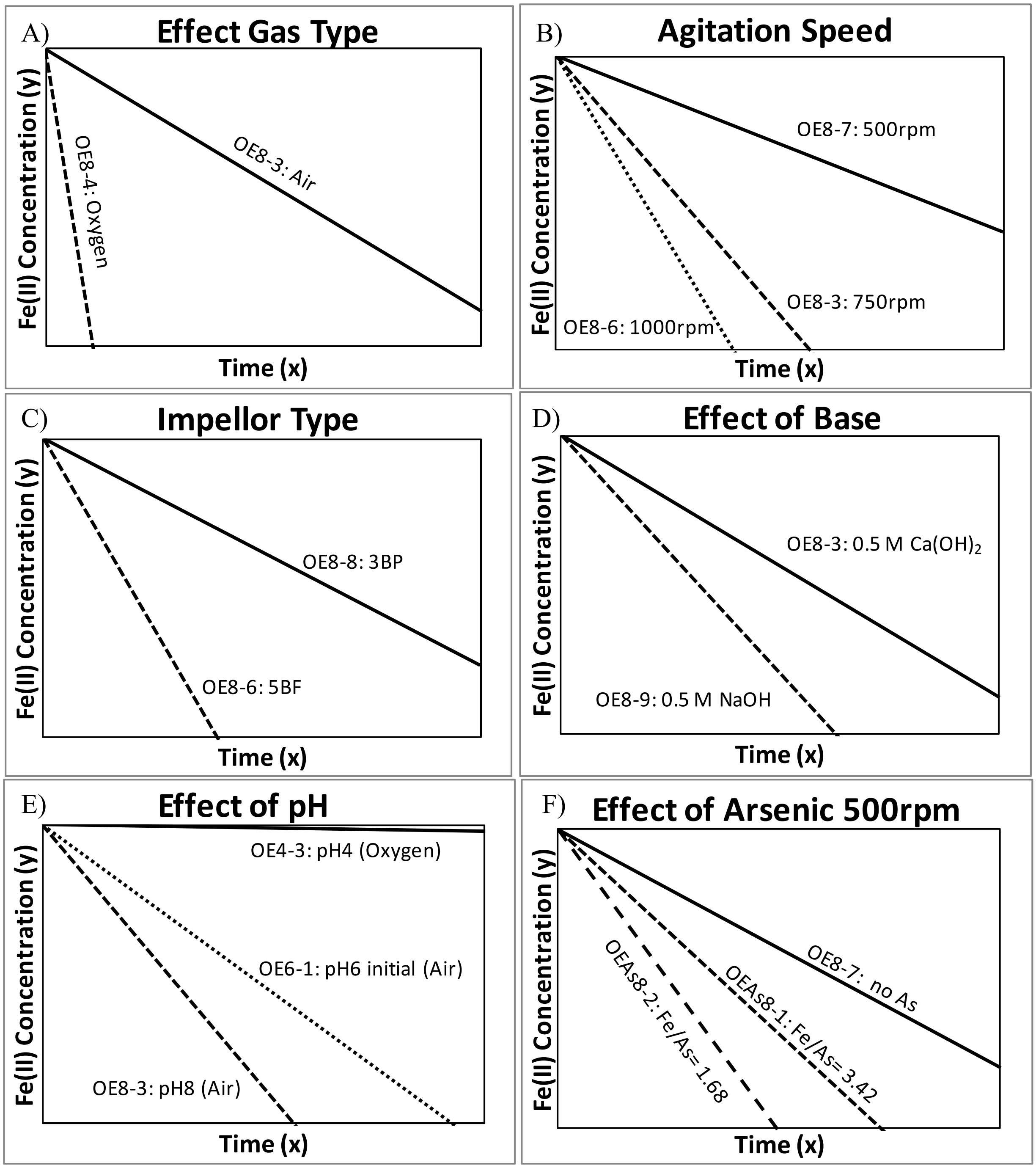

**Figure 38: Presentation of various kinetic plots comparing normalized slopes of ferrous concentration vs. time for experiments with the same conditions apart from the one being examined: A) effect of gas type, B) effect of agitation, C) effect of impeller (3 blades flat vs. 5 blades pitched), D) effect of base, E) effect of pH (note: pure oxygen was used at pH 4), F) effect of arsenic (note: OE8-7 used $Ca(OH)_2$ base instead of NaOH; all conditions and equations are given in Table 12)**

### 6.2.2 Mechanistic Aspects

As the results have shown, oxygen mass-transfer kinetics were apparently controlling the overall oxidation process. The most important parameters describing the mass-transfer kinetics are the mass-transfer coefficient, $k_L$, and the specific gas-liquid interfacial area, $a$, expressed per unit volume of gas-liquid mixture. It is known that this coefficient is dependent on the hydrodynamic conditions around the gas-liquid interface and that the specific surface area is influenced by the mixing conditions in the reactor [38].

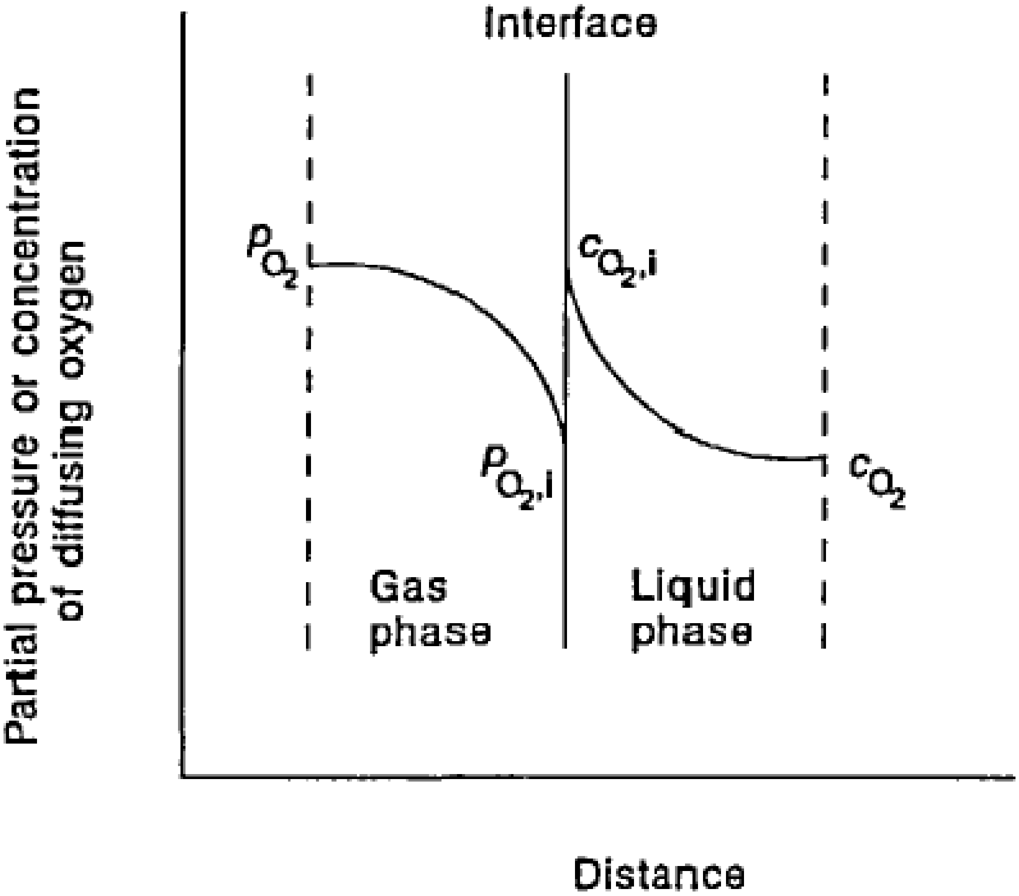

Figure 39: A sketch of the gas-liquid interface and the variation of $pO_2$ and $cO_2$ across it [38]

The difference in chemical potential of oxygen between the gas and liquid phase is the driving force for mass-transfer. Therefore, we can apply Fick's first and second laws of diffusion to express the mass-transfer coefficient. Figure 39 shows that on the gas side of the interface a partial pressure gradient develops and likewise, on the liquid side of the interface, a concentration gradient develops. For instance, the rate of oxygen mass-transfer per unit interfacial area across the liquid side of the interface ($J_L$) can be written as:

$$J_L = k_L(C_{O_2,i} - C_{O_2}) \tag{13}$$

Where $C_{O_2,i}$ is the concentration of oxygen at the interface, $C_{O_2}$ is the concentration of oxygen at the bulk of the solution and $k_L$ is the liquid side mass-transfer coefficient. Therefore, the expression for the molar flux per unit liquid-phase volume per unit volume of gas-liquid mixture derived from the overall mass transfer becomes:

$$J = k_L a\left(C^*_{O_2} - C_{O_2}\right) \tag{14}$$

Based on the literature review of this thesis, the reaction of ferrous iron as a hydrolyzed ferrous hydroxide slurry with oxygen appears to occur rapidly. At a constant pH of 8, if ferrous hydroxide oxidizes as soon as dissolved oxygen is present, the rate limiting step is the transfer of oxygen from the gas phase, $O_{2(g)}$, across the gas-liquid interface into the liquid phase, $O_{2(aq)}$, represented by Equation (15):

$$O_{2(g)} \rightarrow O_{2(aq)} \tag{15}$$

Immediately following that, the reaction of oxygen with ferrous hydroxide proceeds as given by Equation (16):

$$Fe(OH)_2 + \frac{1}{4}O_2 + \frac{1}{2}H_2O \rightarrow Fe(OH)_3 \tag{16}$$

As shown in the previous section (Figure 38), the plots of total ferrous concentration over time for all oxidation experiments at pH 8 yielded a linear curve consistent with oxygen-mass transfer control. However, when looking at the results for the oxidation experiment at pH 6 (Figure 40) we notice a sigmoid curve rather than the typical linear relationship seen for pH 8 OE's.

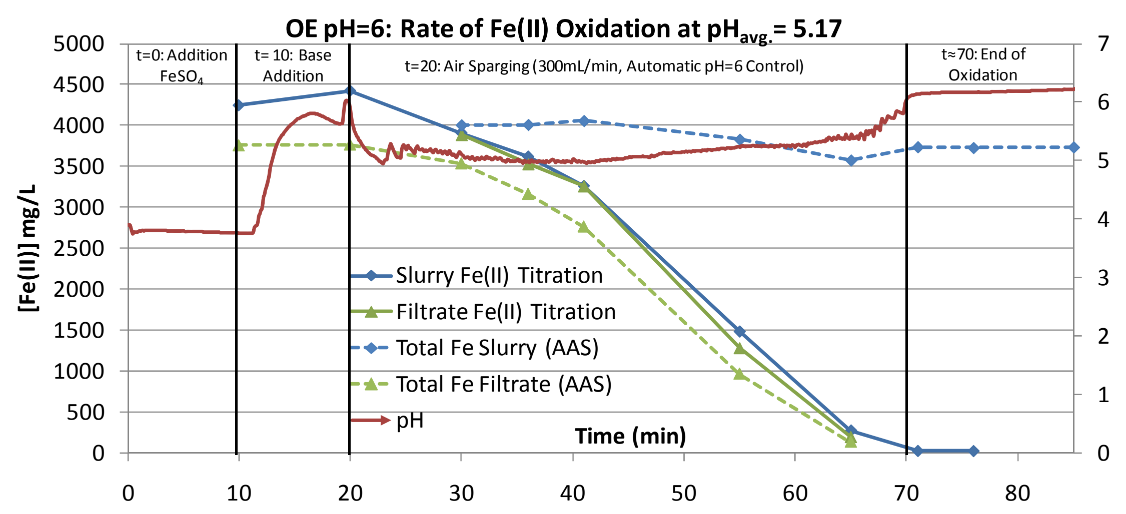

**Figure 40: Sigmoid curve for the oxidation of total Fe(II) at pH=6 by gas sparging. Conditions were as follows: 750 rpm agitation, 300 mL/min air flow rate, 5BF impeller, 0.5 M Ca(OH)$_2$, pH 6 set-point**

If the oxidation curve is separated into two more or less distinctive linear regions (basically a simplified way of dissecting a non-linear curve), namely between t=20-41 and t=41-70, two significantly different linear slopes of $m_{in.} = -54.19$ and $m_{f.} = -111.56$ respectively are obtained. It is apparent that the mechanism of oxidation of ferrous iron at pH 6 is more complex than the one (of simple mass transfer control) at pH 8. It is suggested that in the case of pH 6 the initial slow oxidation step[5] corresponds to the oxidation of soluble ferrous ions to ferric hydroxide (produced as result of immediate hydrolysis of formed ferric ions). Upon significant formation of ferric hydroxide owing to the sorption capacity of the latter, the remaining soluble $Fe^{2+}$ species ions adsorb on it resulting in an autocatalytic effect on the oxidation of ferrous as proposed by Tamura *et al.* [36] and represented by Equation (17) (this constituting the second fast part of the reaction).

$$Fe^{2+} + Fe(OH)_3 \cdot H^+ \rightleftharpoons Fe^{2+}_{ad} \cdot Fe(OH)_3 + H^+ \tag{17}$$

Finally, the oxidation of dissolved ferrous iron at pH 4 has been experimentally shown to occur very slowly. Thus even when pure $O_2$ was substituted for air at an agitation of 750 rpm, there was less than 5 % of the initial [Fe(II)] oxidized after over 3.5 hrs of sparging. At this or lower pH the oxidation of ferrous iron requires elevated temperature and oxygen pressure [38, 71-74].

### 6.2.3 Calculations

As was seen in the previous section, it is possible to show the effects of various parameters on the rate of oxidation of ferrous hydroxide and/or GRII by plotting the linear curves of the depletion of total ferrous iron over time. In addition to this, we may calculate the efficiency of the oxidation during the linear portion of the reaction by comparing the number of moles of oxygen used versus the actual stoichiometric number of moles consumed during the reaction according to Equation (18).

$$Fe^{2+} + \frac{1}{4}O_2 + H^+ \rightarrow Fe^{3+} + \frac{1}{2}H_2O \tag{18}$$

Equation (18) reveals that for every mole of ferrous iron oxidized, a quarter mole of oxygen is required. Knowing the sum of ferrous iron oxidized during a specific time interval we may subsequently calculate the theoretical amount of oxygen consumed and determine the efficiency of the reaction by comparing this value with the actual number of moles of oxygen supplied at a constant gas flow rate.

---

[5] It should be clarified here that the plot evaluating the effect of pH on the rate of oxidation in Figure 38 (E) contains the initial slope of OE6.

The results are shown in Table 13 whereby the calculations where made using the ideal gas constant (R=8.314 J/mol K) and ambient temperature and pressure.

**Table 13: Consumed ferrous iron during sparging, amount of oxygen used during oxidation and calculated oxidizing efficiencies**

| Exp. | Agitation (rpm) | Gas | Blade Type | $[Fe]_{sp.\ in.}$ mg/L | $[Fe]_{sp.\ f.}$ mg/L | $Time_{sp}$ (min) | $O_2$ Flow Rate (mL/min) | $V_{O2}$ ($E^{-3}$ $m^3$) | $nO_2$ (moles) used | $nFe^{2+}$ (moles) oxidized | %Eff. |
|---|---|---|---|---|---|---|---|---|---|---|---|
| OE8-3 | 750 | Air | 5BF | 3294.9 | 102.8 | 35.0 | 62.85 | 2.20 | 0.090 | 0.057 | 15.9 |
| OE8-4 | 750 | $O_2$ | 5BF | 3339.5 | 42.4 | 4.0 | 300.00 | 1.20 | 0.049 | 0.059 | 30.1 |
| OE8-5[a)] | 750 | None | 5BF | 3202.6 | 2390.2 | 60.0 | na | na | na | 0.015 | na |
| OE8-6[b)] | 1000 | Air | 5BF | 2390.2 | 23.5 | 20.0 | 62.85 | 1.26 | 0.051 | 0.042 | 20.6 |
| OE8-7[c)] | 500 | Air | 5BF | 3100.0 | 23.5 | 105.0 | 62.85 | 6.60 | 0.270 | 0.055 | 5.1 |
| OE8-8 | 1000 | Air | 3BP | 3540.6 | 44.7 | 87.5 | 62.85 | 5.50 | 0.225 | 0.063 | 7.0 |
| OE8-9 | 750 | Air | 5BF | 2792.3 | 48.0 | 20.0 | 62.85 | 1.26 | 0.051 | 0.049 | 23.9 |
| OEDrift-1 | 700-740 | Air | 5BF | 3708.1 | 524.9 | 18.0 | 62.85 | 1.13 | 0.046 | 0.057 | 30.8 |
| OEDrift-2 | 721 | Air | 5BF | 3931.5 | 480.3 | 18.0 | 62.85 | 1.13 | 0.046 | 0.062 | 33.4 |
| OEAs-1* | 750 | Air | 5BF | 2479.5 | 390.9 | 20.0 | 62.85 | 1.26 | 0.051 | 0.037 | 18.2 |
| OEAs-2* | 750 | Air | 5BF | 2747.6 | 1083.4 | 10.0 | 62.85 | 0.63 | 0.026 | 0.030 | 29.0 |

[a)] $[Fe]_{sparging}$ estimated with trendline since t=0 digestion not reliable, [b)] $[Fe]_{initial}$ estimated using OE8-5 trendline at t=40 min, [c)] $[Fe]_{sparging}$ estimated with trendline since t=0 sample not taken, * $[Fe]_{sp.\ t=10}$ since first 10 minutes 500 rpm agitation was used

Table 13 contains useful information that appears to be in agreement with the observations made in Section 6.2.1. It confirms that using pure oxygen (OE8-4) as opposed to air (21 % $O_2$ – OE8-3) is nearly twice as effective even at the same gas flow rate. Moreover, the efficiency increases with increasing agitation speed (5.1 %, 500 rpm < 15.9 %, 750 rpm < 20.6 %, 1000 rpm) as discussed earlier. Also, the use of the five blade flat impeller (5BF) which enhances gas-liquid mass transfer proved to be more efficient (20.6 %) than using a three blade pitched impeller (7 %).

In the case of drift oxidation experiments, the two repeat experiments showed very similar oxidation efficiencies at 30.8 % and 33.4 % even when considering the slight discrepancy in the rate of agitation. Once again these results signify good reproducibility. Finally, when comparing the constant pH 8 oxidation of ferrous solutions containing variable arsenic concentrations (discussed later) we noticed an increasing oxidation efficiency with increasing initial arsenic content.

## *6.3 Ferrous Oxidation at Drifting pH*

In addition to oxidation experiments carried out at constant pH, tests were conducted whereby the pH of the solution was allowed to drift during oxidation (refer to section 3.3.2) hence allowing interesting insight into the reaction mechanism. Two series of tests were run. The first one at initial pH ~8.5 and ratio R=[Fe(II)]/$[OH^-]$ of 0.583 (7/12) and the second at initial pH 11.5.

### 6.3.1 Oxidation at Initial [Fe(II)]/$[OH^-]$ of 0.583 Corresponding to pH ~8.5

The ratio R=0.583 was selected based on the investigations by Olowe and Génin [75] and Lin *et al.* [44] who used a similar ratio to study the oxidation of ferrous hydroxide in slightly basic solutions (pH 8.2). Similar to the work of these authors, the pH and $E_h$ were monitored during the course of the oxidation of ferrous sulphate and correlated to changes in the composition of the precipitated phases. The pH and $E_h$ profiles for both drift experiments at R=0.583 (initial pH ~8.5, refer to Table 12) are shown in Figure 41. Prior to the initiation of oxidation for experiments OEDrift-1 & 2, a calculated amount of NaOH ([Fe(II)]/$[OH^-]$=0.583) was added at once to the solution thereby immediately increasing the pH to 8.6 and 8.4 respectively. A few minutes (3-6 min) after the initiation of air sparging an apparent rise in pH (see arrow) occurred. Moreover, it was noticed that throughout the oxidation period (from the onset of air sparging) there were other inflection points and pH plateaus, namely at pH ~7 and ~4.5 (final). At the same time the $E_h$ was shown to drop to -550 mV upon rise of pH to 8.5 thereafter increasing in a ladder form during oxidation finally reaching the terminal value 400-450 mV. In other words, the $E_h$ exhibited a similar behaviour as observed with the constant pH oxidation tests of the previous section.

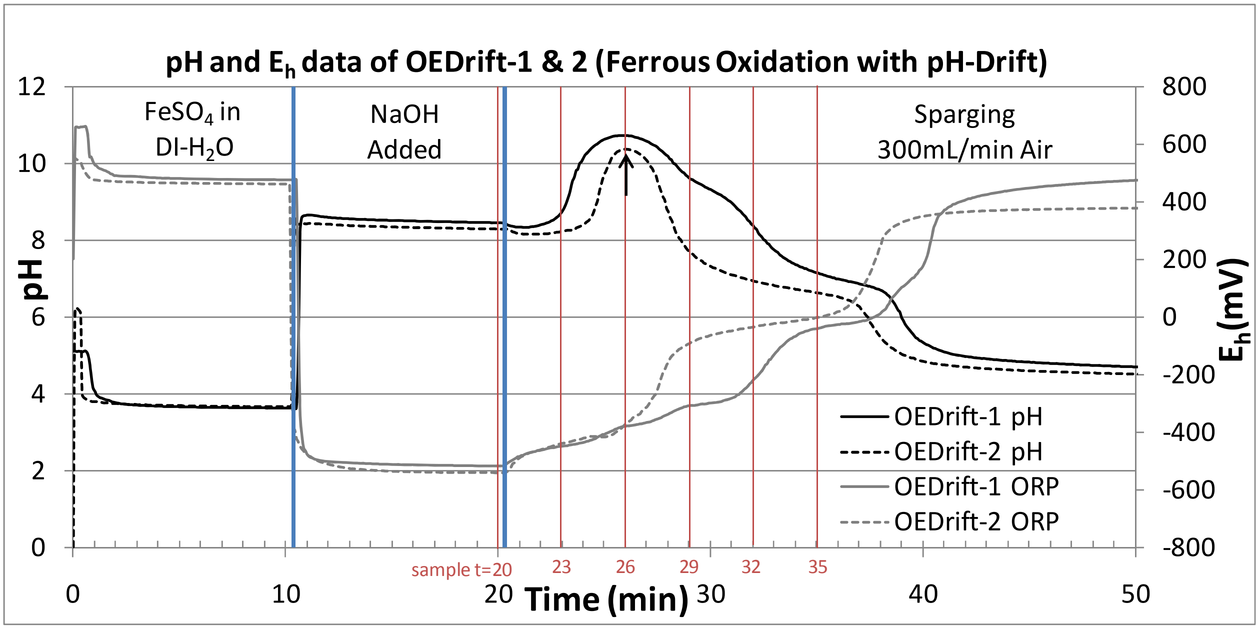

**Figure 41: pH and $E_h$ profiles of ferrous sulphate oxidation at drifting pH (OEDrift-1 & 2). The arrow represents the pH jump and the red vertical lines represent the times of sampling**

The associated precipitation-oxidation behaviour of ferrous hydroxide is illustrated in Figure 42. As it can be seen the bulk of ferrous (>90 %) had precipitated (apparently as ferrous hydroxide) prior the onset of oxidation thereafter converting to ferric iron at a constant rate (linear plot). The constant rate oxidation is consistent with the mass transfer control mechanism discussed in the previous section.

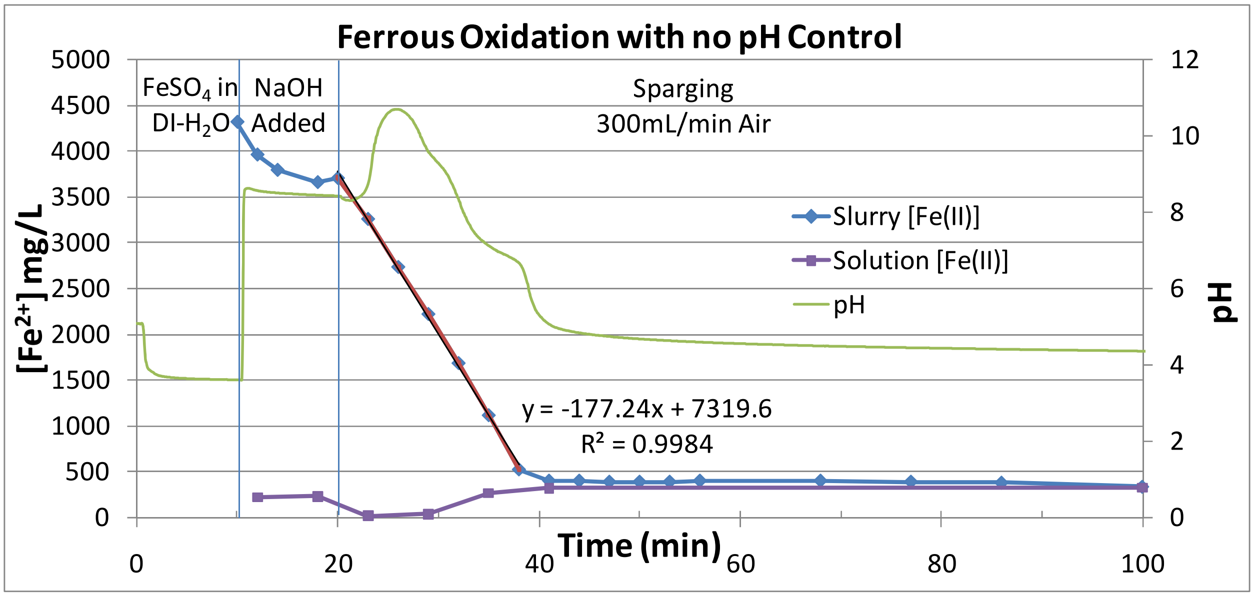

**Figure 42: Variation of [Fe(II)] in slurry and solution during the OEDrift-1 oxidation test ($[Fe(II)]/[OH^-]=0.583$)**

The jump in pH (See arrow in Figure 41) is attributed to the enrichment of the solution with $OH^-$ by the intermediate formation of GRII ($Fe(II)_4Fe(III)_2(OH)_{12}SO_4 \cdot nH_2O$) from the oxidation of $Fe(OH)_2$ at $0.5 \le R \le 0.58$ as discussed and reported by Olowe and Génin [70]:

$$7Fe(OH)_2 + SO_4^{2-} + \frac{1}{2}O_2 \rightarrow GRII + H_2O \quad + 2OH^- \tag{19}$$

Going back to the pH curve of Figure 41, after the initial pH rise there is a pH decrease (going through an initial plateau at pH 7 and a final one at pH ~4.5) due to acid generation arising apparently from the oxidation of the intermediate GRII phase into the final ferric oxyhydroxide phase (goethite):

$$Fe(II)_4Fe(III)_2(OH)_{12}SO_4nH_2O + O_2 \rightarrow 6FeOOH + H_2SO_4 + (n+2)H_2O \tag{20}$$

The above transformation reaction may involve other intermediate steps as evident by the intermediate plateau of pH 7 and the detection of magnetite in an intermediate product as reported in Figure 43.

#### 6.3.1.1 Characterization of Oxidation Products

The oxidation products for OEDrift-1 are shown in Figure 43 as a function of oxidation time. At the onset of oxidation (t=20) it was expected to find a mixture of $Fe(OH)_2$ and GRII (some GRII was suspected to have had already formed prior to air sparging due to the decrease (~10-15 %) in total [Fe(II)] between t=10-20 min). However, instead, lepidocrocite ($\gamma$-FeOOH) was found, which is suspected to be the result of the fast oxidation of the ferrous phase solids upon extraction from the reactor for characterization and hence is not considered a true representative. Between t=26 and t=29 min the formation of well defined magnetite ($Fe_3O_4$) appears after which the crystallinity of the product declines[6] with further oxidation. During sampling, it was observed that the oxidation slurries responded to a permanent magnet confirming the presence of magnetite. As oxidation continues past t=38 min, goethite is the only solid phase left in the slurry as shown by the final XRD pattern. The final product of oxidation for OEDrift-2 was also goethite (not shown). The final goethite products of pH drift oxidation experiments are consistent with the results by Olowe and Génin [75] for an initial $FeSO_4$/NaOH R ratio of 0.58.

---

[6] There are two possible explanations for the decrease in crystallinity of magnetite with time. The first can be attributed to continuous air sparging and agitation for over an hour after all of the intermediate phase (GRII) was oxidized. This prolonged contact time affected the crystallinity and magnetic properties by destroying the incipient ferrous-ferric framework by consumption of ferrous iron followed by subsequent hydrolysis of amorphous iron(III) precipitates [43]. The second was that the samples, which underwent characterization, changed during sample handling. To explain this further it is worth looking at Figure 43 and noticing the times of sampling marked by vertical lines. According to the discussion about the different reaction stages above, the sample at t=26 min was at the height of the transformation of $Fe(OH)_2$ into GRII (Equation (19)), yet the XRD scan provided us with crystalline magnetite. Following that, the samples taken between t=29 and 35 min should have all contained a decreasing fraction of GRII and an increasing fraction of the final ferric oxyhydroxide phase (theoretically - goethite). Therefore it is suggested that each XRD represents an oxidized version of the real sample taken, where the crystallinity of the product was a side effect that depended on the rate of oxidation of the GRII or $Fe(OH)_2$ fraction of the sample. Misawa *et al*. [42] suggests that fast aerial oxidation of an intermediate green complex results in lepidocrocite and that slower oxidation by air results in magnetite. Given that $Fe(OH)_2$ is more sensitive than GRII to air oxidation, it is reasonable to assume that samples at t=20-23 min contained mostly $Fe(OH)_2$ and therefore were reported as lepidocrocite, whereas samples at t=26-35 min contained decreasing amounts of GRII, which oxidized as crystalline magnetite. As the end of the first plateau was reached it (t=35-38 min), we would have expected to find mostly goethite with traces of GRII, which in this case reports as magnetite. If we carefully look at Figure 45, magnetite peaks are noticeable for samples t=32 & 35 min. The final samples at t=100 reported as goethite.

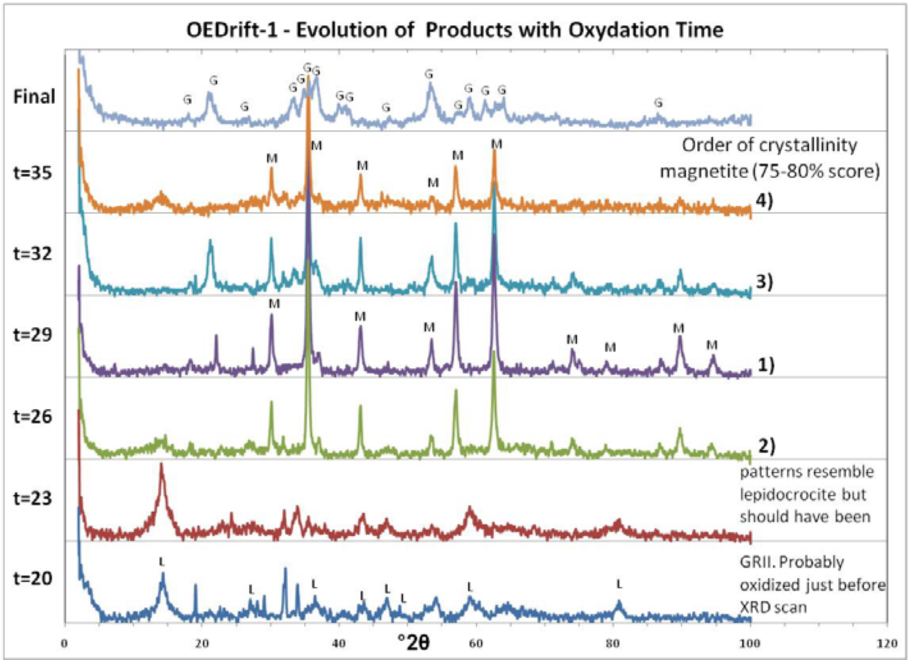

| Magnetite |
|---|
| JCPDS Card# 00-019-0629 |
| 2Theta |
| 30.10 |
| 35.42 |
| 43.05 |
| 53.39 |
| 56.94 |
| 62.52 |
| 73.95 |
| 78.93 |
| 89.62 |
| 94.43 |

**Figure 43: XRD patterns documenting the evolution of phases as a function of oxidation time (y-axis in min) for OEDrift-1. M=Magnetite (with 2Theta position on the right), G=Goethite, L=Lepidocrocite**

## 6.3.2 Oxidation at Initial pH 11.5

Oxidation tests with pH drifting were also run following hydrolysis of single ferrous sulphate solutions to pH 11.5 (Tests HEFe-1 and 2; data presented in Chapter 5, Figure 30). The combined hydrolysis (up to pH 11.5) and oxidation (drifted pH) data for Test HEFe-1 is plotted in Figure 44. The onset of air sparging is marked by a blank symbol along with an ORP spike. The oxidation slurry titration measurements show a linear decrease of the total Fe(II) concentration up to data point at t=213 min after which the ORP tends to rise quickly marking the end of oxidation. The last measured slurry oxidation data point gave 156 mg/L Fe(II) at t=240 min, beyond which further Fe(II) oxidation kinetics were slowed down.

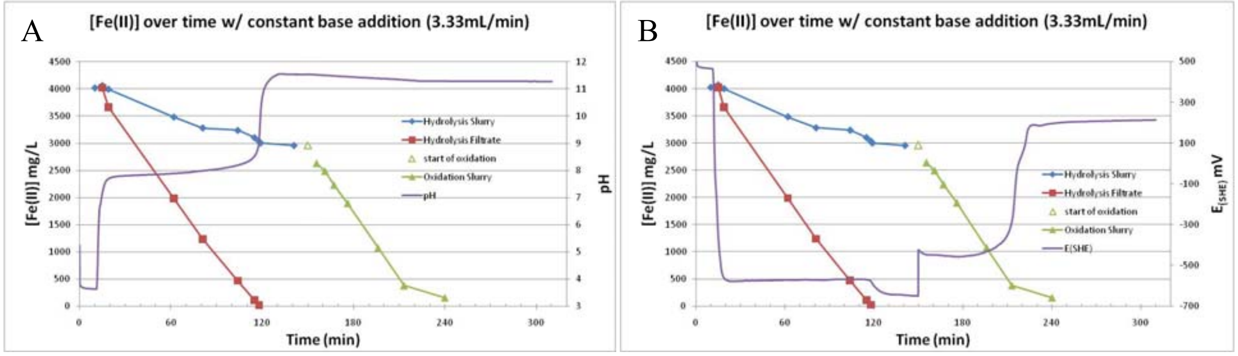

**Figure 44: Hydrolysis of Fe(II) followed by air oxidation shown with A) pH and B) ORP evolution**

In contrast to the tests OEDrift-1 & 2 that showed significant pH variation during oxidation, the present test showed minimal pH change with a drop of only 0.24 units. Similar results were obtained with the post-hydrolysis oxidation following test HEFe-2, this time recording a pH drop of 0.45 units and a linear slurry Fe(II) oxidation curve (Table 12).

Characterization of the final products of oxidation from tests HEFe-1 and 2 by both XRD and Raman spectroscopy (data not shown) confirms goethite (JCPDS card# 00-029-0713) as was found with the OEDrift-1 & 2 tests run at lower pH. Given, however, the different pH response in the former tests (pH 11.5), it is possible that in this case the oxidation of ferrous hydroxide to goethite is direct not involving intermediate phases like GRII and magnetite.

## 6.4 Ferrous Oxidation in the Presence of Arsenic(V)

In this section the oxidation at constant pH=8[7] of hydrolyzed ferrous sulphate solutions containing arsenic(V) at two Fe(II)/As(V) molar ratios, namely 4 and 1.65 (targeted), is investigated (Table 14). The initial pH of the solution was approximately 1.5 in order to prevent any premature precipitation. As in Section 5.1.2 of the Hydrolysis Studies Chapter, the pH was increased by constant NaOH base addition however only up to pH=8, during which precipitation occurred. The pH was subsequently manually maintained at that pH for one hour after which the slurry solution was sparged with air at constant pH=8. The concentration profiles of $Fe(II)_{slurry}$, $Fe(II)_{filtrate}$, $Fe_{tot}$ and $As(V)_{filtrate}$ over time and over pH for Fe/As solutions equal (actual values) to 3.52 and 1.68 are shown in Figure 46 and Figure 47 respectively. The ramping up of the oxidation experiments containing arsenic before air sparging follows the same footsteps as was used during the hydrolysis experiments containing arsenic (discussed in Chapter 5). Therefore it can be expected that the iron and arsenic concentration profiles for both OEAs-1 and HEAs-1, with similar Fe/As molar ratios of 3.52 and 3.99 respectively, are equal. The same applies for OEAs-2 and HEAs-2 with Fe/As molar ratios of 1.68 and 1.49. These comparisons are shown graphically in Figure 67 and Figure 68 in the Appendix Section 8.5 with good agreement confirming indirectly the good inherent reproducibility of these test results.

---

[7] Another series of oxidation tests were done following hydrolysis of similar mixed Fe(II)/As(V) solutions to pH 11.5 this time under pH drifting conditions. These tests were continuation of the hydrolysis tests HEAs-1 & 2 discussed in Section 5.2 of Chapter 5. The results from these supplementary post-hydrolysis tests are reported in the Appendix Section 8.3.

**Table 14: Pre-oxidation hydrolysis conditions and data for experiments OEAs-1 & 2**

| Exp. | Fe/As molar ratio | % Fe(II) oxidized during hydrolysis to pH=8 | Time to reach pH=8 | $Fe(II)]_{in.}/[OH^{-}]$ at pH=8 |
|---|---|---|---|---|
| OEAs-1 | 3.52 | 27 | 98 min | 0.588 |
| OEAs-2 | 1.68 | 20 | 147 min | 0.379 |

## 6.4.1 Pre-Oxidation Hydrolysis of the Fe(II)/As Solution

During pre-oxidation hydrolysis induced by constant base addition some 20-25 % of the ferrous iron was found to oxidize due to air infiltration (data in Table 14). The pH (and $E_h$) evolution during solution titration (hydrolysis) was monitored and shown in Figure 45 for the OEAs-1 test. Additional data is provided in the Appendix Section 8.5. The pH evolution curves provide some interesting features (inflection points summarized in Table 15) that can be linked to the precipitation behaviour of ferrous and arsenate depicted graphically in Figure 46 and Figure 47.

**Table 15: pH inflection points for pre-oxidation hydrolysis of ferrous-arsenic(V) containing solutions**

| Experiment | Fe/As=4 | | Fe/As=1.65 | |
|---|---|---|---|---|
| | HEAs-1 | OEAs-1 | HEAs-2 | OEAs-2 |
| pH of 1st inflection point | 4.05 | 4.05 | 3.41 | 3.64 |
| pH of 2nd inflection point | 7.08 | 7.38 | 7.64 | 8* |

*The second inflection point is assumed to have occurred exactly where the hydrolysis stopped.

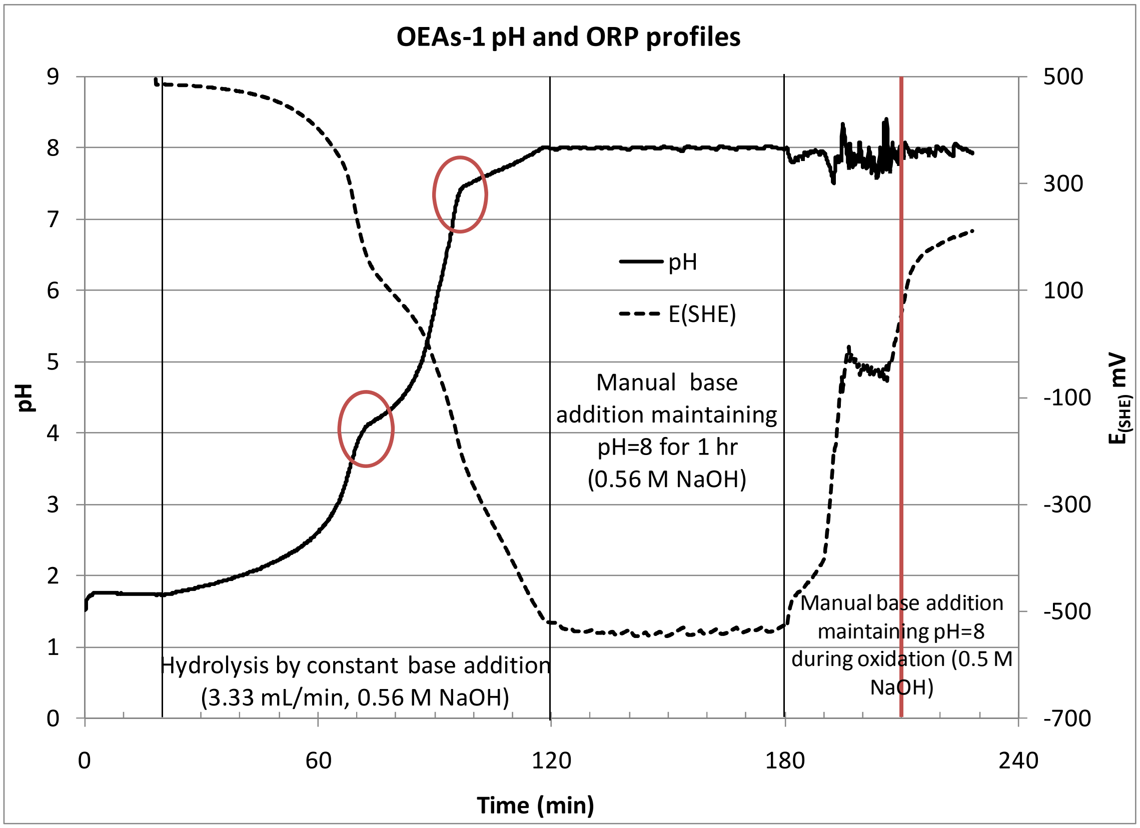

**Figure 45: pH and ORP evolution during hydrolysis and oxidation of ferrous-arsenate containing solution [Fe(II)/As(V)=3.52]**

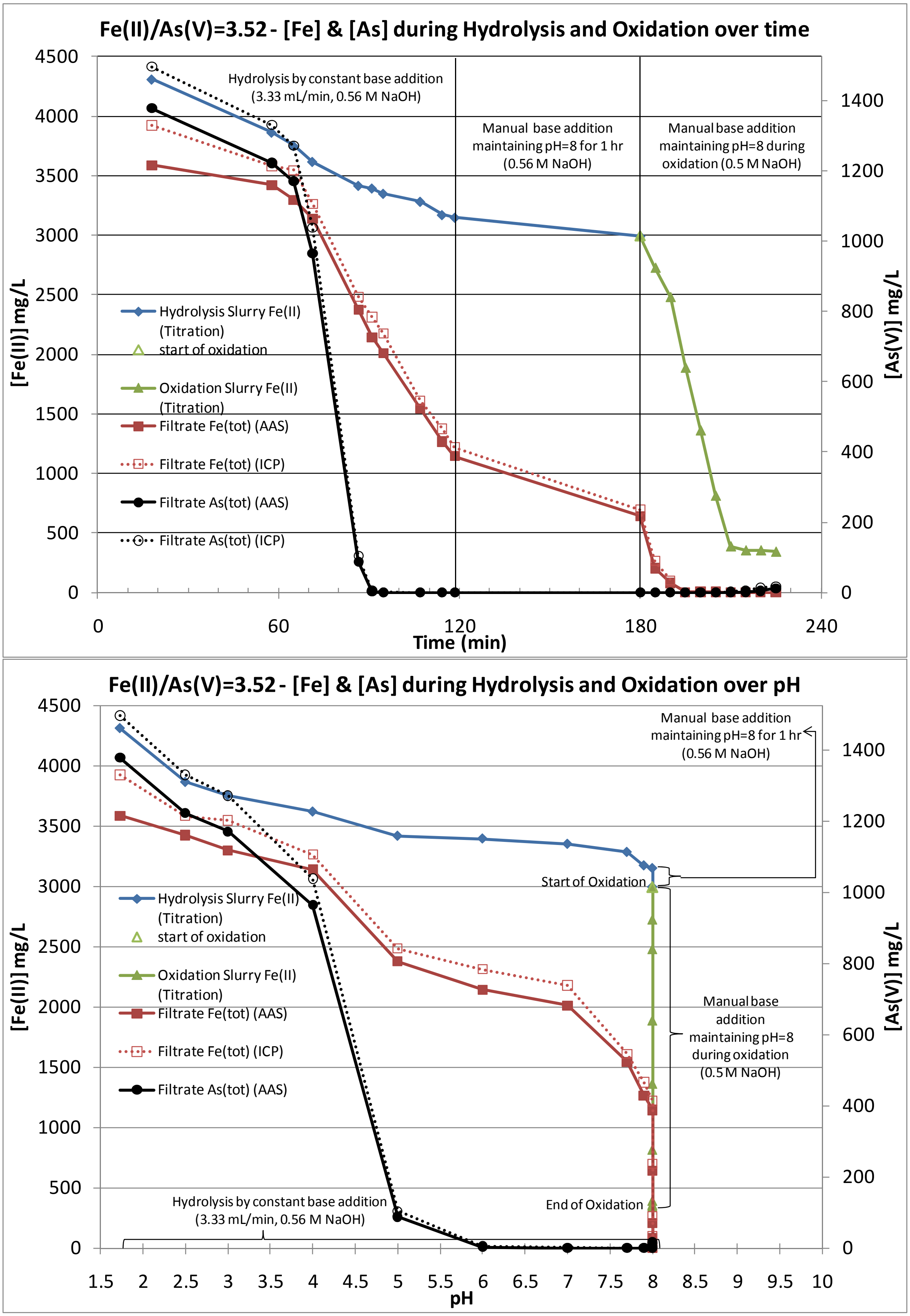

Figure 46: Hydrolysis up to pH=8 and constant pH=8 oxidation as a function of time (top) and pH (bottom) of an Fe(II)/As(V)=3.52 solution

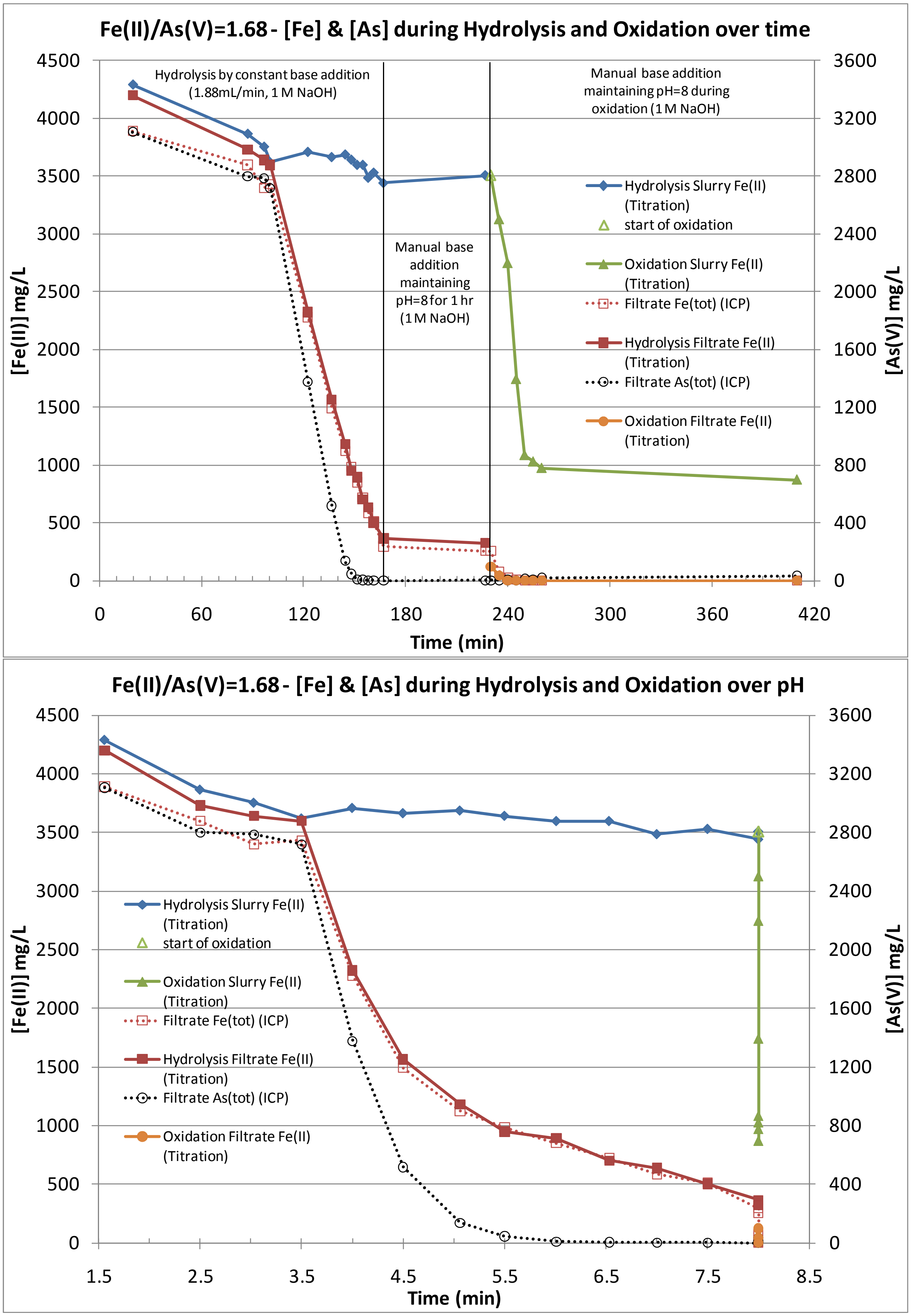

**Figure 47: Hydrolysis up to pH=8 and constant pH=8 oxidation as a function of time (top) and pH (bottom) of an Fe(II)/As(V)=1.68 solution**

As it can be seen from the figures above, As(V) was slowly removed from solution at the start of base addition between pH=1.5 and pH≈3.5-4. During that pH range, the As(V) concentration dropped together with Fe(II) at an Fe/As molar ratio of 1.94 and 1.58 for OEAs-1 & 2 respectively (comparable to values of 1.79 and 1.56 for HEAs-1 & 2 over similar pH range, data presented in Chapter 5). It should be emphasized that up to the first pH inflection point, the arsenic that was removed from solution ranged between 7.5 and 30.5 % of the total. Subsequently, near the inflection point noticeable in the pH and ORP profiles (Figure 45 plus data in the Appendix Section 8.5), As(V) was removed from solution at a much faster rate. By calculating (as best as possible depending on the number of data points) the molar ratio of Fe(II)/As(V) that precipitated between the first and second inflection points (see Table 15) the values of 1.40 and 1.55 for OEAs-1 & 2 respectively were obtained. As discussed in Section 5.2, these molar ratios may represent the phase that is formed between the two inflection points, which is close to the stoichiometric Fe(II)/As(V) ratio of 1.5 for ferrous arsenate (symplesite) [54].

The precipitation of ferrous arsenate in this context has led to effective removal of arsenic(V). Thus in the case of Fe(II)/As(V) molar ratio of 3.52, the residual arsenic concentration past pH=7.7 was found to be below the detection limit of the ICP-OES instrument (<0.1 mg/L), while in the case of Fe(II)/As(V) molar ratio of 1.68, the residual [As] reached a low value of 0.65 mg/L at pH=8.

### 6.4.2 Constant pH 8 Post-Hydrolysis Oxidation

After the initial hydrolysis of the Fe(II)/As(V) solution up to pH=8, the solution was equilibrated at that pH for one hour before the onset of air sparging. During that time the concentration of As(V) did not change for OEAs-1 and increased only slightly to 0.94 mg/L for OEAs-2. Figure 48 presents the change in [As] during the combined hydrolysis-oxidation treatment of experiments OEAs-1 & 2.

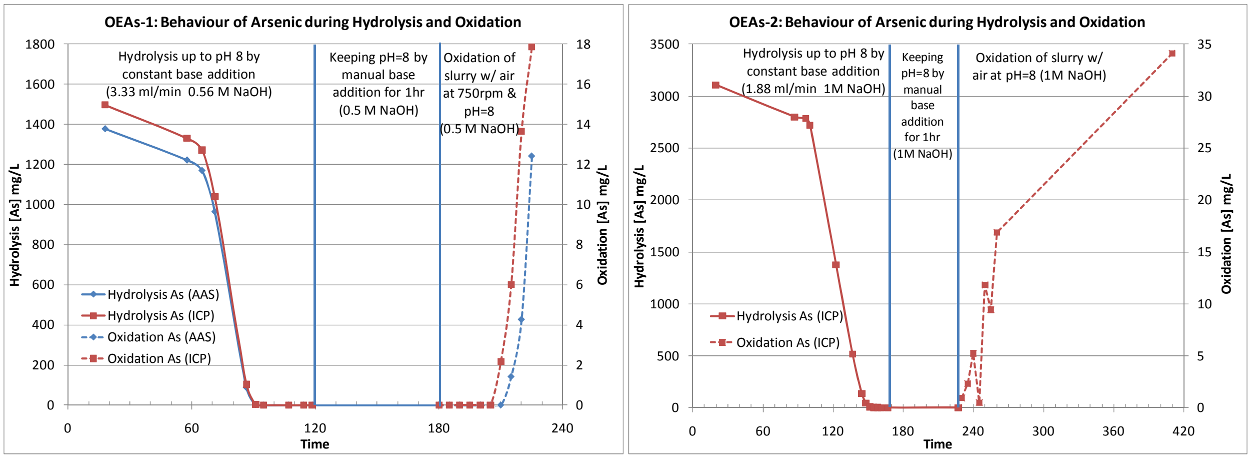

**Figure 48: Arsenic concentration profiles for OEAs-1 (left) and OEAs- 2 (right) tests**

In contrast to Figures 46 and 47 that showed no change in [As] during oxidation due to the scale difference, Figure 48 clearly shows oxidation of the ferrous arsenate slurry at pH 8 led to arsenic release. For OEAs-1 (Fe(II)/As(V)=3.5), a rise in [As] was not noticed until 30 minutes into air sparging. When examining the pH and ORP evolution during oxidation (Figure 45), we notice a sharp rise in $E_h$ from ~ -550 mV to an initial plateau at ~ -20 mV corresponding to the first 30 min (180→210 min) followed by a last rise in $E_h$ near the 200 mV level. Frequent manual base additions had to be made up to the start of the last rise in $E_h$ as indicated by the large fluctuations of pH[8] (see red vertical line in Figure 45), which diminished as the $E_h$ rises. The time, t=210 min, at which the [As] in solution started to increase corresponds to the last rise in $E_h$ and also the last data point part of the linear decrease of total [Fe(II)][9] in slurry samples (Figure 46 top). It is apparent therefore that destabilization of ferrous arsenate by oxidation led to the release of arsenic. The control of arsenic in the latter case was switched from ferrous arsenate to ferric arsenate or more likely to arsenate adsorption on the iron(III) hydroxide forming in situ[10]. Considering the arsenic release (albeit limited) upon oxidation of the ferrous arsenate precipitate by air sparging led to the conclusion that the former could be a more effective sink for arsenic in tailings than arsenical ferrihydrite/ferric arsenate only if it can be maintained in an air restricted environment.

---

[8] As discussed in Chapter 5 the excess (over the symplesite stoichiometry) Fe(II) precipitated as $Fe(OH)_2$ and/or GRII. As such, the net proton generating reactions taking place during sparging, which required base addition to maintain pH 8 constant, were the oxidation of Fe(II) containing phases and their subsequent hydrolysis into iron(III) hydroxides.

[9] There appears that a fraction of ferrous corresponding to Fe(II) concentration equal to 390 mg/L at t=210 min resisted further oxidation. Assuming that this remaining fraction of ferrous iron was in the form of ferrous arsenate (symplesite), then the associated concentration of arsenic in this solid would equal 350 mg/L, which represented 25 % of the original amount of arsenic.

[10] Similar observations can be made for OEAs-2 by examining the data in Figure 47 and Figure 48 (right) to the pH and $E_h$ evolution (Figure 69 in the Appendix Section 8.5). In this case ~28 % of arsenic was found at the end of the oxidation test to be associated with the resisting oxidation fraction of ferrous (871 mg/L Fe(II)) and the remaining arsenic in the solids was most likely again adsorbed on the in-situ formed iron(III) hydroxide.

### 6.4.3 Characterization

*XRD analysis:*

The XRD patterns for the oxidation products of experiments OEAs-1 and 2 are shown in Figure 49. The patterns contain distinctive but not well developed peaks akin to semi-crystalline products. However, PANanalytical HighScore XRD phase identification software could not match these patterns to any known compounds. It is interesting to note that similar patterns were exhibited by the oxidation products obtained from tests HEAs-1 & 2 involving hydrolysis to pH 11.5 and subsequent oxidation under drifting pH (see Figure 70 in the Appendix Section 8.5). The similarity of the two sets of patterns may be linked to the fact that the final pH in the HEAs series was ~8 like the OEAs series.

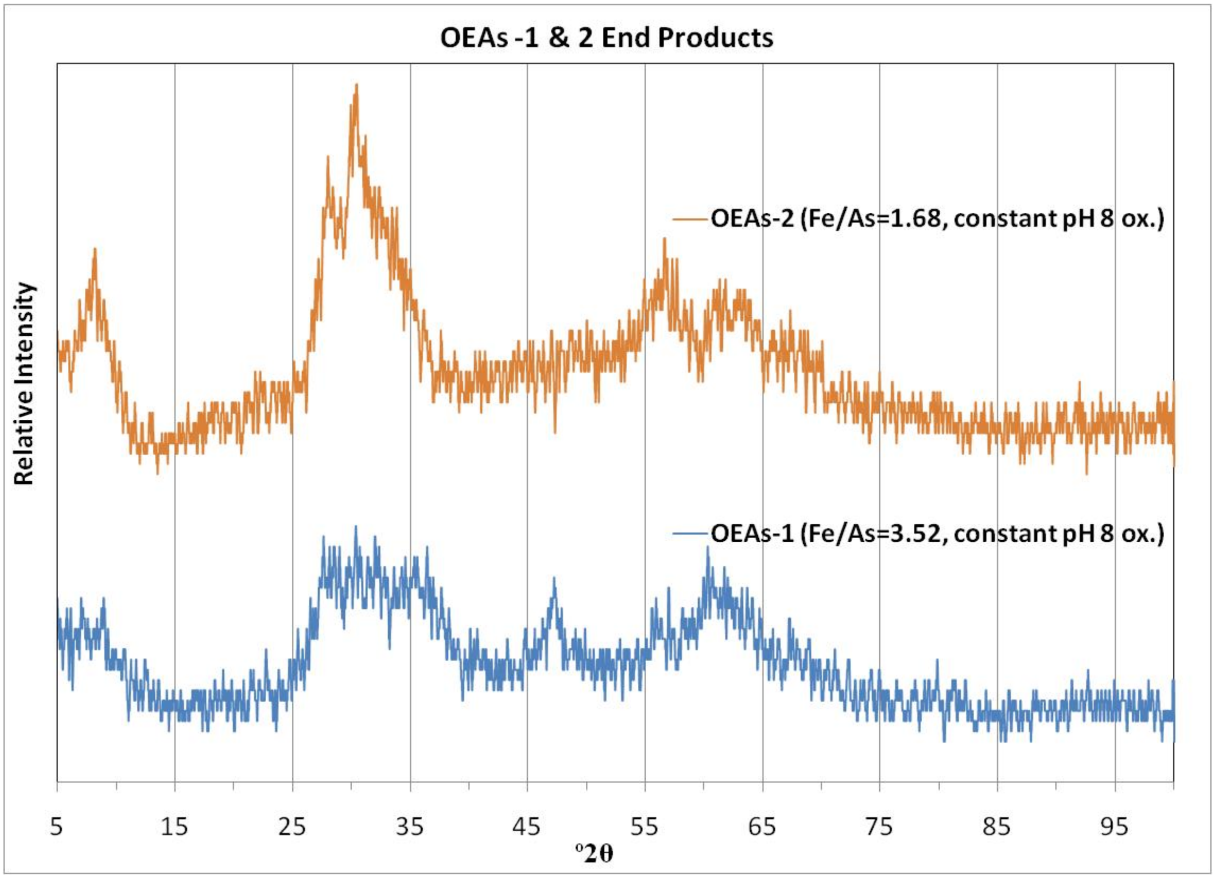

**Figure 49: XRD patterns of OEAs-1 & 2 final oxidation products**

*RAMAN Spectroscopy:*

In an effort to obtain some insight as to the nature of these arsenate-containing oxidation products Raman spectra were collected as well shown in Figure 50. Both spectra are very similar with the only difference being the strong signals for the As-O stretching bands at ~850 $cm^{-1}$, which is expectedly higher for OEAs-2 then OEAs-1. Other than that, it is noticed that the bands between 150 cm$^{-1}$ and 700 cm$^{-1}$ are characteristic of iron hydroxide phases. Further characterization is required for identifying these products.

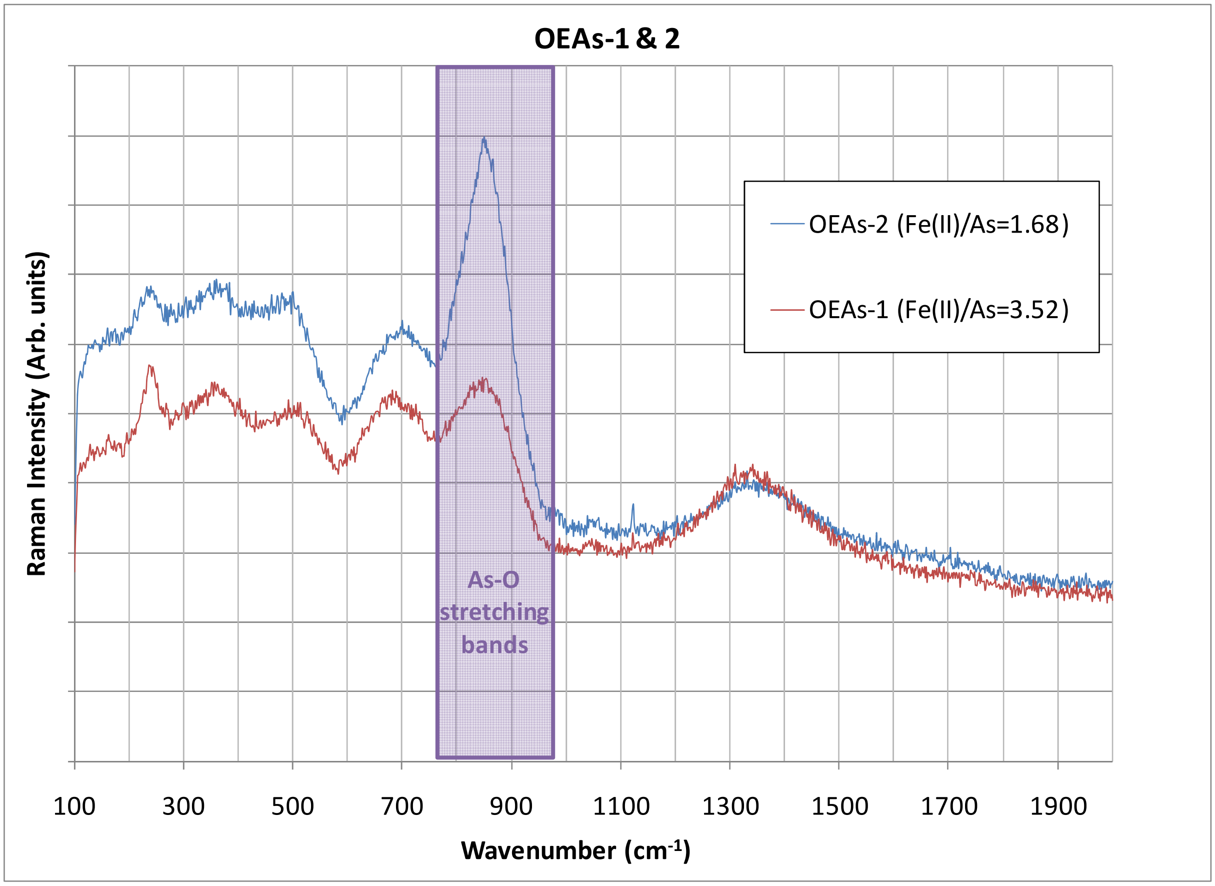

**Figure 50: Raman scans for the final products of OEAs-1 & 2**

## *6.5 Partial Conclusions*

- Oxidation of ferrous hydroxide slurry formed by hydrolysis to pH=8 was associated with gradual increase of $E_h$ from -550 mV to an intermediate plateau of -200 mV to finally (upon completion of oxidation) 400 mV. At the same time pH drifting experiments during oxidation revealed characteristic inflection points.

- These $E_h$ and pH features were interpreted as a series of transformations occurring during oxidation starting from ferrous hydroxide to green rust, to magnetite and finally goethite.

- The oxidation kinetics of ferrous hydroxide was governed by oxygen mass transfer exhibiting characteristic linear plots that were empirically modeled for different conditions.

- The ferrous hydroxide oxidation kinetics were found to increase upon oxygen substitution for air, increase in agitation speed, use of radial rather than axial impeller, pH increase and increasing arsenic(V) concentration.

- The ferrous arsenate that formed during hydrolysis of mixed Fe(II)-As(V) solutions led to effective removal of arsenic to <1 mg/L at pH 8. Upon oxidation, however, via air sparging, ferrous arsenate was destabilized leading to arsenic release (> than the 1 mg/L level) with the bulk of arsenic subsequently controlled via (at all likelihood) adsorption on the in situ forming ferrihydrite.

- It was not possible to positively identify the oxidation products despite the appearance of clearly distinguishable XRD peaks as they did not match any of the known phases. Similarly, Raman spectroscopy did not provide positive identification.

# 7 Synopsis

In this chapter first the major findings from this work are summarized and then some ideas for continuing this research are provided.

## *7.1 Global Conclusions*

A 2-stage (pH4, pH8) lime neutralization continuous coprecipitation (CCPTN) circuit was used to study the removal of high arsenic(V) concentrations (1400 mg/L) from acidic sulphate effluent waters containing various ratios of ferrous to ferric at Fe(total)/As(V) molar ratio equal to 4. The substitution of ferrous for ferric iron resulted in an increase of arsenic concentration in the CCPTN process effluent. However, by comparison arsenic levels from isomolar Fe(III)-As(V) solutions in the absence of ferrous were at least three orders higher showing that excess iron above the stoichiometric ratio one contribute to effective arsenic retention/precipitation, even when present as ferrous. The beneficial effect of ferrous on arsenic(V) retention was attributed to formation of ferrous arsenate (symplesite).

Long term ageing of the coprecipitates at various temperatures showed slow release of arsenic reaching apparent (pseudo) equilibrium after a few months of equilibration. Ageing under drifting pH conditions led to lower arsenic release than pH-controlled ageing. For example, the stability of aged CCPTs at 20 ºC having an initial Fe(II) fraction no greater than half the total iron was satisfactory with less than 1 mg/L As(V) released after 463 days at final (stabilized) pH ~5. A pH adjustment to 8 following ageing near pseudoequilibrium resulted to much lower arsenic levels than the corresponding ones reached by constant pH 8 ageing from the beginning. At Fe(II)/Fe(III)=1 and Fe(III)/As(V)=2 (RD7) the pseudoequilibrium arsenic release level following mid-way pH adjustment/ageing to pH 8 was only 1.9 mg/L. The retention of arsenic in the presence of ferrous may be achieved via a combination of paths including formation of ferrous arsenate (symplesite), arsenate adsorption on green rust, and re-adsorption of arsenate on ferrihydrite (ferric hydroxide) produced during ageing by partial oxidation of ferrous hydroxide.

Batch hydrolysis experiments involving the addition of base to ferrous sulphate solutions with or without arsenic(V) provided valuable insight in support of the observed arsenic removal and retention behaviour during the CCPTN tests. Thus hydrolysis of ferrous solutions containing ferric iron and arsenic(V) showed precipitation of ferrous to take place at much lower pH than that of single ferrous solutions; this having been attributed to adsorption onto precipitated iron(III) hydroxide and precipitation of a ferrous-arsenate compound (symplesite) respectively. In the case of the hydrolysis of Fe(II)-As(V) solutions, arsenic was shown to be successfully removed from solution below 1 mg/L beyond pH 6.5 before being released back into solution above pH 10. According to the present investigation, the obtained results clearly show the ability of Fe(II) to remove As(V) from solution unlike ever seen before. By extrapolation it is deduced that in a CCPTN system any ferrous iron present unambiguously contributes to removal of As(V) from solution.

Following the batch hydrolytic precipitation of ferrous alone as hydroxide or together with arsenic(V) as ferrous arsenate, it was subjected to intentional oxidation by air sparging to monitor the resultant phase changes and arsenic release/retention behaviour. Thus it was found in the case of ferrous hydroxide, oxidation at pH 8 led to its conversion to green rust, magnetite and finally goethite. The oxidation kinetics were governed by oxygen mass transfer. In the case of ferrous arsenate, air sparging was found to cause its destabilization and the release of arsenic to significant levels (~18 mg/L for the system with initial Fe(II)/As(V)=3.52). This suggests that ferrous arsenate was more stable than the corresponding ferric arsenate and/or arsenate-adsorbed ferrihydrite at pH ~8. As such, in order to take advantage of its low solubility, appropriate measures need to be taken during disposal to restrict its exposure to air, for example via sub-aqueous deposition. To this end further research needs to be undertaken.

## *7.2 Ideas for Future Research*

Work that was initiated by this author involving oxidation during CCPTN and was not included in this thesis requires to be continued and completed. Basically the continuous coprecipitation campaign, this time incorporating in-situ oxidation of ferrous only and mixed ferrous and ferric solutions along As(V), is proposed followed by stability testing and characterization studies.

Based on the results from Chapter 5 and 6, notably that of the formation of a ferrous-arsenate compound, it is worthwhile to continue studying the As(V)-Fe(II) system as a legitimate method for removing arsenic from solution in a partially reducing environment. For this, the author recommends additional test work (Batch and CCPTN) coupled with stability testing especially for Fe(II)/As(V) molar ratios of 1.5 and possibly unity. Furthermore, the ageing procedure could be modified in order to simulate reducing environments with different redox potentials via the regulated addition of a strong reducing agent such as sodium sulphite ($Na_2SO_3$).

Another issue to be dealt with is the characterization of the produced products that are sensitive to oxidation. New methods and techniques for the preservation of ferrous compounds are needed to effectively characterize them. As a result, the ferrous arsenate solid that has been shown to precipitate can be further characterized to establish its real stoichiometry.

# 8 Appendix

This Appendix contains additional figures and results relevant to the results presented in Chapters 4, 5 and 6.

## 8.1 Continuous Coprecipitation (CCPTN)

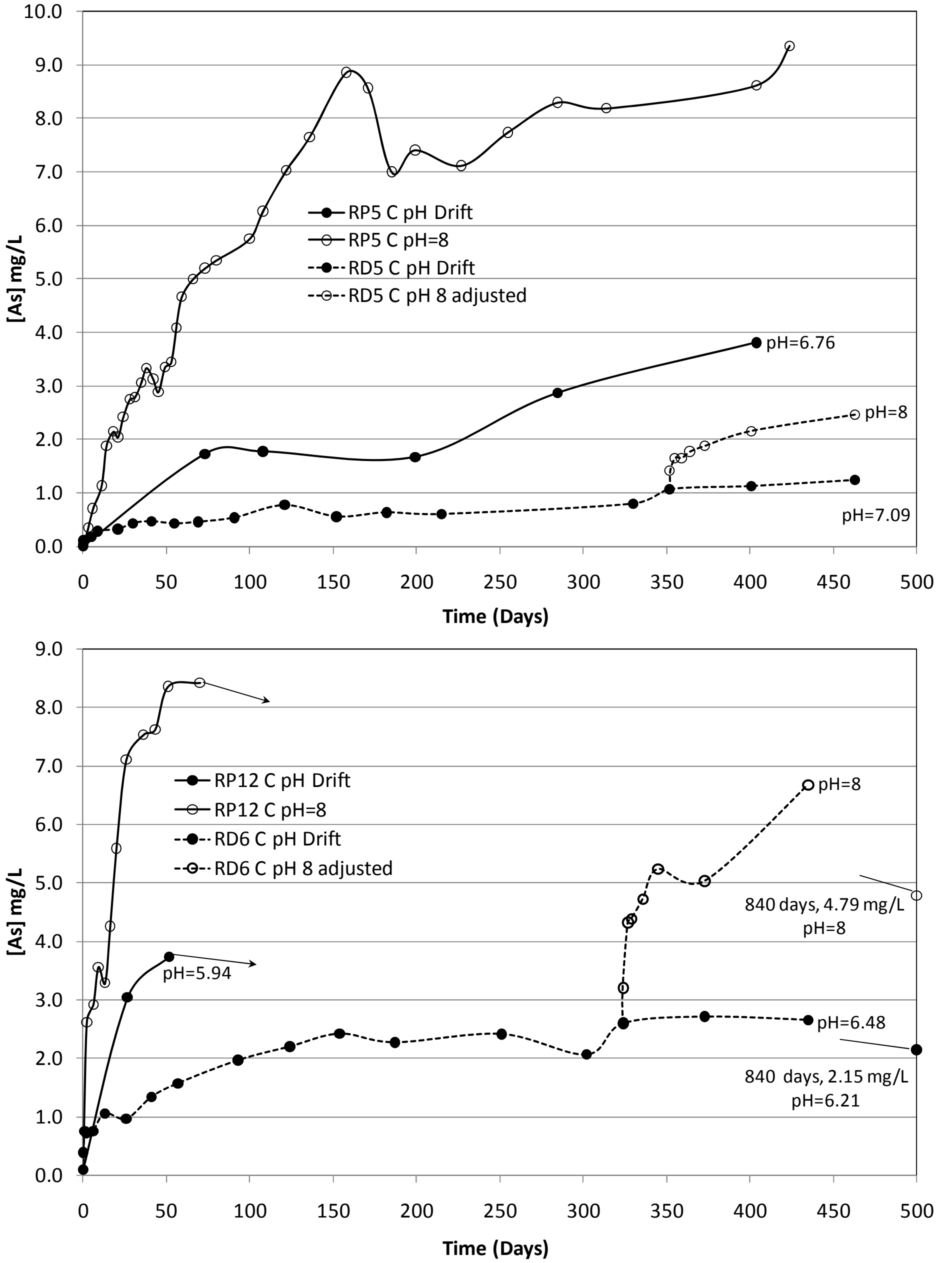

**Figure 51: Long term ageing data-comparison between RD5 and RP5 [8] (top) and RD6 and RP12 [8] (bottom) at 70 ºC accelerated ageing temperature. Note: solids from RD5 and RD6 had been pre-aged in their final coprecipitation liquor at room temperature for 12 weeks; t=0 represents the extension of ageing following solids concentration by reducing by half the liquor volume. "pH adjusted" involved splitting of the ageing slurry in two halfs with one of them continuing on free pH drift while the other was regularly adjusted to pH 8**

Table 16 contains the ageing data collected ([As], pH) for experiments RD5 Drift, RP5 Drift and RP5 constant pH 8 at 20, 40 and 70 °C ageing temperature given in blue, yellow and red columns respectively. Likewise, Table 17 shows the data for experiments RD6 Drift, RP12 Drift and RP12 constant pH 8.

**Table 16: Complete Ageing Data for experiments RD5 Drift and RP5 Drift and constant pH 8. The final data points before ageing shutdown highlighted in black**

| RD5 | | | | | | | | | | | |
|---|---|---|---|---|---|---|---|---|---|---|---|
| 20°C DRIFT | | | | 40°C DRIFT | | | | 70°C DRIFT | | | |
| Age (t=0) | Age | [As] | pH | Age (t=0) | Age | [As] | pH | Age (t=0) | Age | [As] | pH |
| Days | Days | mg/L | | Days | Days | mg/L | | Days | Days | mg/L | |
| -84 | 0 | 0.01 | | -84 | 0 | 0.01 | | -84 | 0 | 0.01 | |
| -44 | 40 | 0.04 | | -44 | 40 | 0.04 | | -44 | 40 | 0.04 | |
| -42 | 42 | 0.04 | | -42 | 42 | 0.04 | | -42 | 42 | 0.04 | |
| -40 | 44 | 0.03 | | -40 | 44 | 0.03 | | -40 | 44 | 0.03 | |
| -36 | 48 | 0.03 | | -36 | 48 | 0.03 | | -36 | 48 | 0.03 | |
| -33 | 51 | 0.04 | | -33 | 51 | 0.04 | | -33 | 51 | 0.04 | |
| -27 | 57 | 0.05 | | -27 | 57 | 0.05 | | -27 | 57 | 0.05 | |
| 0 | 84 | 0.05 | | 0 | 84 | 0.05 | | 0 | 84 | 0.12 | |
| 1 | 85 | 0.05 | | 1 | 85 | 0.06 | | 1 | 85 | 0.12 | |
| 5 | 89 | 0.05 | 7.20 | 5 | 89 | 0.07 | 7.08 | 5 | 89 | 0.18 | 6.91 |
| 9 | 93 | 0.05 | | 9 | 93 | 0.08 | | 9 | 93 | 0.29 | |
| 21 | 105 | 0.05 | 6.68 | 21 | 105 | 0.09 | 6.49 | 21 | 105 | 0.32 | 6.63 |
| 29 | 113 | 0.06 | 7.15 | 30 | 114 | 0.12 | | 30 | 114 | 0.44 | |
| 41 | 125 | 0.07 | | 41 | 125 | 0.12 | | 41 | 125 | 0.47 | |
| 55 | 139 | 0.12 | 7.07 | 55 | 139 | 0.10 | 6.90 | 55 | 139 | 0.43 | 6.88 |
| 69 | 153 | 0.06 | 7.11 | 69 | 153 | 0.10 | 6.96 | 69 | 153 | 0.46 | 6.93 |
| 91 | 175 | 0.08 | 7.15 | 91 | 175 | 0.17 | 7.01 | 91 | 175 | 0.54 | 6.92 |
| 121 | 205 | 0.11 | 7.11 | 121 | 205 | 0.18 | 6.96 | 121 | 205 | 0.77 | 6.94 |
| 166 | 250 | 0.08 | 7.10 | 152 | 236 | 0.13 | 7.06 | 152 | 236 | 0.56 | 6.88 |
| 182 | 266 | | 7.08 | 182 | 266 | 0.14 | 6.90 | 182 | 266 | 0.64 | 6.82 |
| 272 | 356 | | 7.00 | 215 | 299 | 0.27 | 6.98 | 215 | 299 | 0.61 | 7.07 |
| 330 | 414 | | 7.04 | 272 | 356 | | 7.08 | 279 | 363 | | 6.94 |
| 352 | 436 | 0.09 | 7.07 | 330 | 414 | 0.28 | 7.01 | 330 | 414 | 0.80 | 7.04 |
| 401 | 485 | 0.13 | 7.14 | 352 | 436 | 0.36 | 7.15 | 352 | 436 | 1.07 | 7.08 |
| 463 | 547 | 0.14 | 7.09 | 401 | 485 | 0.59 | 7.11 | 401 | 485 | 1.13 | 7.15 |
| | | | | 463 | 547 | 0.40 | 7.06 | 463 | 547 | 1.25 | 7.09 |

| RP5 | | | | | | | | | | | | | | | |
|---|---|---|---|---|---|---|---|---|---|---|---|---|---|---|---|
| 40°C DRIFT | | | 70°C DRIFT | | | 20°C pH=8 | | 40°C pH=8 | | 70°C pH=8 | |
| Age | [As] | pH | Age | [As] | pH | Age | [As] | Age | [As] | Age | [As] |
| days | mg/L | | days | mg/L | | days | mg/L | days | mg/L | days | mg/L |
| 0 | 0.01 | | 0 | 0.01 | | 0 | 0.01 | 0 | 0.03 | 0 | 0.03 |
| 49 | | 6.71 | 49 | | 6.61 | 1 | 0.02 | 3 | 0.09 | 3 | 0.35 |
| 53 | | 6.80 | 53 | | 6.69 | 2 | 0.03 | 6 | 0.12 | 6 | 0.71 |
| 56 | | 6.85 | 56 | | 6.81 | 5 | 0.05 | 11 | 0.27 | 11 | 1.14 |
| 59 | | 7.01 | 59 | | 6.78 | 8 | 0.06 | 14 | 0.41 | 14 | 1.88 |
| 63 | | 6.92 | 63 | | 6.88 | 13 | 0.10 | 18 | 0.42 | 18 | 2.15 |
| 66 | | 6.80 | 66 | | 6.73 | 16 | 0.09 | 21 | 0.59 | 21 | 2.05 |
| 73 | 0.38 | 6.80 | 73 | 1.73 | 6.77 | 20 | 0.11 | 24 | 0.66 | 24 | 2.42 |
| 80 | | 6.91 | 80 | | 6.87 | 23 | 0.11 | 28 | 0.71 | 28 | 2.75 |
| 88 | | 6.92 | 88 | | 6.89 | 26 | 0.11 | 31 | 0.74 | 31 | 2.79 |
| 95 | | 6.87 | 95 | | 6.82 | 30 | 0.15 | 35 | 0.80 | 35 | 3.07 |
| 108 | 0.43 | 6.92 | 108 | 1.78 | 6.82 | 37 | 0.21 | 38 | 0.90 | 38 | 3.34 |
| 122 | | 6.92 | 122 | | 6.85 | 44 | 0.28 | 42 | 1.03 | 42 | 3.13 |
| 136 | | 6.78 | 136 | | 6.73 | 51 | 0.26 | 45 | 1.20 | 45 | 2.89 |
| 158 | | 6.74 | 158 | | 6.47 | 58 | 0.30 | 49 | 1.03 | 49 | 3.35 |
| 199 | 0.36 | 6.88 | 171 | | | 68 | 0.34 | 53 | 1.05 | 53 | 3.45 |
| 285 | 0.59 | 6.80 | 185 | | | 82 | 0.38 | 56 | 1.16 | 56 | 4.09 |
| 404 | 0.74 | 6.90 | 199 | 1.67 | 6.76 | 97 | 0.38 | 59 | 1.21 | 59 | 4.67 |
| | | | 227 | | | 110 | 0.46 | 66 | 1.38 | 66 | 5.00 |
| | | | 255 | | | 124 | 0.42 | 73 | 1.35 | 73 | 5.20 |
| | | | 285 | 2.87 | 6.77 | 138 | 0.46 | 80 | 1.36 | 80 | 5.35 |
| | | | 404 | 3.81 | 6.76 | 160 | 0.51 | 88 | 1.40 | 100 | 5.75 |
| | | | | | | 173 | 0.56 | 95 | 1.43 | 108 | 6.27 |
| | | | | | | 187 | 0.59 | 100 | 1.50 | 122 | 7.03 |
| | | | | | | 201 | 0.64 | 108 | 1.67 | 136 | 7.65 |
| | | | | | | 229 | 0.65 | 122 | 1.87 | 158 | 8.86 |
| | | | | | | 257 | 0.69 | 136 | 1.93 | 171 | 8.57 |
| | | | | | | 287 | 0.77 | 158 | 1.99 | 185 | 7.00 |
| | | | | | | 316 | 0.80 | 171 | 2.05 | 199 | 7.41 |
| | | | | | | 406 | 0.87 | 185 | 1.91 | 227 | 7.12 |
| | | | | | | 427 | 0.88 | 199 | 2.01 | 255 | 7.74 |
| | | | | | | 455 | 0.97 | 227 | 2.15 | 285 | 8.30 |
| | | | | | | 1085 | 1.15 | 255 | 2.33 | 314 | 8.19 |
| | | | | | | $pH_f$=7.68 | | 285 | 2.65 | 404 | 8.62 |
| | | | | | | | | 314 | 2.49 | 424 | 9.36 |
| | | | | | | | | 404 | 2.93 | | |
| | | | | | | | | 425 | 2.51 | | |
| | | | | | | | | 905 | 1.08 | | |
| | | | | | | | | 1083 | 1.58 | | |
| | | | | | | | | **1188** | **2.08** | | |
| | | | | | | | | **$pH_f$=7.3** | | | |

**Table 17: Complete Ageing Data for experiments RD6 Drift and RP12 Drift and constant pH 8. The final data points before ageing shutdown highlighted in black**

| RDG | | | | | | | | | | | |
|---|---|---|---|---|---|---|---|---|---|---|---|
| 20°C DRIFT | | | | 40°C DRIFT | | | | 70°C DRIFT | | | |
| Age (t=0) | Age | [As] | pH | Age (t=0) | Age | [As] | pH | Age (t=0) | Age | [As] | pH |
| Days | Days | mg/L | | Days | Days | mg/L | | Days | Days | mg/L | |
| -84 | 0 | 0.04 | | -84 | 0 | 0.04 | | -84 | 0 | 0.04 | |
| -75 | 9 | 0.04 | | -75 | 9 | 0.04 | | -75 | 9 | 0.04 | |
| -72 | 12 | 0.06 | | -72 | 12 | 0.06 | | -72 | 12 | 0.06 | |
| -70 | 14 | 0.05 | | -70 | 14 | 0.05 | | -70 | 14 | 0.05 | |
| -68 | 16 | 0.08 | | -68 | 16 | 0.08 | | -68 | 16 | 0.08 | |
| -64 | 20 | 0.10 | | -64 | 20 | 0.10 | | -64 | 20 | 0.10 | |
| -61 | 23 | 0.23 | | -61 | 23 | 0.23 | | -61 | 23 | 0.23 | |
| -55 | 29 | 0.23 | | -55 | 29 | 0.23 | | -55 | 29 | 0.23 | |
| -22 | 62 | | 6.52 | -22 | 62 | | | -22 | 62 | | |
| -7 | 77 | 0.40 | 6.28 | -7 | 77 | 0.40 | | -7 | 77 | 0.40 | |
| 0 | 84 | 0.39 | 6.51 | 0 | 84 | 0.39 | | 0 | 84 | 0.39 | |
| 1 | 85 | 0.49 | | 1 | 85 | 0.52 | 6.47 | 1 | 85 | 0.76 | 6.47 |
| 2 | 86 | | 6.58 | 2 | 86 | 0.46 | 6.41 | 2 | 86 | 0.72 | 6.35 |
| 13 | 97 | 0.39 | | 6 | 90 | 0.52 | 6.38 | 6 | 90 | 0.76 | 6.24 |
| 26 | 110 | 0.37 | 6.46 | 13 | 97 | 0.54 | | 13 | 97 | 1.06 | |
| 41 | 125 | 0.36 | 6.46 | 26 | 110 | 0.53 | 6.43 | 26 | 110 | 0.97 | 6.39 |
| 57 | 141 | 0.46 | 6.53 | 41 | 125 | 0.58 | 6.47 | 41 | 125 | 1.34 | 6.34 |
| 93 | 177 | 0.61 | 6.48 | 57 | 141 | 0.63 | 6.58 | 57 | 141 | 1.57 | 6.46 |
| 138 | 222 | 0.47 | 6.51 | 93 | 177 | 0.78 | 6.42 | 93 | 177 | 1.97 | 6.34 |
| 244 | 328 | 0.54 | 6.47 | 124 | 208 | 0.85 | 6.50 | 124 | 208 | 2.20 | 6.24 |
| 302 | 386 | 0.47 | 6.44 | 154 | 238 | 0.83 | 6.40 | 154 | 238 | 2.42 | 6.29 |
| 324 | 408 | 0.66 | 6.58 | 187 | 271 | 1.36 | 6.47 | 187 | 271 | 2.28 | 6.47 |
| 373 | 457 | 0.61 | 6.55 | 244 | 328 | 1.32 | 6.54 | 251 | 335 | 2.42 | 6.30 |
| 435 | 519 | 0.64 | 6.58 | 302 | 386 | 1.07 | 6.45 | 302 | 386 | 2.07 | 6.37 |
| | | | | 324 | 408 | 1.28 | 6.47 | 324 | 408 | 2.60 | 6.40 |
| | | | | 373 | 457 | 1.19 | 6.52 | 373 | 457 | 2.71 | 6.47 |
| | | | | 435 | 519 | 1.28 | 6.52 | 435 | 519 | 2.66 | 6.48 |

| RP12 | | | | | | | | | | | | | | | | | |
|---|---|---|---|---|---|---|---|---|---|---|---|---|---|---|---|---|---|
| 20°C DRIFT | | | 40°C DRIFT | | | 70°C DRIFT | | | 20°C pH=8 | | | 40°C pH=8 | | | 70°C pH=8 | | |
| Age | [As] | pH | Age | [As] | pH | Age | [As] | pH | Age | [As] | pH | Age | [As] | pH | Age | [As] | pH |
| Days | mg/L | | Days | mg/L | | Days | mg/L | | Days | mg/L | | Days | mg/L | | Days | mg/L | |
| 0 | 0.18 | | 0 | 0.11 | | 0 | 0.11 | | 0 | 0.18 | | 0 | 0.11 | | 0 | 0.11 | |
| 3 | | | 3 | | | 3 | | | 1 | 0.11 | | 2 | 2.18 | | 2 | 2.62 | |
| 7 | | 7.40 | 7 | | 6.91 | 7 | | 6.83 | 3 | 0.89 | | 6 | 2.23 | | 6 | 2.92 | |
| 10 | | | 10 | | | 10 | | | 7 | 1.54 | | 9 | 2.74 | | 9 | 3.56 | |
| 14 | | 7.20 | 14 | | 6.74 | 14 | | 6.69 | 10 | 1.25 | | 13 | 3.08 | | 13 | 3.29 | |
| 17 | | | 17 | | | 17 | | | 14 | 1.57 | | 16 | 3.47 | | 16 | 4.26 | |
| 21 | | | 21 | | | 21 | | | 17 | 1.62 | | 20 | 4.03 | | 20 | 5.59 | |
| 27 | 0.71 | 6.32 | 27 | 1.56 | 6.41 | 27 | 3.04 | 6.14 | 21 | 1.64 | | 26 | 4.60 | | 26 | 7.11 | |
| 37 | | 6.33 | 37 | | 6.40 | 37 | | 6.19 | 27 | 1.67 | | 36 | 4.90 | | 36 | 7.53 | |
| 44 | | | 44 | | | 44 | | | 37 | 1.60 | | 43 | 5.43 | | 43 | 7.62 | |
| 52 | 0.63 | 6.35 | 52 | 1.74 | 6.35 | 52 | 3.74 | 5.94 | 44 | 2.04 | | 51 | 5.91 | | 51 | 8.36 | |
| 71 | | | 71 | | | 757 | 2.02 | 6.14 | 52 | 2.41 | | 70 | 6.31 | | 70 | 8.42 | |
| 593 | 1.07 | 6.45 | 579 | 2.13 | 6.34 | **839** | **2.15** | **6.21** | 71 | 2.74 | | 138 | 5.83 | | 579 | 2.75 | 8.00 |
| 757 | 1.07 | 6.42 | 756 | 2.27 | 6.36 | | | | 80 | 2.71 | | 579 | 6.77 | 7.91 | 757 | 4.12 | 7.97 |
| | | | **839** | **2.65** | **6.46** | | | | 99 | | | 757 | 6.67 | 7.87 | **840** | **4.79** | **8.18** |
| | | | | | | | | | 593 | 3.56 | 7.74 | **839** | **7.36** | **8.00** | | | |
| | | | | | | | | | 757 | 3.52 | 7.65 | | | | | | |

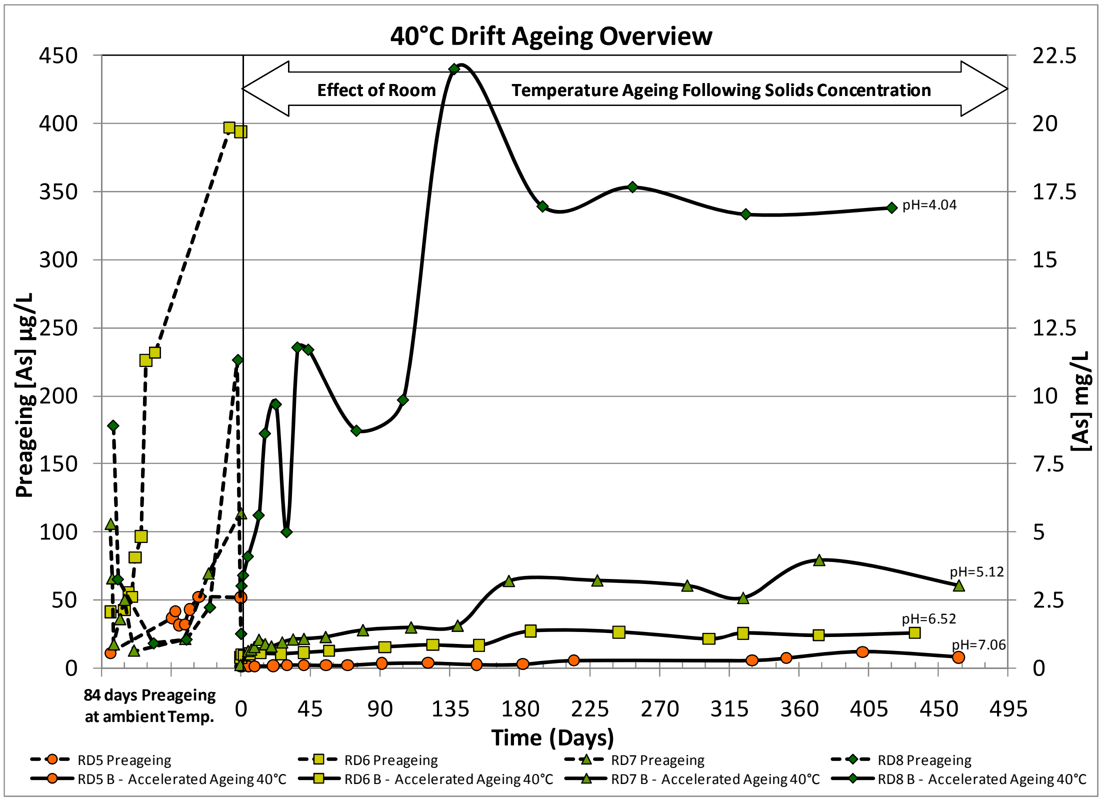

Figure 52: Comparison of long term "drift" stability curves of experiments RD5, 6, 7 & 8 at 40ºC. RD5 contains no addition of ferrous sulphate while RD6, 7 & 8 contain increasing amount ferrous

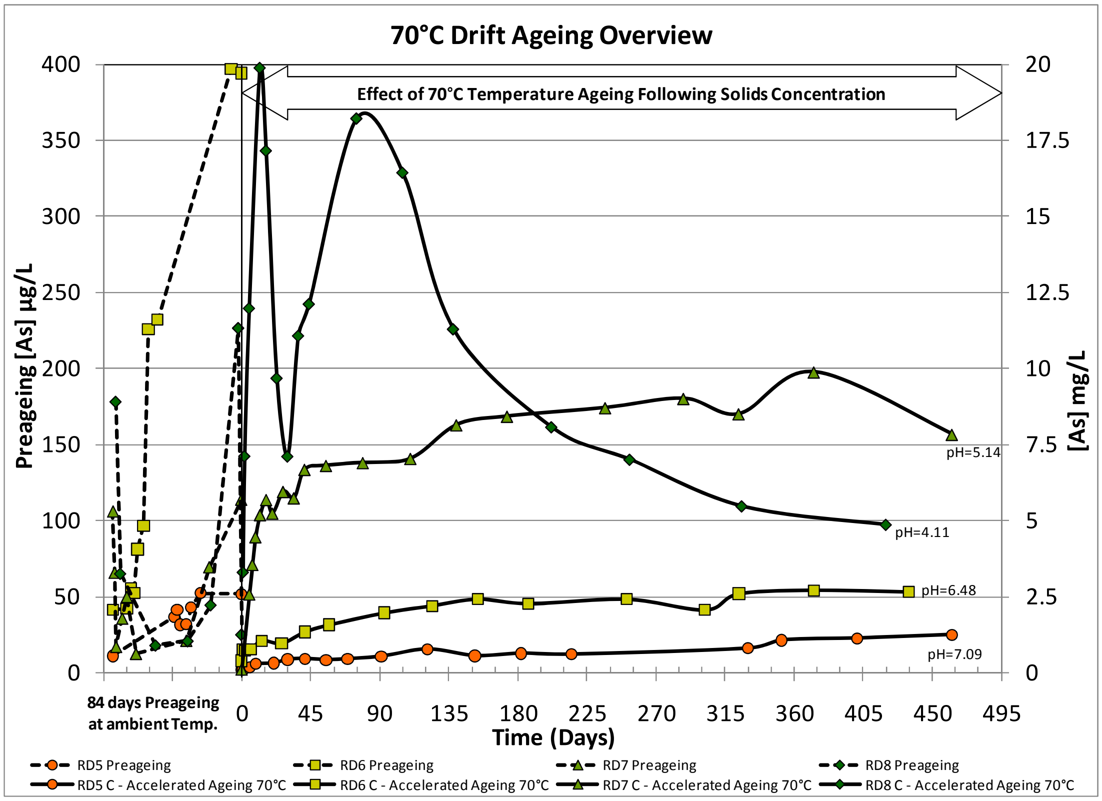

Figure 53: Comparison of long term "drift" stability curves of experiments RD5, 6, 7 & 8 at 70ºC. RD5 contains no addition of ferrous sulphate while RD6, 7 & 8 contain increasing amount ferrous

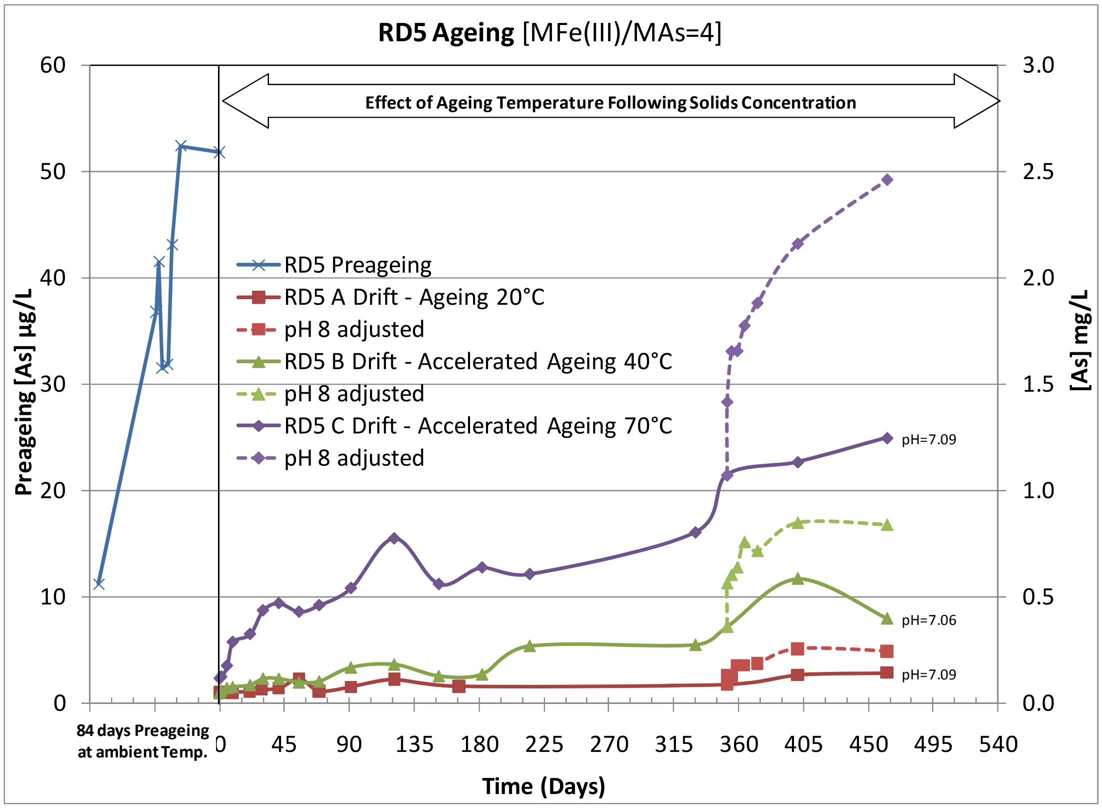

Figure 54: Long term “drift” stability curves (solid lines) for experiment RD5. The pH values represent the last stable “drift” pH measurement. At t= 352 $Ca(OH)_2$ was added to raise the pH to 8 (broken lines)

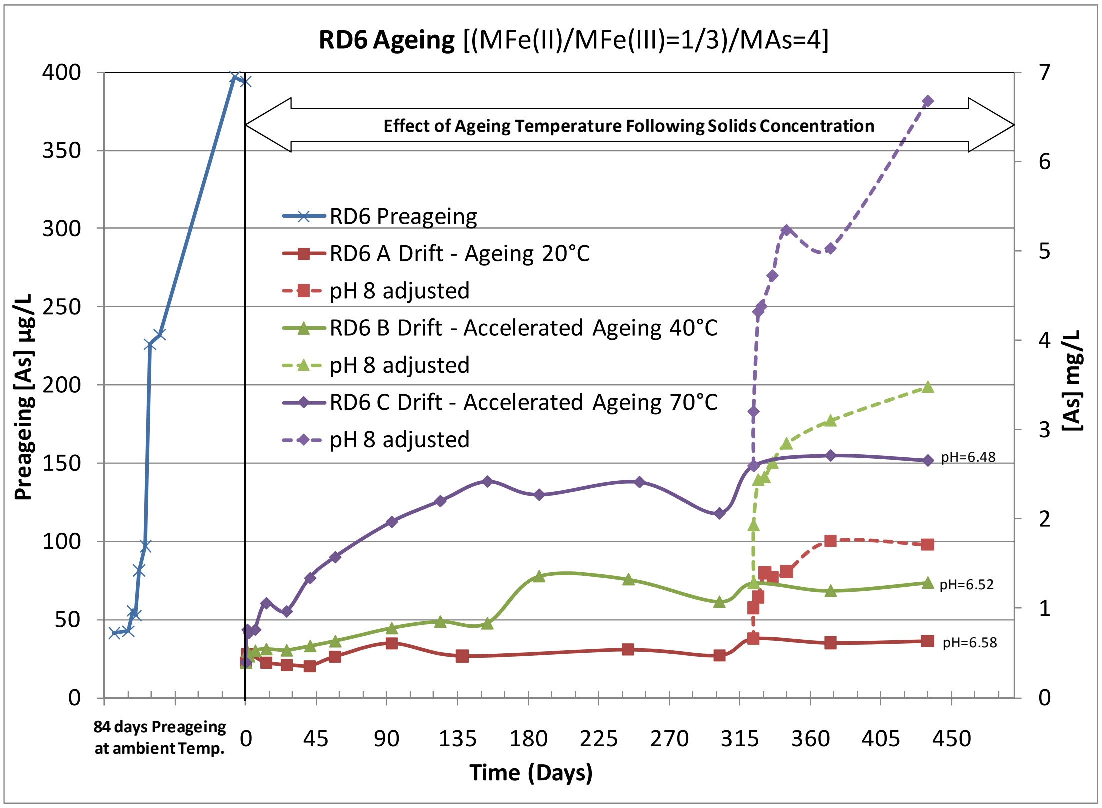

Figure 55: Long term “drift” stability curves (solid lines) for experiment RD6. The pH values represent the last stable “drift” pH measurement. At t= 324 $Ca(OH)_2$ was added to raise the pH to 8 (broken lines)

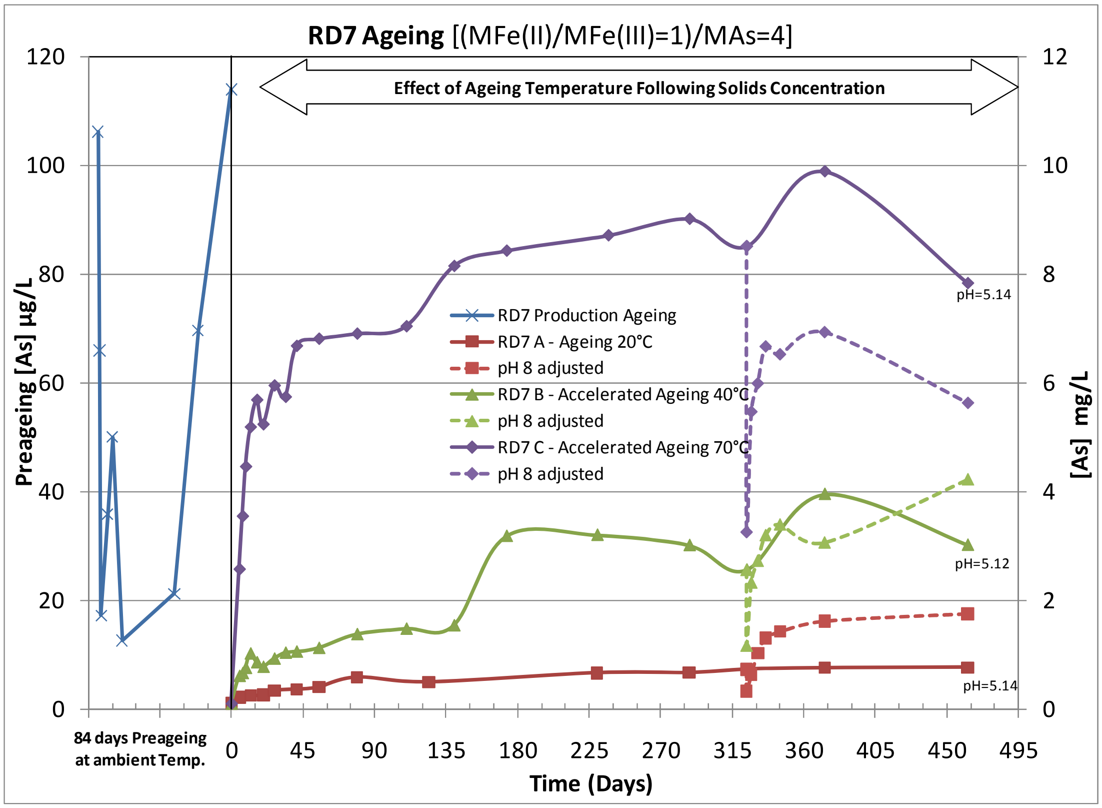

Figure 56: Long term "drift" stability curves (solid lines) for experiment RD7. The pH values represent the last stable "drift" pH measurement. At t= 324 $Ca(OH)_2$ was added to raise the pH to 8 (broken lines)

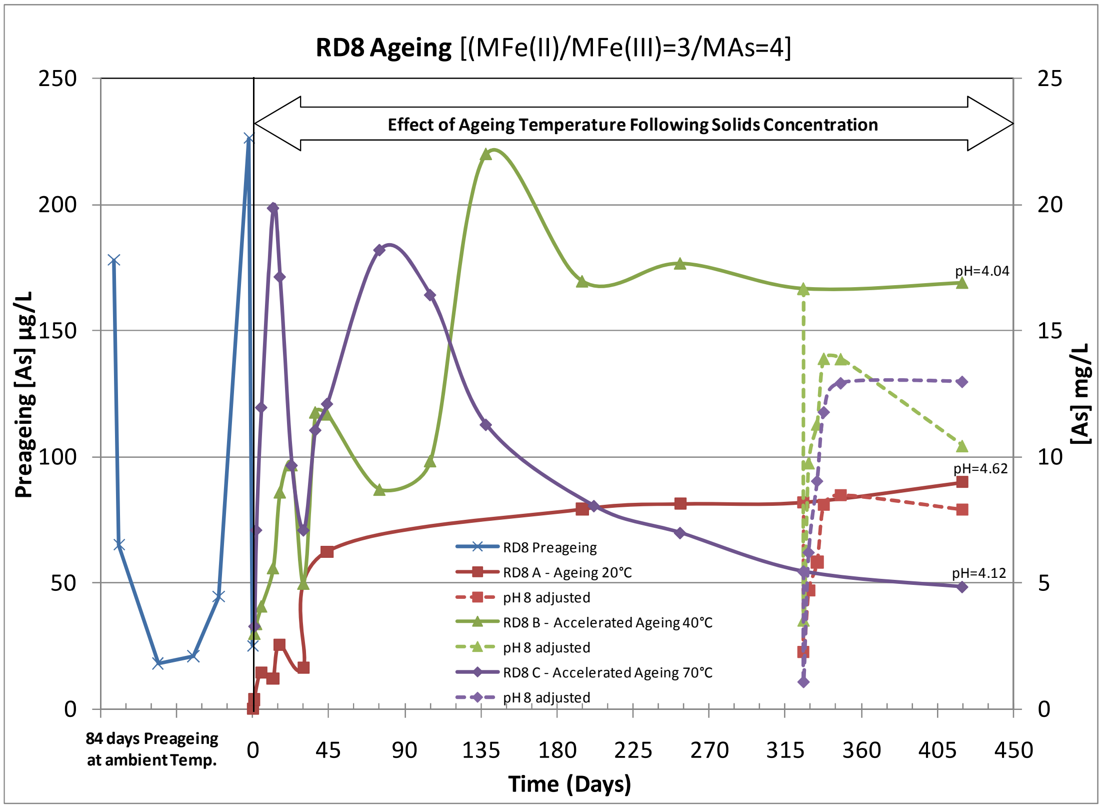

Figure 57: Long term "drift" stability curves (solid lines) for experiment RD8. The pH values represent the last stable "drift" pH measurement. At t=326 $Ca(OH)_2$ was added to raise the pH to 8 (broken lines)

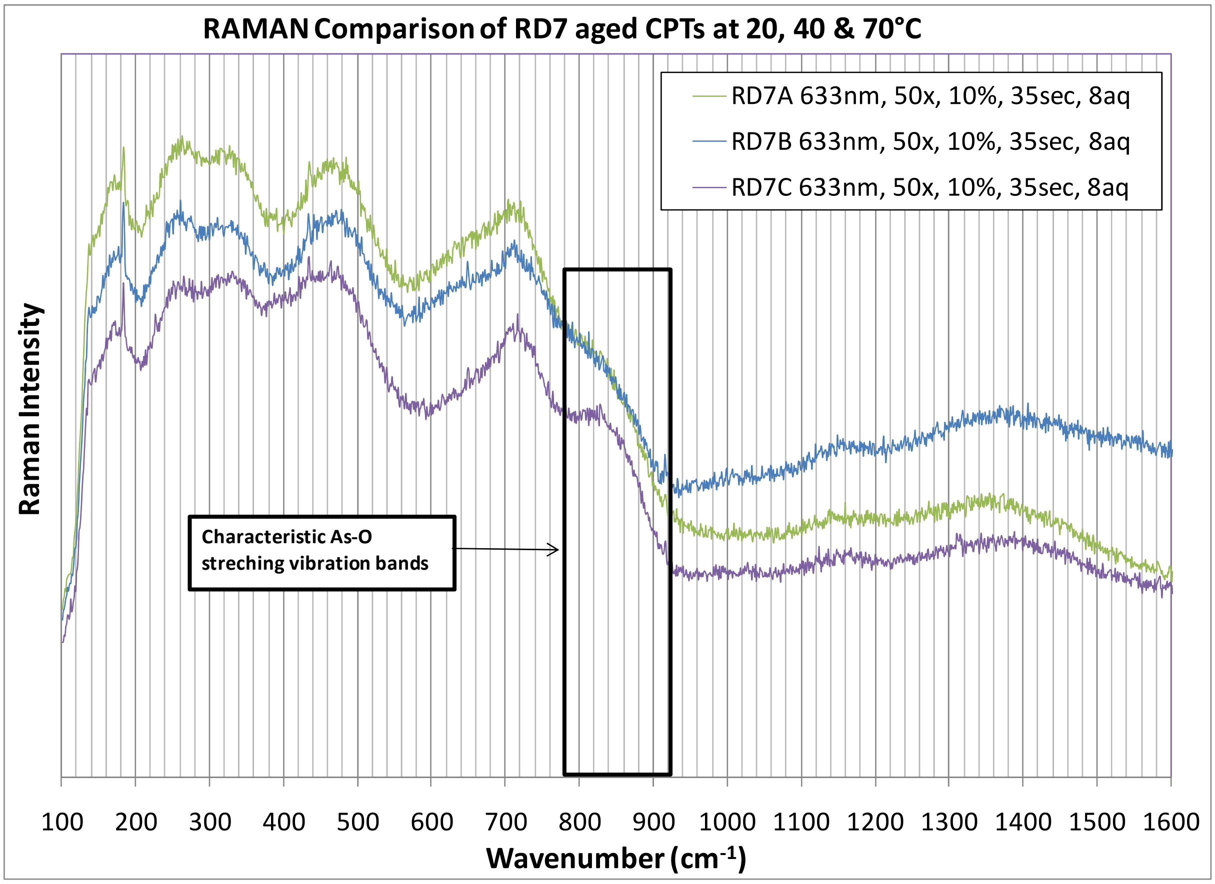

**Figure 58: Raman Spectra for RD7 at different ageing temperatures (A = 20°C, B = 40°C, C = 70°C), showing the shoulders at ~840 cm$^{-1}$ representing the characteristic arsenate stretching vibration bands**

## *8.2 Ferrous Only Hydrolysis Experiments*

Here the pH and $E_h$ evolution with time for the test HEFe-1 of Figure 29 is provided as additional information. The pH and ORP (adjusted to the standard hydrogen electrode, $E_{(SHE)}$) profiles during hydrolysis is shown in Figure 59. Ten minutes into the start of base introduction, the pH reached 7.7 and the ORP dropped to ~ -570 mV. For the next 100 minutes the pH increased only slightly corresponding to the release of protons generated by the hydrolysis of ferrous ions into ferrous hydroxides portrayed by Equation (21).

$$Fe^{2+} + 2H_2O \rightarrow Fe(OH)_2 + 2H^+ \tag{21}$$

Moreover, the slight ORP drop before the start of oxidation coincides with the last steep rise in pH from 8.3 to 11.5 at time 110 and 130 min respectively. It was also observed that this ORP drop started as soon as all Fe(II) in solution (Filtrate [Fe(II)]) was depleted at t=120 min (See Figure 44).

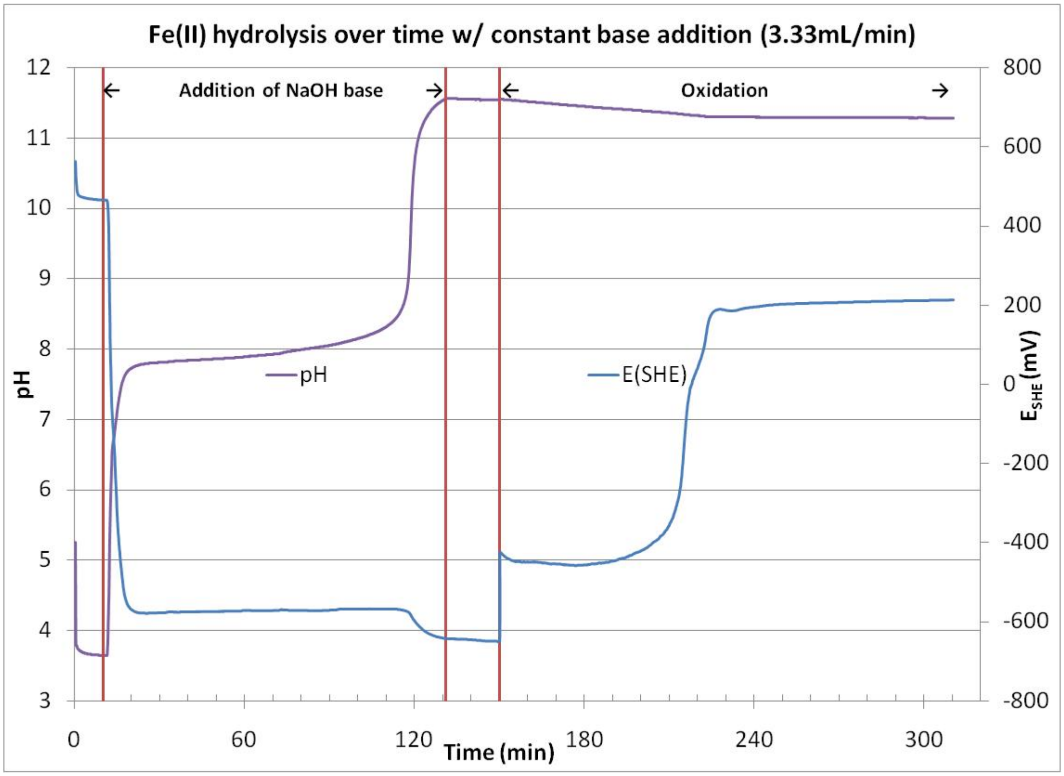

Figure 59: pH and ORP profile over time for HEFe-1 (Figure 29)

## 8.3 Post Hydrolysis Oxidation of Fe(II)-As(V) Solutions at Drifting pH

In this section the oxidation of the hydrolysis products obtained at pH 11.5 from mixed Fe(II)-As(V) solutions (tests HEAs-1 & 2 presented in Chapter 5) are described. This set of data is placed in this Appendix as it was collected at much higher pH than commonly encountered in the arsenic coprecipitation practice.

### 8.3.1 Post Hydrolysis Oxidation of Fe(II)/As(V)= 4 with Drifting pH (Test HEAs-1)

The post hydrolysis oxidation was very fast such that not enough data points were taken to plot a curve showing the rate of ferrous oxidation in the slurry. However, it was recorded that within the first five minutes of oxidation the total [Fe(II)] and soluble [As(V)] dropped from 3552 to 268 mg/L and 81.2 to 7.2 mg/L respectively. These concentration decreases came in addition to a pH drop from 11.5 to 10.85 and ultimately to 7.02 over the course of two hours of continuous oxidation. Past the two hour mark, the iron and arsenic concentrations did not significantly change from the values at 5 minutes (See Table 18). In contrast to the results of tests OEAs-1 & 2 (refer to Chapter 6), in this case arsenic was removed from solution rather than being released most likely by adsorbing onto the newly formed iron(III) hydroxide.

**Table 18: Oxidation of Fe(II)/As(V)=4 Solution after Hydrolysis to pH 11.5 (Air sparging at 300 ml/min and 500 rpm)**

| Time Oxidation (min) | pH | [Fe(II)] in Slurry (Titration) mg/L | [As(V)] in Filtrate (ICP) mg/L |
|---|---|---|---|
| 0 | 11.50 | 3552 | 81.2 |
| 5 | 10.85 | 268 | 7.2 |
| 132 | 7.02 | 279 | 8.8 |

The products of oxidation are discussed in Section 8.3.3.

### 8.3.2 Post Hydrolysis Oxidation of Fe(II)/As(V)= 1.65 with Drifting pH (Test HEAs-2)

The next day following the hydrolysis of the Fe(II)/As(V) = 1.65 solution up to pH 11.3 (refer to Section 5.2.2 in Chapter 5), air sparging was provided and the resultant Fe(II) and As(V) concentrations are shown in Figure 60.

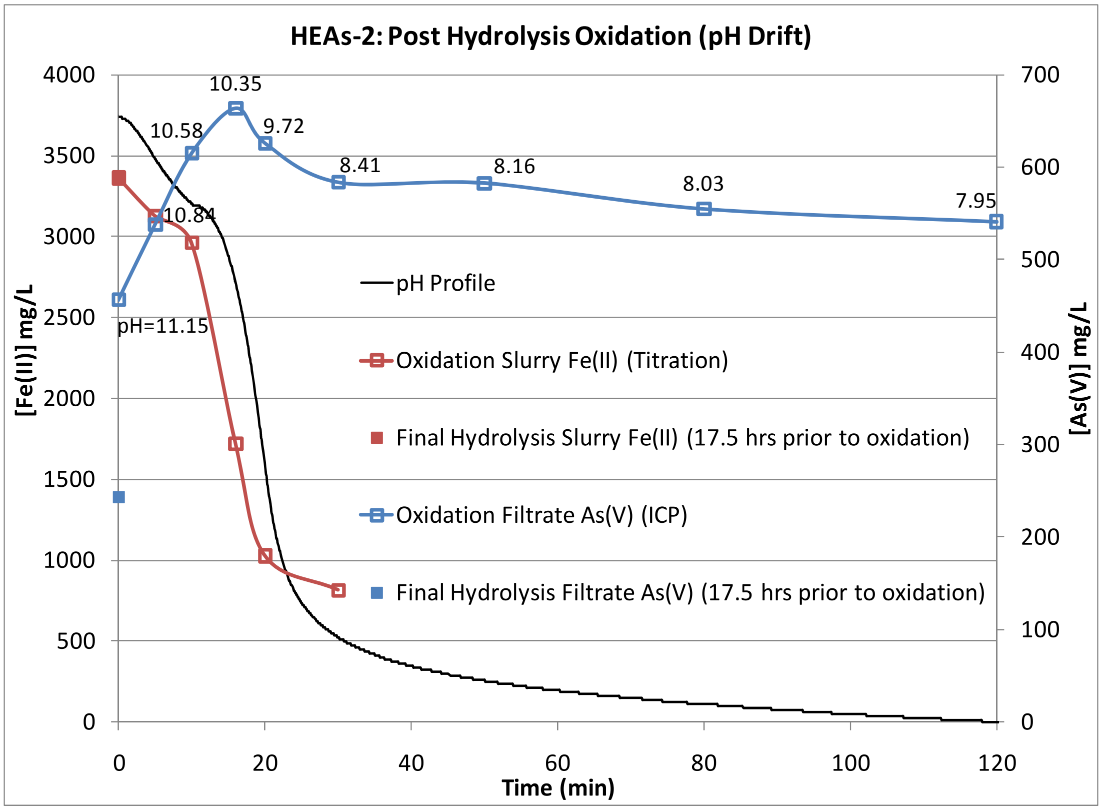

**Figure 60: Post hydrolysis oxidation with drifting pH (Test HEAs-2). The black line represents the pH profile where the data labels above oxidation [As(V)] curve are actual pH values; time 0 represents the onset of oxidation**

On the basis of this graph the following observations can be made:

- Overnight, the concentration of As(V) in solution increased from 243 to 456 mg/L while the total Fe(II) concentration in the slurry remained constant at 3362 mg/L. This suggests that while no oxidation occurred, arsenic managed to dissolve back into solution.

- During the first 10 minutes the rate of Fe(II) oxidation was slower than between t=10 and 20 min. This is due to the change in the impeller agitation speed. Past t=20 min the rate of oxidation decreased and seemed to be controlled by the oxidation products.

- During oxidation, dissolved [As] increased up to a maximum of 663 mg/L at t=16 min before decreasing and apparently stabilizing at 541 mg/L after 2 hours of continuous oxidation.

- It seems that after a certain point (t≈30 min) the pH of oxidation started to stabilize to a value of ~8 and simultaneously the oxidation products became resistant to further oxidation.

### 8.3.3 Characterization of Post-Hydrolysis Oxidation Products

Figure 61 shows the XRD patterns of post-hydrolysis oxidation products. The bottom two patterns, those corresponding HEFe-1 & 2, strongly match to goethite (JCPDS card# 00-029-0713). However, in the case of the final oxidation products of arsenic-bearing hydrolysis experiments (HEAs-1 & 2), the XRD matching software did not find any matching patterns.

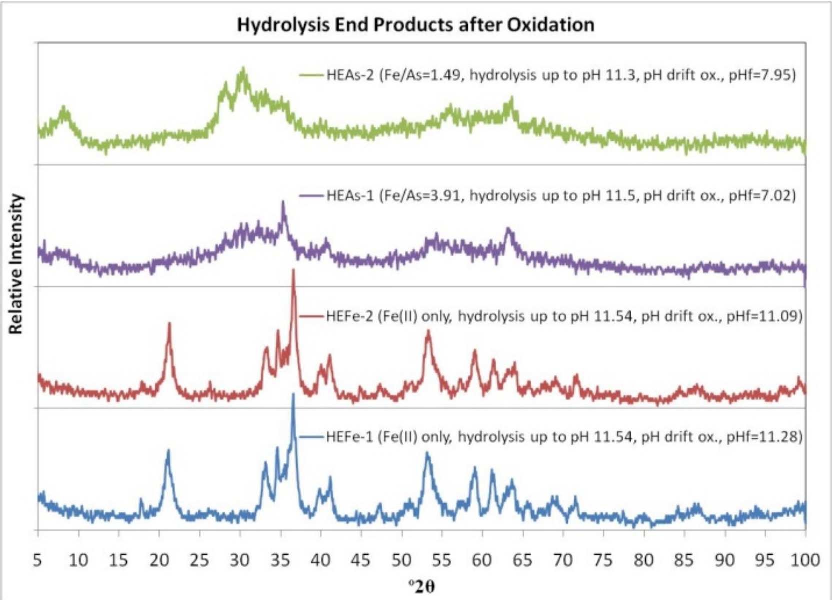

**Figure 61: XRD patterns of post-hydrolysis oxidation products (experiments HEFe1-2 & HEAs1-2)**

Lastly, it was observed that during oxidation of HEAs solutions without pH adjustments, the pH dropped significantly down from 11.5 and 11.3 for HeAs-1 & 2 to 7.02 and 7.95 respectively. In contrast the final pH of oxidation for ferrous only solutions was at most 0.45 pH units. This indicates that the oxidation of the initial Fe(II)-$AsO_4$ phase followed by the hydrolysis of $Fe^{3+}$ to from iron(III) hydroxides generated lots of protons. This is especially true for HEAs-1 where there was a significant excess of initial ferrous iron which likely precipitated as $Fe(OH)_2$ and/or GRII during hydrolysis. As these phases oxidize and subsequently generate new iron(III) hydroxides the pH of the solution is known to decrease [44, 76]. We can also see that there are multiple inflection points in the pH and ORP curves during the oxidation of HEAs-1 (Figure 32) indicating the transformation (oxidation) of one phase to another.

## *8.4 Mass Balance and $E_h$-pH Pourbaix Diagrams*

This section consists of additional information regarding the relationship between a Pourbaix diagram, such as the one depicted in Figure 37 (Section 6.1), and $E_h$ and pH curves. In their publication, authors Ruby *et al.* [45] explain there is a clear and distinct relationship that can be established between a mass balance diagram and a Pourbaix diagram. In a very simple system consisting of only dissolved mixed valence iron, one can establish the phase regions. More specifically, corresponding equivalent points from titrations of mixed iron(II) and iron(III) solutions can be plotted onto a mass-balance diagram with reasonable accuracy [46]. Furthermore, relatively constant pH and ORP values to be found during plateaus in these titration curves can be plotted into Pourbaix diagrams, thereby representing the phases present. Ruby *et al.* [45] have shown the advantages and importance of $E_h$ and pH monitoring for corrosion scientists and, in parallel, its application in aqueous processing. For instance, during a controlled oxidation of Fe(II) species, the oxidation path can be drawn in the mass-balance diagram and the phases at any given time can be predicted. Simultaneously, $E_h$ and pH values to be found in "buffering" regions during oxidation may be plotted in a constructed Pourbaix diagram demonstrating that the expected species are in fact "temporally" electrochemically in equilibrium. Without getting into too much detail, a brief look at Figure 62 to Figure 64 will illustrate the aforementioned application.

The line $L_{ox}$ in the mass-balance diagram describes the oxidation path (by addition of sodium persulphate, generating a slope of the reaction path equal to 0) of initially dissolved Fe(II) ions after addition of NaOH base at an $[OH^-]/[Fe(II)]$ molar ratio of 1.5 equivalent to raising the pH to ~8. Between points $P_0$ and $P_1$ oxidation of $Fe(OH)_2$ into GR(II) occurs, where dissolved Fe(II) ions are not involved in the oxidation. According to the mass-balance diagram (Figure 62), at $P_1$ all $Fe(OH)_2$ is oxidized to GR(II). At the same time when looking at the $E_h$-pH monitoring of this reaction (Figure 63), one can see an equivalent point $t_1$. To represent this relationship with a visual aid, the last two figures are superimposed in Figure 64 showing an intersection of equivalent point $t_1$ and its abscissa x=0.23 with the line $L_{ox}$ at $P_1$. Likewise, the same occurs at point $P_2$ with equivalent point $t_2$ where all GR(II) is oxidized into FeOOH.

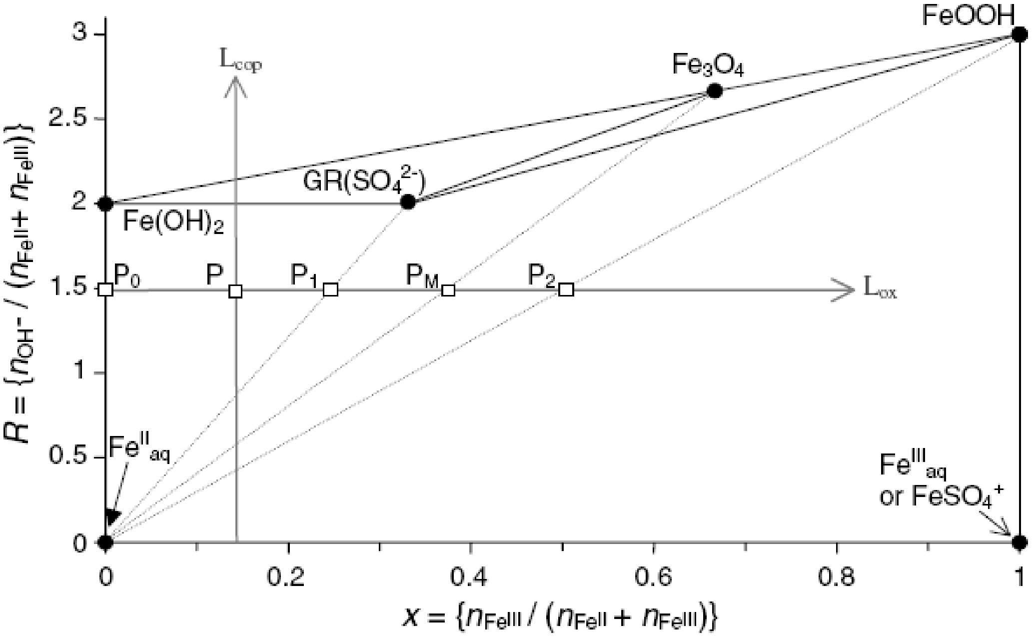

**Figure 62: Fe(II)-Fe(III) mass-balance diagram showing the route of an oxidation of Fe(II) species by $Na_2S_2O_8$ (line $L_{ox}$) [45]**

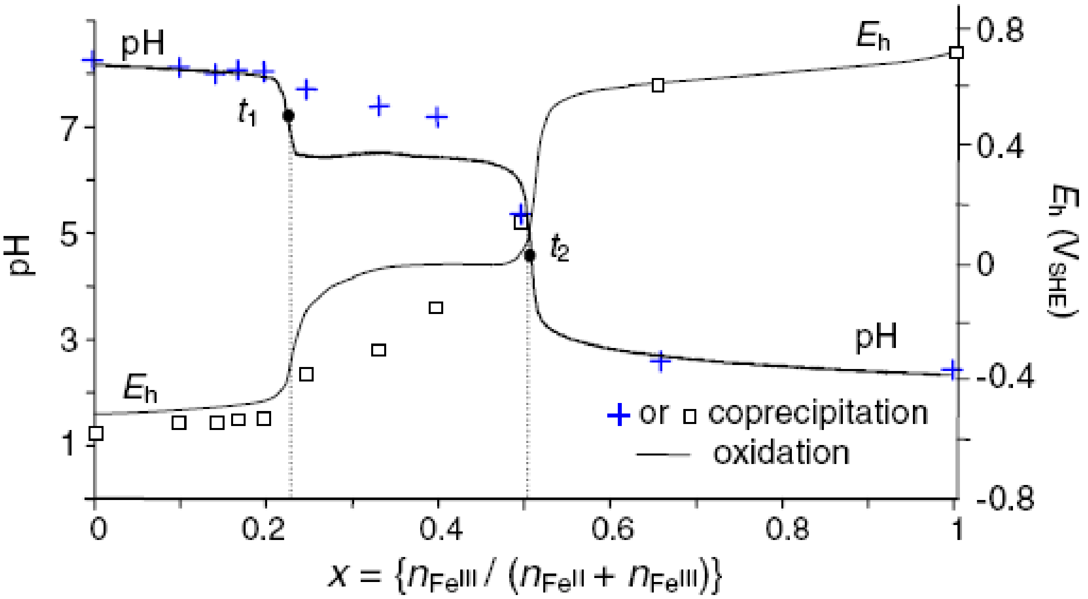

**Figure 63: Evolution of pH and ORP during the oxidation of Fe(II) species by $Na_2S_2O_8$ (full lines) [45]**

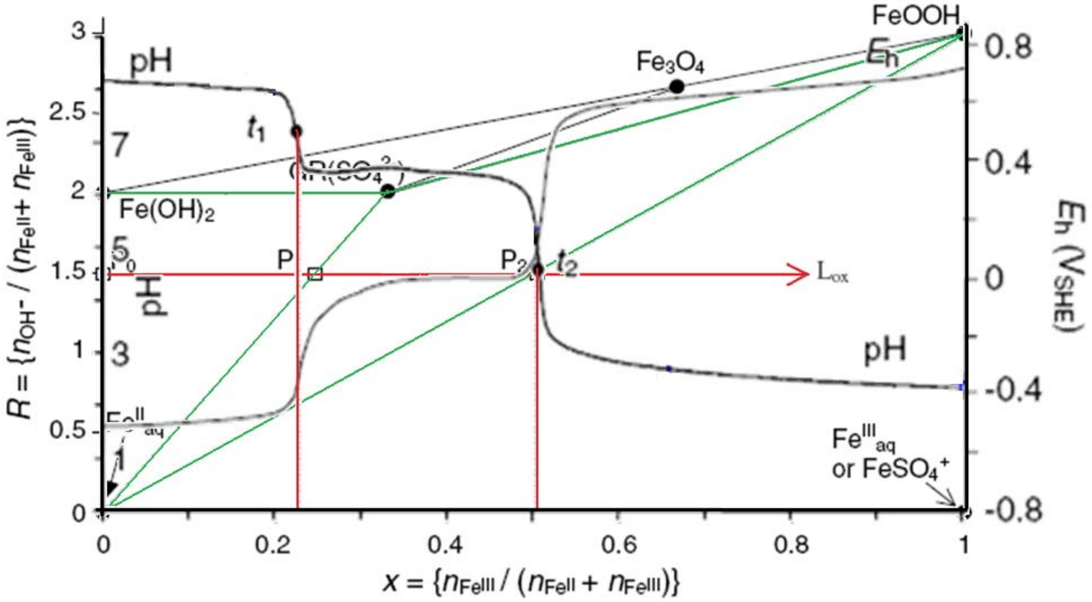

**Figure 64: Superimposing Figure 62 and Figure 63 to show how equivalent points $t_1$ & $t_2$ occur as the oxidation path represented by $L_{ox}$ cross over to a new ternary system [45]**

Finally, the pH and $E_h$ values of the three plateau regions seen in Figure 63 can be accurately plotted into an $E_h$-pH Pourbaix diagram (Figure 37) specifically constructed for the experimental conditions of the study [45].

From this example, it is shown that measurements of ORP and pH can provide important insights on the oxidation of species and the subsequent transformation of precipitates into different phases. In the case of arsenic coprecipitation with mixed Fe(II) and Fe(III) sulphate media the analogous system would be significantly more complex. In 1991 Khoe *et al.* [53] were the first authors to attempt to produce thermochemical data on the iron(II)-arsenate system. At the present time it is beyond the scope of this Thesis to delve further into this topic, however future research should not omit these valuable concepts.

## *8.5 Oxidation Experiments with Arsenic at Constant pH=8*

Figure 65 and Figure 66 show the increase of the pH as a function of time during automatic constant base addition. These figures also validate the accuracy of the data logging software and show its ability to capture detailed pH fluctuations such as those during air oxidation.

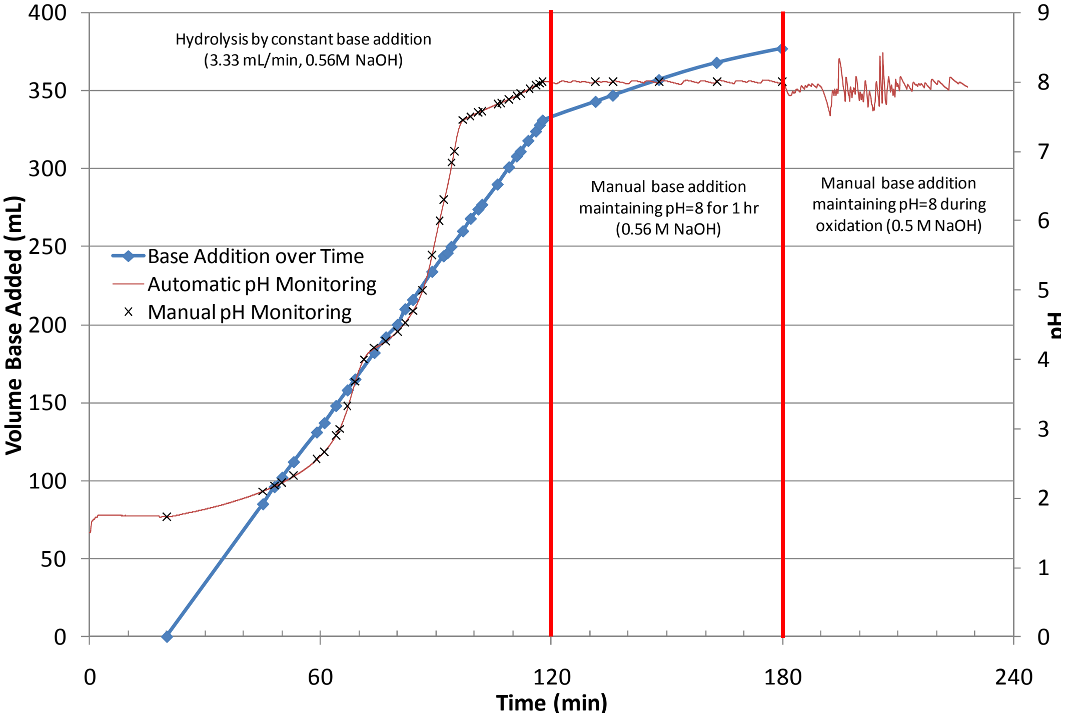

Figure 65: OEAs-1 – Base addition over time and pH monitoring

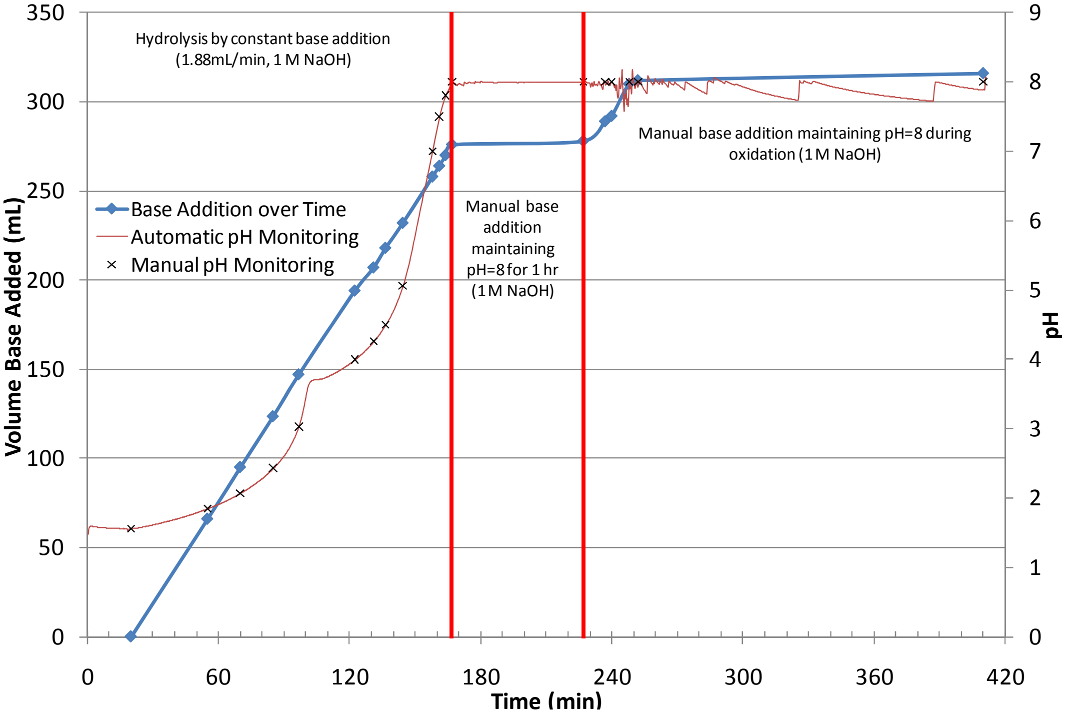

Figure 66: OEAs-2 – Base addition over time and pH monitoring

Figure 67 and Figure 68 compare the concentration profiles during hydrolysis of two types of experiments (OEAs and HEAs) with similar Fe/As molar ratio. These curves show good reproducibility in terms of the behaviour of Fe and As concentrations during constant pH addition.

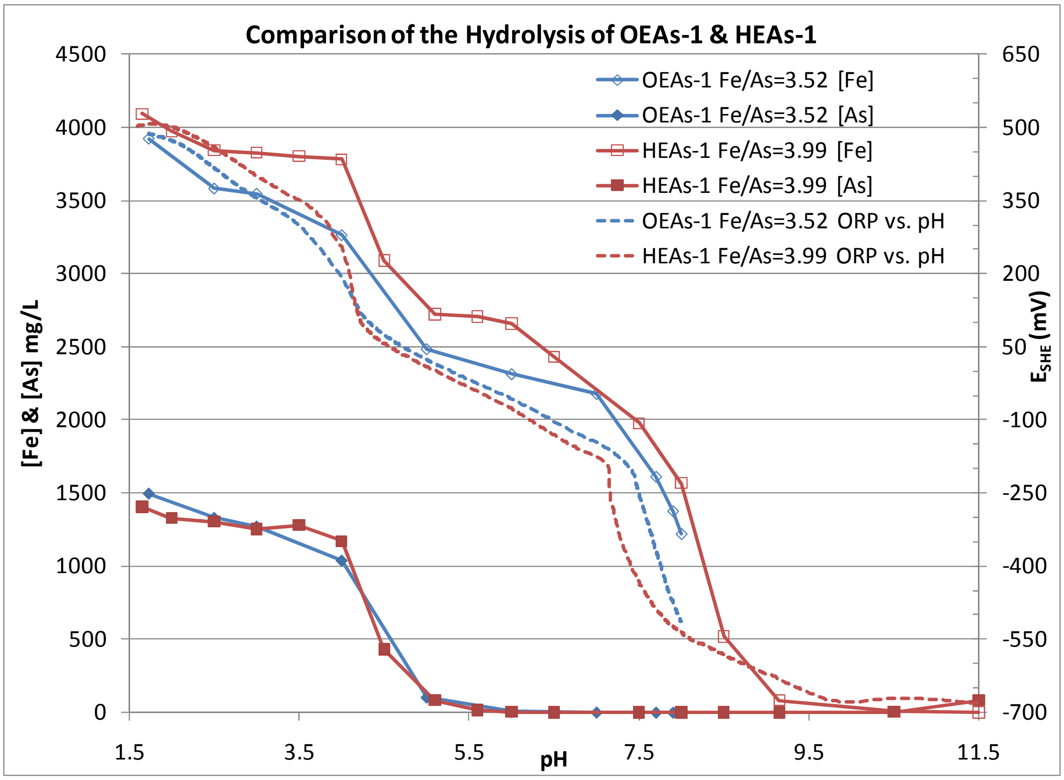

Figure 67: Comparing [As] & [Fe] in filtered samples as a function of pH during the hydrolysis of experiments HEAs-1 and OEAs-1, both which have a targeted Fe/As molar ratio of 4. Also plotted are the ORP's given with respect to the standard hydrogen electrode ($E_{SHE}$) in mV as a function of pH

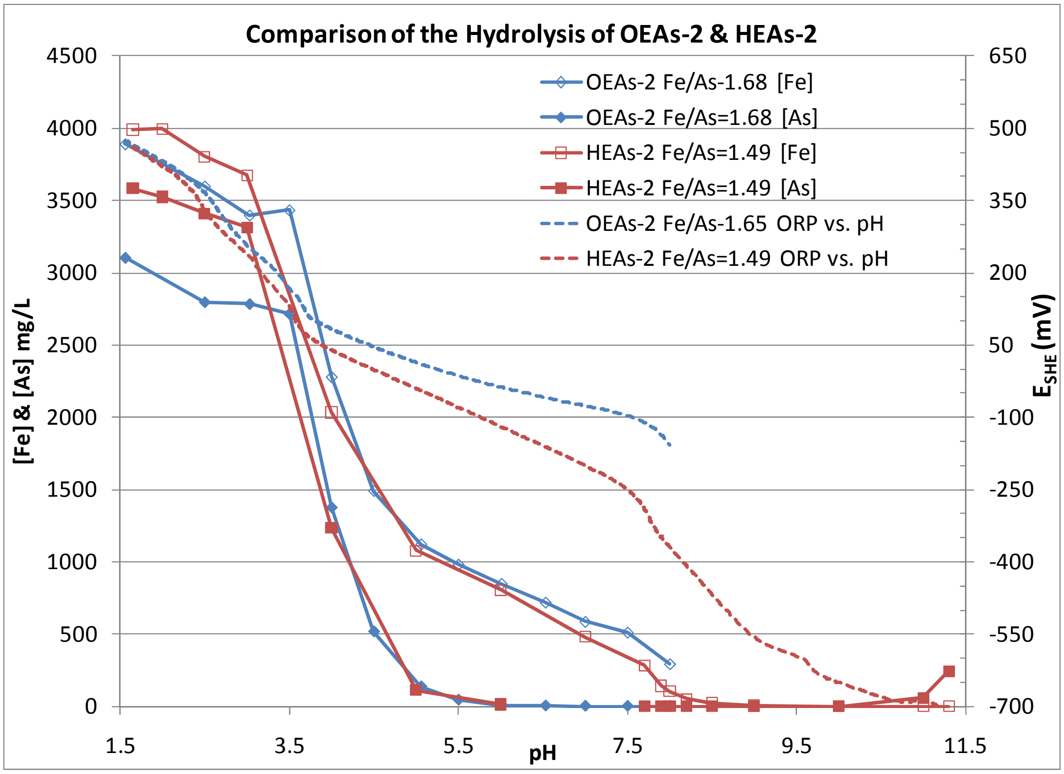

Figure 68: Comparing [As] & [Fe] in filtered samples as a function of pH during the hydrolysis of experiments HEAs-2 and OEAs-2, both which have a targeted Fe/As molar ratio of 1.65. Also plotted are the ORP's given with respect to the standard hydrogen electrode ($E_{SHE}$) in mV as a function of pH

Figure 69 shows the $E_h$ and pH evolution during constant base addition to an Fe(II)/As(V) solution at a molar ratio of 1.68.

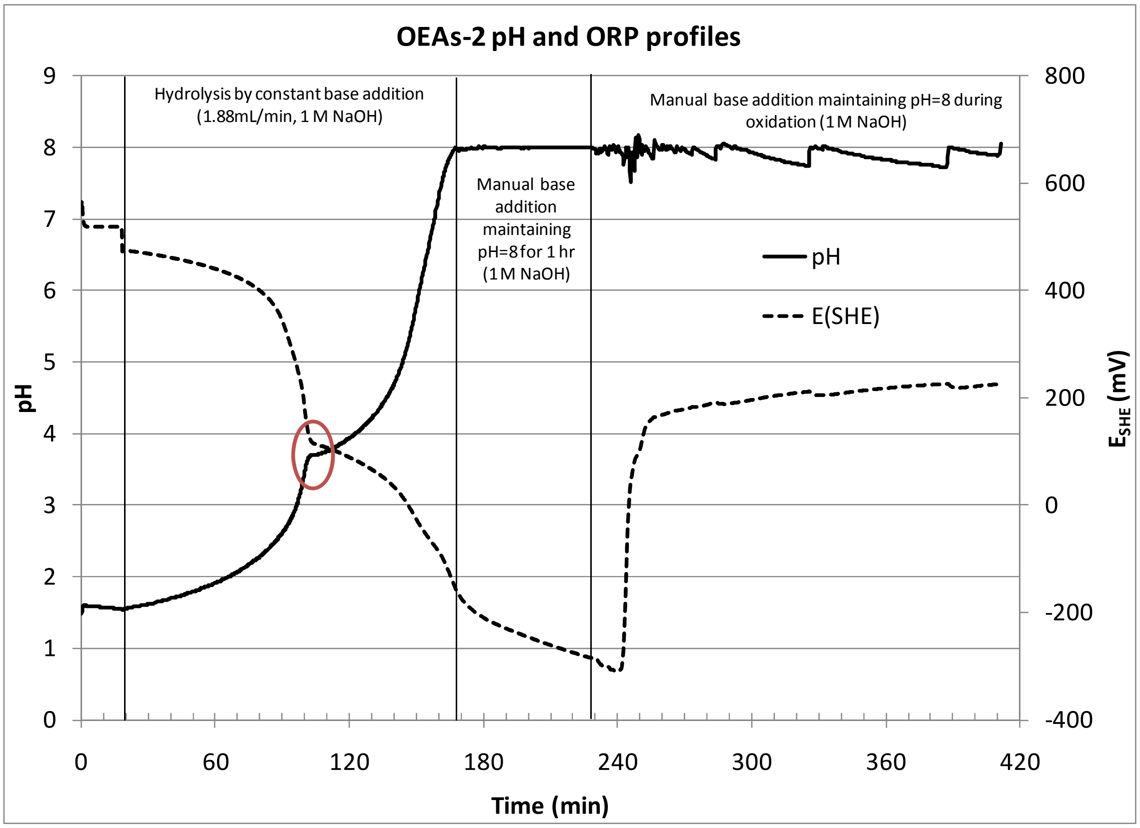

**Figure 69: pH and ORP evolution during hydrolysis and oxidation of ferrous-arsenate containing solution [Fe(II)/As(V)=1.68]**

The same discussion that applied for OEAs-1 found in Section 6.4.2 can be said for OEAs-2, which had a similar fate for arsenic. At time t=250 or 20 minutes into oxidation, a sharp rise in $E_h$ occured (Figure 69). This time also coincided with the last data point of the linear portion of the total [Fe(II)] curve (Figure 47 top). At this point, 1083 mg/L ferrous iron remained as a solid phase which was resistant to further oxidation only dropping to 871 mg/L after 160 minutes of air sparging. If we make the same assumption as for OEAs-1, the symplesite phase containing 1083 mg/L Fe(II) of corresponds to 969 mg/L of the initial 3106 mg/L As(V). Therefore, the majority of the arsenic liberated upon oxidation of the predominant ferrous arsenate phase must have been instantly adsorbed by subsequently formed iron(III) oxidation products. It is noteworthy to bring attention to Figure 48 (right) where the [As] curve during oxidation shows multiple concentration drops as oxidation proceeds with time. This could imply a short delay for arsenate uptake between the simultaneous breakdown of symplesite (releasing arsenates to solution) and the oxidation of ferrous iron to form new iron(III) hydroxide arsenate adsorption sites.

From these results it can be concluded that under oxidizing conditions at a constant pH of 8 for a substantial amount of time, the final phase contains soluble arsenic concentrations below 18 and 35 mg/L for OEAs-1 and 2 respectively.

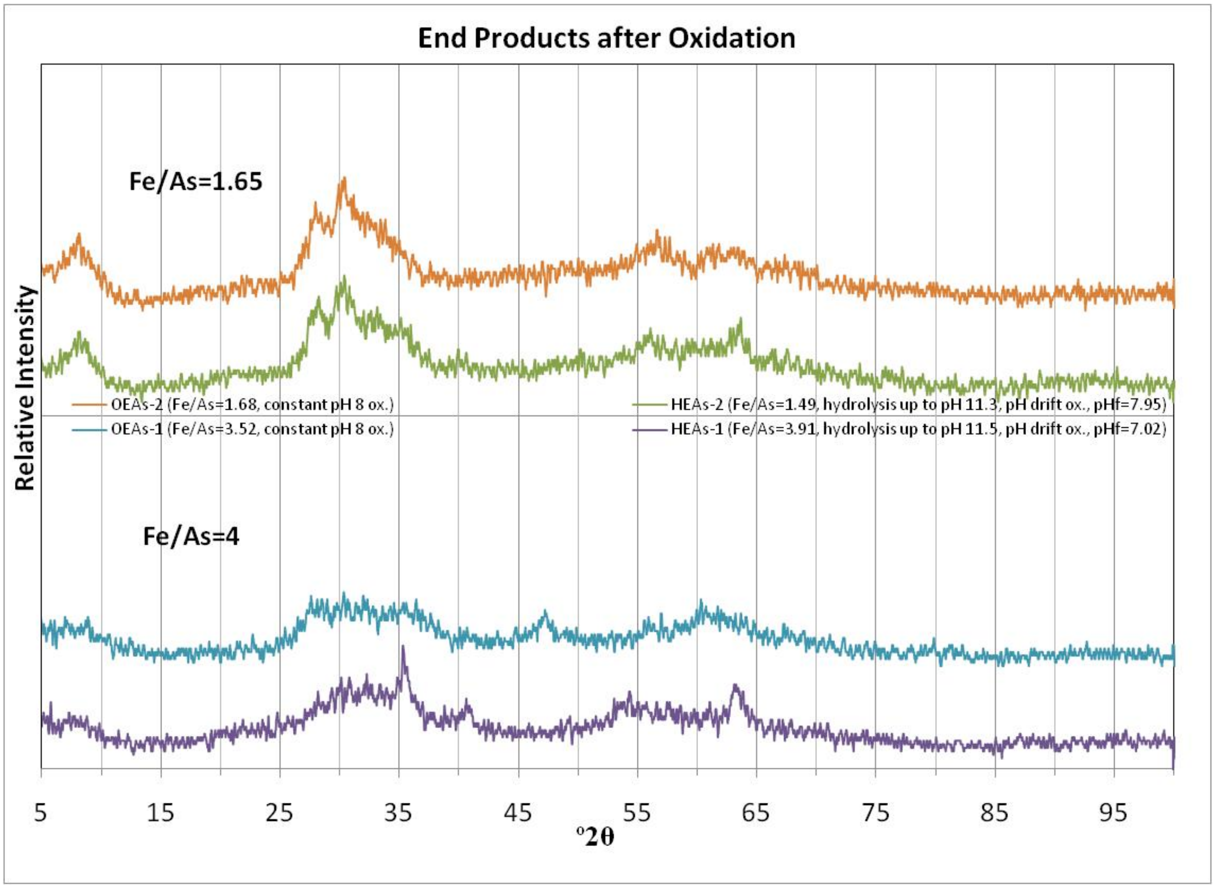

**Figure 70: Comparing XRD patterns for HEAs and OEAs experiments with respect to their initial solution Fe/As molar ratios**

## 8.6 Consumption of Hydroxyl Anions during Hydrolysis of Ferrous Sulphate Solutions with and without Arsenic

Figure 71 compares the accumulation of $[OH^-]$/total initial [Fe(II)] versus pH for each experiment involving the hydrolysis of Fe(II)/As(V) or Fe(II) only solutions by constant base addition. The dotted curves are for solution containing arsenic whose initial pH was kept lower than pH 2 in order to prevent precipitation of arsenic.

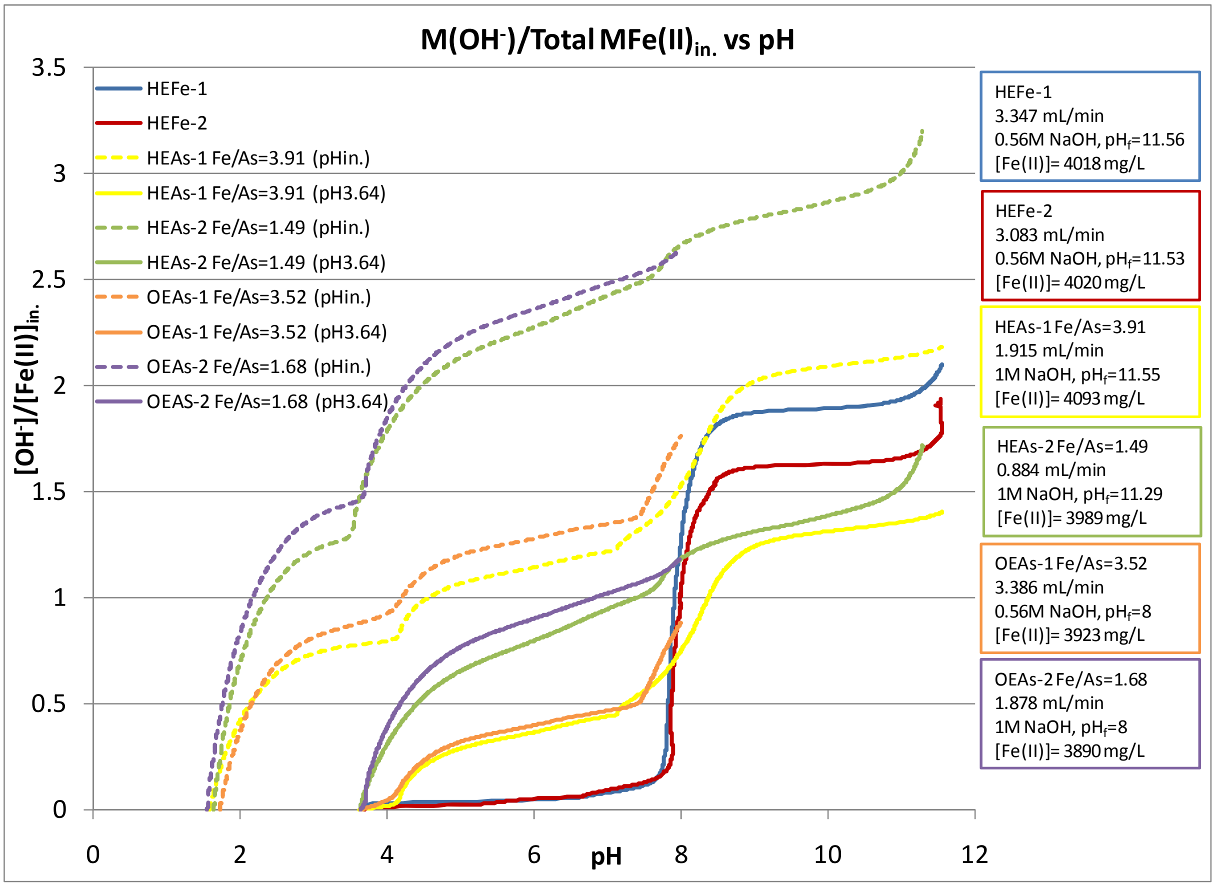

**Figure 71: Accumulation of moles of OH$^-$/total initial moles of Fe(II) plotted over pH for all enhanced hydrolysis tests and the hydrolysis portion of constant pH 8 Fe-As solution oxidation tests. Dotted lines represent the accumulation of M(OH$^-$) over total MFe(II)$_{in.}$ starting from the initial pH of the solution, whereas solids lines represent the accumulation of M(OH$^-$) over total MFe(II)$_{in,}$ starting from pH 3.64**

The curves basically show how much base was needed in order to achieve a certain pH. In other words, we can clearly see that increasing the initial arsenic concentration in a solution required more hydroxyl anions to reach say pH 6. Moreover, the curves show the reproducibility of the hydrolysis for solution containing similar starting Fe/As molar ratios. Therefore these curves show that during the hydrolysis of solutions containing arsenic, reactions occur which release protons in the solution that are effectively offset by the constant base addition. Another way of looking at it is to select a fixed ratio of [OH$^-$]/[Fe(II)], say 0.5, and see what the pH of the different starting solutions are. In that case, a solution that contained only Fe(II) initially reached a pH of 8 whereas solutions with an initial Fe/As molar ratio of 4 and 1.5 reached pH values of 7.1 and 4.3 respectively. These curves also have the purpose of showing the inflection points discussed in Chapters 5 and 6.

## 8.7 pyConsort Software

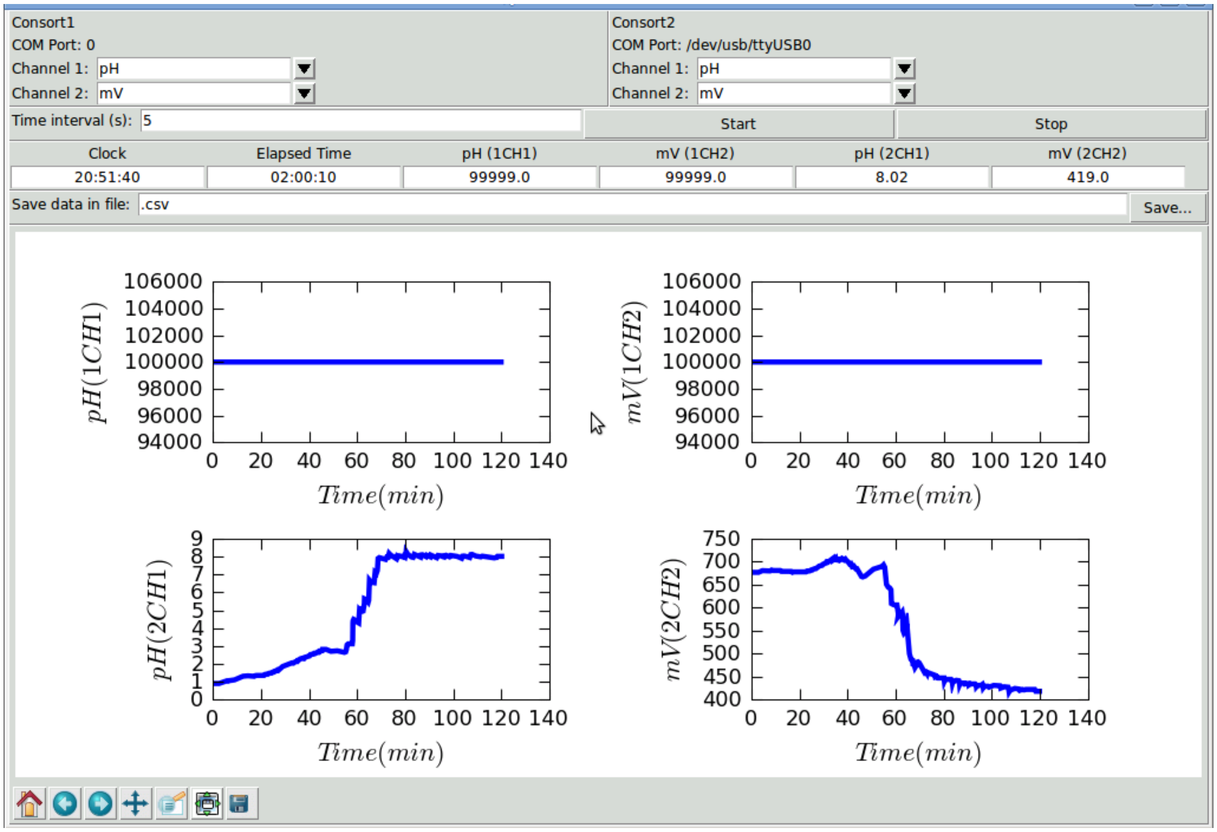

Consort1
COM Port: 0
Channel 1: pH
Channel 2: mV

Consort2
COM Port: /dev/usb/ttyUSB0
Channel 1: pH
Channel 2: mV

Time interval (s): 5

| Clock | Elapsed Time | pH (1CH1) | mV (1CH2) | pH (2CH1) | mV (2CH2) |
|---|---|---|---|---|---|
| 20:51:40 | 02:00:10 | 99999.0 | 99999.0 | 8.02 | 419.0 |

Save data in file: .csv

**Figure 72: Screen shot of pyConsort program showing live data acquisition from Consort R305 unit**

This open source program written in Python (>2.5) was developed by Philippe Tétreault-Pinard. Third party libraries used include pySerial and matplotlib. The source code and GUI code are both available for download at the following website: http://consort.sourceforge.net

# 9 References

[1] C. Rinas, J. Rowson*, et al.* "*Aging of reduced arsenic minerals in uranium mill tailings at the McClean Lake operation*", in Uranium 2010 The Future is U; Saskatoon, Saskatchewan. Eds. E. K. Lam, J. W. Rowson*, et al.*, pp. 377-387, 2010: Canadian Institute of Mining, Metallurgy and Petroleum

[2] E. Krause and V. A. Ettel, "*Solubilities and stabilities of ferric arsenate compounds*", Hydrometallurgy*,* vol. 22(3), 1989, pp. 311-337.

[3] B. J. Moldovan and M. J. Hendry, "*Characterizing and quantifying controls on arsenic solubility over a pH range of 1−11 in a uranium mill-scale experiment*", Environmental Science & Technology*,* vol. 39(13), 2005, pp. 4913-4920.

[4] D. Langmuir, J. Mahoney*, et al.*, "*Predicting arsenic concentrations in the porewaters of buried uranium mill tailings*", Geochimica et Cosmochimica Acta*,* vol. 63(19-20), 1999, pp. 3379-3394.

[5] D. Langmuir, J. Mahoney*, et al.*, "*Solubility products of amorphous ferric arsenate and crystalline scorodite ($FeAsO_4 \cdot 2H_2O$) and their application to arsenic behavior in buried mine tailings*", Geochimica et Cosmochimica Acta*,* vol. 70(12), 2006, pp. 2942-2956.

[6] J. Mahoney, M. Slaughter*, et al.*, "*Control of As and Ni releases from a uranium mill tailings neutralization circuit: Solution chemistry, mineralogy and geochemical modeling of laboratory study results*", Applied Geochemistry*,* vol. 22(12), 2007, pp. 2758-2776.

[7] N. Chen, D. T. Jiang*, et al.*, "*Structural characterization of poorly-crystalline scorodite, iron(III)-arsenate co-precipitates and uranium mill neutralized raffinate solids using X-ray absorption fine structure spectroscopy*", Geochimica et Cosmochimica Acta*,* vol. 73(11), 2009, pp. 3260-3276.

[8] R. J. De Klerk "*Investigating the continuous circuit coprecipitation of arsenic(V) with ferric iron in sulphate media*", M.Eng. Thesis, McGill University, 2008

[9] S. Hirano, X. Cui*, et al.*, "*Difference in uptake and toxicity of trivalent and pentavalent inorganic arsenic in rat heart microvessel endothelial cells*", Archives of Toxicology*,* vol. 77(6), 2003, pp. 305-312.

[10] S. Dixit and J. G. Hering, "*Comparison of arsenic(V) and arsenic(III) sorption onto iron oxide minerals: Implications for arsenic mobility*", Environmental Science & Technology*,* vol. 37(18), 2003, pp. 4182-4189.

[11] P. L. Smedley and D. G. Kinniburgh, "*A review of the source, behaviour and distribution of arsenic in natural waters*", Applied Geochemistry*,* vol. 17(5), 2002, pp. 517-568.

[12] R. A. Root, S. Dixit*, et al.*, "*Arsenic sequestration by sorption processes in high-iron sediments*", Geochimica et Cosmochimica Acta*,* vol. 71(23), 2007, pp. 5782-5803.

[13] "*Minor Clarification of National Primary Drinking Water Regulation for Arsenic"*, E. P. Agency, Editor. 2003, Federal Register: Washington.

[14] F.-P.-T. C. o. D. Water, "*Arsenic - Guidlines for Canadian Drinking Water Quality"*, W. Q. a. H. Bureau, Editor. 2006, Health Canada: Ottawa.

[15] "*CRC Handbook of Chemistry and Physics*", Journal of the American Chemical Society, vol. 127, pp. 4542-4542, 2005.

[16] D. Paktunc, J. Dutrizac, *et al.*, "*Synthesis and phase transformations involving scorodite, ferric arsenate and arsenical ferrihydrite: Implications for arsenic mobility*", Geochimica et Cosmochimica Acta, vol. 72(11), 2008, pp. 2649-2672.

[17] P. A. Riveros, J. E. Dutrizac, *et al.*, "*Arsenic disposal practices in the metallurgical industry*", Canadian Metallurgical Quarterly, vol. 40(4), 2001, pp. 395-420.

[18] G. B. Harris and E. Krause "*The disposal of arsenic from metallurgical processes: Its status regarding ferric arsenate*", in Extractive Metallurgy of Copper, Nickel and Cobalt: Fundamental Aspects; Denver, CO. Eds. R. G. Reddy and R. Weizenbach, pp. 1221-1237, 1993: Minerals, Metals, & Materials Society

[19] B. Harris "*The removal of arsenic from process solutions: Theory and industrial practice*", in Hydrometallurgy 2003; Vancouver. Eds. C. A. Young, A. M. Alfantazi, *et al.*, pp. 1889-1902, 2003: TSM

[20] "*Metal Mining Effluent Regulations"*, F. Act, Editor. 2002, the Queen's Pinter for Canada: Ottawa. p. 1246-1543.

[21] R. G. Robins, J. C. Y. Huang, *et al.* "*The adsorption of arsenate ion by ferric hydroxide*", in Arsenic Metallurgy: Fundamentals and Applications; Phoenix, AZ. Eds. R. G. Reddy, J. L. Hendrix, *et al.*, pp. 99-112, 1988: The Minerals, Metals and Materials Society

[22] Y. Jia and G. P. Demopoulos, "*Adsorption of arsenate onto ferrihydrite from aqueous solution: Influence of media (sulfate vs nitrate), added gypsum, and pH alteration*", Environ. Sci. Technol., vol. 39(24), 2005, pp. 9523-9527.

[23] J. A. Wilkie and J. G. Hering, "*Adsorption of arsenic onto hydrous ferric oxide: effects of adsorbate/adsorbent ratios and co-occurring solutes*", Colloids and Surfaces A: Physicochemical and Engineering Aspects, vol. 1071996, pp. 97-110.

[24] Y. Jia and G. P. Demopoulos, "*Coprecipitation of arsenate with iron(III) in aqueous sulfate media: Effect of time, lime as base and co-ions on arsenic retention*", Water Research, vol. 42(3), 2008, pp. 661-668.

[25] J. Mahoney, D. Langmuir, *et al.*, "*Raffinate neutralization experiments at the McClean Lake mill - Removal of arsenic and nickel"*, in *Uranium in the Environment*, B. J. Merkel and A. Hasche-Berger, Editors. 2006, Springer: Berlin. p. 225-234.

[26] L. C. Roberts, S. J. Hug, *et al.*, "*Arsenic removal with iron(II) and iron(III) in waters with high silicate and phosphate concentrations*", Environ. Sci. Technol., vol. 38(1), 2004, pp. 307-315.

[27] J. W. Hohn, L. G. Twidwell, *et al.* "*A comparison of ferrihydrite and aluminum-modified ferrihydrite for the removal of arsenate from aqueous solution by co-precipitation*", in Iron Control in Hydrometallurgy; Montreal. Eds. J. E. Dutrizac and P. A. Riveros, pp. 911-926, 2006: CIM

[28] C. C. Fuller, J. A. Davis, *et al.*, "*Surface chemistry of ferrihydrite: Part 2. Kinetics of arsenate adsorption and coprecipitation*", Geochimica et Cosmochimica Acta, vol. 57(10), 1993, pp. 2271-2282.

[29] G. A. Waychunas, B. A. Rea, *et al.*, "*Surface chemistry of ferrihydrite: Part 1. EXAFS studies of the geometry of coprecipitated and adsorbed arsenate*", Geochimica et Cosmochimica Acta, vol. 57(10), 1993, pp. 2251-2269.

[30] J. L. Jambor and J. E. Dutrizac, "*Occurrence and constitution of natural and synthetic ferrihydrite, a widespread iron oxyhydroxide*", Chemical Reviews, vol. 98(7), 1998, pp. 2549-2586.

[31] Y. Jia, L. Xu, *et al.*, "*Observation of surface precipitation of arsenate on ferrihydrite*", Environ. Sci. Technol., vol. 40(10), 2006, pp. 3248-3253.

[32] T. Sato, T. Goto, *et al.*, "*The oxidation of iron(II) sulfate with sulfur dioxide and oxygen mixtures*", Bulletin of the Chemical Society of Japan, vol. 57(8), 1984, p. 5.

[33] W. Davison and G. Seed, "*The kinetics of the oxidation of ferrous iron in synthetic and natural waters*", Geochimica et Cosmochimica Acta, vol. 47(1), 1983, pp. 67-79.

[34] W. Sung and J. J. Morgan, "*Kinetics and product of ferrous iron oxygenation in aqueous systems*", Environmental Science & Technology, vol. 14(5), 1980, pp. 561-568.

[35] W. Stumm and G. F. Lee, "*Oxygenation of Ferrous Iron*", Industrial & Engineering Chemistry, vol. 53(2), 1961, pp. 143-146.

[36] H. Tamura, K. Goto, *et al.*, "*The effect of ferric hydroxide on the oxygenation of ferrous ions in neutral solutions*", Corrosion Science, vol. 16(4), 1976, pp. 197-207.

[37] H. Tamura, K. Goto, *et al.*, "*Effect of anions on the oxygenation of ferrous ion in neutral solutions*", Journal of Inorganic and Nuclear Chemistry, vol. 38(1), 1976, pp. 113-117.

[38] D. Filippou, T. C.-M. Cheng, *et al.*, "*Gas-liquid oxygen mass-transfer; from fundamentals to applications in hydrometallurgical systems*", Mineral Processing and Extractive Metallurgy Review: An International Journal, vol. 20(4), 2000, pp. 447-502.

[39] B. Morgan and O. Lahav, "*The effect of pH on the kinetics of spontaneous Fe(II) oxidation by $O_2$ in aqueous solution - basic principles and a simple heuristic description*", Chemosphere, vol. 68(11), 2007, pp. 2080-2084.

[40] F. J. Millero, "*The effect of ionic interactions on the oxidation of metals in natural waters*", Geochimica et Cosmochimica Acta, vol. 49(2), 1985, pp. 547-553.

[41] S. R. Randall, D. M. Sherman, *et al.*, "*Sorption of As(V) on green rust (*$Fe_4(II)Fe_2(III)(OH)_{12}SO_4\cdot 3H_2O$*) and lepidocrocite ([gamma]-FeOOH): Surface complexes from EXAFS spectroscopy*", Geochimica et Cosmochimica Acta, vol. 65(7), 2001, pp. 1015-1023.

[42] T. Misawa, K. Hashimoto, *et al.*, "*Formation of* $Fe(II)_1$*-*$Fe(III)_1$ *intermediate green complex on oxidation of ferrous ion in neutral and slightly alkaline sulphate solutions*", Journal of Inorganic and Nuclear Chemistry, vol. 35(12), 1973, pp. 4167-4174.

[43] O. P. Perez and Y. Umetsu, "*ORP-monitored magnetite formation from aqueous solutions at low temperatures*", Hydrometallurgy, vol. 55(1), 2000, pp. 35-56.

[44] R. Lin, R. L. Spicer, *et al.*, "*A study of the oxidation of ferrous hydroxide in slightly basic solution to produce [gamma]-FeOOH*", Colloids and Surfaces A: Physicochemical and Engineering Aspects, vol. 113(1-2), 1996, pp. 79-96.

[45] C. Ruby, A. Géhin, *et al.*, "*Mass-balance and Eh-pH diagrams of FeII-III green rust in aqueous sulphated solution*", Corrosion Science, vol. 48(11), 2006, pp. 3824-3837.

[46] C. Ruby, A. Géhin, *et al.*, "*Coprecipitation of Fe(II) and Fe(III) cations in sulphated aqueous medium and formation of hydroxysulphate green rust*", Solid State Sciences, vol. 5(7), 2003, pp. 1055-1062.

[47] M. Mukiibi, W. P. Ela, *et al.*, "*Effect of ferrous iron on arsenate sorption to amorphous ferric hydroxide*", Annals of the New York Academy of Sciences, vol. 1140(Environmental Challenges in the Pacific Basin), 2008, pp. 335-345.

[48] J. Jönsson and D. M. Sherman, "*Sorption of As(III) and As(V) to siderite, green rust (fougerite) and magnetite: Implications for arsenic release in anoxic groundwaters*", Chemical Geology, vol. 255(1-2), 2008, pp. 173-181.

[49] Z. Lin and R. W. Puls, "*Potential indicators for the assessment of arsenic natural attenuation in the subsurface*", Advances in Environmental Research, vol. 7(4), 2003, pp. 825-834.

[50] P. Refait, P. Girault, *et al.*, "*Influence of arsenate species on the formation of Fe(III) oxyhydroxides and Fe(II-III) hydroxychloride*", Colloids and Surfaces A: Physicochemical and Engineering Aspects, vol. 332(1), 2009, pp. 26-35.

[51] J. Majzlan, L. Mazeina, *et al.*, "*Enthalpy of water adsorption and surface enthalpy of lepidocrocite ([gamma]-FeOOH)*", Geochimica et Cosmochimica Acta, vol. 71(3), 2007, pp. 615-623.

[52] Y. Jia, L. Xu, *et al.*, "*Infrared spectroscopic and X-ray diffraction characterization of the nature of adsorbed arsenate on ferrihydrite*", Geochimica et Cosmochimica Acta, vol. 71(7), 2007, pp. 1643-1654.

[53] G. H. Khoe, J. C. Huang*, et al.* "*Precipitation chemistry of the aqueous ferrous-arsenate system*", in EPD Congr. 91, Proc. Symp. TMS Annual Meeting Menai, Australia. Ed. D. R. Faskell, pp. 103-105, 1991: Miner. Met. Mater. Soc.

[54] R. B. Johnston and P. C. Singer, "*Solubility of symplesite (ferrous arsenate): implications for reduced groundwaters and other geochemical environments*", Soil Sci Soc Am J*,* vol. 71(1), January 1, 2007 2007, pp. 101-107.

[55] M. G. Babechuk, C. G. Weisener*, et al.*, "*Microbial reduction of ferrous arsenate: Biogeochemical implications for arsenic mobilization*", Applied Geochemistry*,* vol. 24(12), 2009, pp. 2332-2341.

[56] T. C.-M. Cheng "*Measurement of oxygen mass transfer rates in a laboratory batch pressure reactor*", M.Eng. Thesis, McGill University, 1994

[57] J. W. Rowson, *Personal Communication*, Saskatoon, August 18th 2010

[58] J. F. Le Berre, R. Gauvin*, et al.*, "*Characterization of poorly-crystalline ferric arsenate precipitated from equimolar Fe(III)-As(V) solutions in the pH range 2 to 8*", Metallurgical and Materials Transactions B*,* vol. 38(5), 2007, pp. 751-762.

[59] J. F. Le Berre, R. Gauvin*, et al.*, "*A study of the crystallization kinetics of scorodite via the transformation of poorly crystalline ferric arsenate in weakly acidic solution*", Colloids and Surfaces A: Physicochemical and Engineering Aspects*,* vol. 315(1-3), 2008, pp. 117-129.

[60] M. A. Gomez, L. Becze*, et al.*, "*Molecular and structural investigation of yukonite (synthetic & natural) and its relation to arseniosiderite*", Geochimica et Cosmochimica Acta*,* vol. 74(20), 2010, pp. 5835-5851.

[61] R. L. Frost, W. Martens*, et al.*, "*Raman spectroscopic study of the vivianite arsenate minerals*", Journal of Raman Spectroscopy*,* vol. 34(10), 2003, pp. 751-759.

[62] J. Raposo, M. Olazábal*, et al.*, "*Complexation and precipitation of arsenate and iron species in sodium perchlorate solutions at 25°C*", Journal of Solution Chemistry*,* vol. 35(1), 2006, pp. 79-94.

[63] G. P. Demopoulos, "*Aqueous precipitation and crystallization for the production of particulate solids with desired properties*", Hydrometallurgy*,* vol. 96(3), 2009, pp. 199-214.

[64] P. G. Weidler, "*BET sample pretreatment of synthetic ferrihydrite and its influence on the determination of surface area and porosity*", Journal of Porous Materials*,* vol. 4(3), 1997, pp. 165-169.

[65] H. Liu, Y. Wang*, et al.*, "*The microstructure of ferrihydrite and its catalytic reactivity*", Chemosphere*,* vol. 79(8), 2010, pp. 802-806.

[66] J. Bessière, M. Perdicakis, *et al.*, "*Formation de la rouille verte II sulfatée* $Fe_2(OH)_{12}SO_4$ *par oxydation du sulfate ferreux par l'eau*", Comptes Rendus de l'Académie des Sciences, vol. 2(2), 1999, pp. 101-105.

[67] P. M. L. Bonin, M. S. Odziemkowski, *et al.*, "*In situ identification of carbonate-containing green rust on iron electrodes in solutions simulating groundwater*", Journal of Solution Chemistry, vol. 29(10), 2000, pp. 1061-1074.

[68] P. Refait, C. Bon, *et al.*, "*Chemical composition and Gibbs standard free energy of formation of Fe(II)-Fe(III) hydroxysulphate green rust and Fe(II) hydroxide*", Clay Minerals, vol. 34(3), September 1 1999, pp. 499-510.

[69] M. H. I. Baird, N. V. Rama Rao, *et al.*, "*Oxygen absorption in a baffled tank agitated by delta paddle impeller*", The Canadian Journal of Chemical Engineering, vol. 71(2), 1993, pp. 195-201.

[70] T. Nishimura and R. G. Robins "*Removal of arsenic in gold cyanide processes* ", in Minor Elements 2000: Processing and Environmental Aspects of As, Sb, Se, Te, and Bi; Salt Lake City, UT. Ed. C. A. Young, pp. 135-140, 2000: SME

[71] T. C.-M. Cheng "*Production of hematite in acidic zinc sulphate media*", Ph.D. Thesis, McGill Univeristy, 2002

[72] T. Chmielewski and W. A. Charewicz, "*The oxidation of Fe(II) in aqueous sulphuric acid under oxygen pressure*", Hydrometallurgy, vol. 12(1), 1984, pp. 21-30.

[73] D. B. Dreisinger and E. Peters, "*The oxidation of ferrous sulphate by molecular oxygen under zinc pressure-leach conditions*", Hydrometallurgy, vol. 22(1-2), 1989, pp. 101-119.

[74] B. Verbaan and F. K. Crundwell, "*An electrochemical model for the leaching of a sphalerite concentrate*", Hydrometallurgy, vol. 16(3), 1986, pp. 345-359.

[75] A. A. Olowe and J. M. R. Génin, "*The mechanism of oxidation of ferrous hydroxide in sulphated aqueous media: Importance of the initial ratio of the reactants*", Corrosion Science, vol. 32(9), 1991, pp. 965-984.

[76] J.-M. R. Génin, C. Ruby, *et al.*, "*Synthesis of green rusts by oxidation of* $Fe(OH)_2$*, their products of oxidation and reduction of ferric oxyhydroxides; Eh-pH Pourbaix diagrams*", Comptes Rendus Geosciences, vol. 338(6-7), 2006, pp. 433-446.